INVESTIGATION OF NEUTRON THERMALIZATION IN POLYCRYSTALLINE MODERATORS

A THESIS

Presented to

The Faculty of the Division of Graduate

Studies and Research

by

Bangalore Inamati Shamasundar

In Partial Fulfillment

of the Requirements for the Degree

Doctor of Philosophy

in the School of Nuclear Engineering

Georgia Institute of Technology

January, 1974

INVESTIGATION OF NEUTRON THERMALIZATION IN POLYCRYSTALLINE MODERATORS

Approved:

F. M. Kallfelz, Chairman

G. G. Eichholz

J. D. Clement

S. Spooner

Date approved by Chairman: 14 Jan 1974

ACKNOWLEDGMENTS

I would like to extend my deepest gratitude to Dr. John Kallfelz, my thesis adviser, who suggested the thesis topic and provided advice and generous assistance over the years of our association. I would like to thank the members of my reading committee, Dr. Geoffrey G. Eichholz, Dr. Joseph D. Clement, and Dr. Stephen Spooner, for providing invaluable professional support. My thanks also are extended to Dr. Joe Johnson for his encouragement and inspiration during my studies.

I wish to thank my friend, Dr. James Lake, for his contribution and assistance in numerous aspects of this work. My thanks also go to Mr. Dhunjishaw Lal for his efforts in initiating the computer codes, GASKET and FLANGE, here at Georgia Tech. I am grateful to Dr. M. M. R. Williams of the University of London, Queen Mary College, and Dr. J. N. Davidson of Georgia Tech, for their discussions which resolved many questions. My appreciation is extended to Dr. A. I. M. Ritchie, Australian Atomic Energy Commission, Australia, who suggested that the extinction effects present in crystalline materials might have influence on some of our results.

Financial support throughout this research has been provided by the Research Corporation, under the Frederick Gardner Cottrell grant, as well as by a graduate research assistantship by the School of Nuclear Engineering, Georgia Tech.

My thanks are extended to Mr. Ward Engle of Oak Ridge National Laboratory for his discussions which elucidated many questions regarding

the ANISN computer code and for his help in making the DOT calculations. I would like to thank Mr. Leonard Ballard of the Oak Ridge Y-12 Plant for his generous help in providing the beryllium oxide samples. The beryllium samples used in the cross section measurements were part of an inventory, on loan from the Argonne National Laboratory.

I am indebted to the reactor supervisors, Mr. Robert Kirkland and Mr. Fred Apple, and the members of the Georgia Tech Research Reactor staff for their cooperation in carrying out the experimental phases of this research. My thanks go to my friend, Mr. Mike Burke, who was exceptionally cooperative in planning and helping with the construction of various pieces of equipment. Mr. B. D. Statham of the School of Nuclear Engineering Electronic Shop has always extended his prompt and proficient assistance.

My appreciation is extended to Lydia Geeslin for her typing and editing assistance on this manuscript and other papers.

I express my most sincere appreciation to my beloved wife, Rekha, for her love and understanding during the times that this thesis took priority.

TABLE OF CONTENTS

TABLE OF CONTENTS

LIST OF TABLES

LIST OF ILLUSTRATIONS

LIST OF ILLUSTRATIONS (Continued)

LIST OF ILLUSTRATIONS (Concluded)

SUMMARY

In recent years, a question of interest to reactor physicists has been, under what circumstances the discrete fundamental mode eigenvalue (decay constant) and the eigenfunction (equilibrium spectra) can exist for the neutron transport equation, which describes the motion of thermal neutrons in a moderating assembly. Theoretical analysis has shown that thermal neutrons, diffusing in a moderating medium, cannot reach an equilibrium distribution for certain time-dependent and steady-state cases when the system size or the absorption concentration are varied beyond some "critical" values.

A series of measurements to determine accurately the total cross section of polycrystalline beryllium, beryllium oxide, and graphite, below the Bragg cut-off energy, has been made. These measured results are one of the parameters crucial to an accurate determination of the "critical" dimensions of these moderators below which the discrete fundamental mode eigenvalue cannot exist.

Measurements were also made to establish accurately the total cross section, above the Bragg cut-off energy, of the beryllium moderator used in the experiments of Lake and Kallfelz. Over a certain energy range, the results of the measured total cross section have been found to be less than the values generally used for theoretical calculations. This is caused by the extinction effects due to the presence of relatively large grain sizes.

A theoretical study of the space, angle-dependent spectra, in a 35.56 x 35.56 x 50.0 cm long beryllium moderator, has been made using the adjoint Monte Carlo technique. The calculated energy spectrum, in the forward positive z direction, at 10.2 cm from the source, is in good agreement with the experimental results of Lake and Kallfelz. This theoretical analysis has shown that the first term of the Placzek kernel, normalized to yield the correct inelastic cross section, can provide a good representation of the inelastic scattering properties of a beryllium moderator.

A theoretical study of the total angle-integrated flux, as a function of distance from the source, has been made in finite sizes of a beryllium moderator, using the S_N method. Here the transverse leakage term has been approximated by the energy-dependent transverse buckling concept, whereas the transport of neutrons along the axis of the assembly has been treated exactly. It has been found that, in a 150 x 150 cm beryllium assembly, the neutron distribution reaches an equilibrium condition fairly rapidly, whereas in 35.56 x 35.56 cm and 60 x 60 cm beryllium assemblies the neutron distribution does not reach an equilibrium condition even after a distance of 100 cm from the source plane.

These results are in agreement with the published asymptotic transport theory predictions and are in direct disagreement with the corresponding diffusion theory results which predict that equilibrium conditions should exist in beryllium assemblies with transverse dimensions as low as 30 x 30 cm. This demonstrates the limitations on the use of diffusion theory for small systems with strong transverse leakage. The reasons for the breakdown of diffusion theory have been discussed in some detail.

CHAPTER I

INTRODUCTION

Fast neutrons, if produced in a moderating medium from any of the usual sources, will collide with the nuclei of the moderator and lose energy by elastic and inelastic processes. As long as the energy of the neutrons is greater than about one electron volt (eV), the scattering law, which determines the rate of slowing down, will be independent of the physical state of the moderator and will be determined solely by the nuclear forces between the neutron and the nuclei. At about one eV, depending on the temperature of the medium, the thermal motions of the scattering atoms will start to become significant compared with that of the neutron. The scattering law will be dependent on the nature of the molecular binding of the moderating medium. As the neutron energy decreases still more these effects become more important, and the neutron will be both losing energy to the moderator atoms, as well as gaining energy from them. Eventually in an infinite, non-absorbing medium a situation will be reached where the neutrons, on the average, receive as much energy as they lose and an equilibrium is reached. The equilibrium distribution of neutrons will, in general, not be Maxwellian because of absorption, leakage, and slowing down effects. It is the last stage of the slowing down process, that is, from one eV to zero eV, with which one associates the name "thermalization." The thermalization rate and the

final equilibrium distribution of neutrons in space and energy will be determined in part by the scattering kernel. The latter is a measure of the probability that a neutron which has a particular initial energy will end up after a collision with a particular final energy and will have been scattered through a certain angle. Part of the thermalization theory entails the calculation of this quantity, which clearly depends on whether the scatterer is liquid, solid, or gaseous, and also on its temperature and state of chemical binding.

Thermal neutrons diffusing in an infinite, non-absorbing medium will always attain a Maxwellian equilibrium distribution, irrespective of the nature of the energy exchange mechanism of the scattering kernel of the moderating medium. To obtain information on the nature of the scattering kernel, the spectrum must be distorted from the Maxwellian in some manner; this distortion is often accomplished by either increasing the absorption or the leakage of neutrons from the moderating medium. The former method is used in the "diffusion length" problem where the spatial decay of neutrons diffusing into the medium from a planar source is studied as a function of the absorption concentration.

The latter method is used in the "pulsed neutron" problem where the time decay of an initial pulse of neutrons is observed as a function of the transverse buckling of the moderating system. By adopting such methods, one extracts the diffusion parameters, such as the diffusion coefficient D and the diffusion cooling coefficient C which are sensitive to the thermalization properties of the moderator.

There have been many experimental and theoretical studies of the

diffusion length and pulsed neutron problem. Crystalline moderators like beryllium, beryllium oxide, and graphite, with their relatively weak energy transfer characteristics[1] and strongly fluctuating neutron transport cross section, have received special attention from experimental and theoretical investigators. Recently these studies have concentrated on the question of how severely one can distort the spectrum and under what conditions an equilibrium spectrum can exist in such moderating systems with high absorption concentration or severe transverse leakage.

It has been shown that there exists a limit on the maximum absorption concentration or the minimum size of the system beyond which a discrete eigenvalue and the associated eigenfunction cannot exist. That is, the decay is no longer asymptotic at long times or distances from the source. This means that the assumption of space- (or time-) energy separability, often used for solving the neutron transport equation, is no longer valid, as the solution is in the continuum region.[2,3,4]

Upper Limit on the Decay Constants

Let us consider an elementary discussion concerning the existence of an upper limit for the space eigenvalue in the diffusion length problem. The steady-state diffusion length problem is essentially a study of the spatial decay of neutrons, diffusing into a moderating medium from a planar source, as a function of either the absorption concentration or the leakage induced by the finite transverse size of the system.

Consider the homogeneous part of the transport equation for an essentially infinite half-space of an isotropic scattering medium:

$$\mu \frac{\partial \varphi(E,\mu,x)}{\partial x} + \Sigma_T(E)\ \varphi(E,\mu,x) = \frac{1}{2}\int_o^\infty\int_{-1}^{+1} \Sigma_S(E'\rightarrow E)\ \varphi(E',\mu',x)dE'd\mu' \qquad (1)$$

where $\varphi(E,\mu,x)$ is the space, angle, and energy-dependent neutron flux, μ is the cosine of the scattering angle, $\Sigma_T(E)$ is the total macroscopic cross section, and $\Sigma_S(E'\rightarrow E)$ is the differential scattering cross section. Substituting $\varphi(E,\mu,x) = \varphi(E,\mu)\ e^{-\kappa x}$, we have

$$(\Sigma_T(E) - \kappa\mu)\ \varphi(E,\mu) = \frac{1}{2}\int_o^\infty\int_{-1}^{+1} \Sigma_S(E'\rightarrow E)\ \varphi(E',\mu')dE'd\mu' \qquad (2)$$

The inscattering integral is always greater than or equal to zero, the flux is always non-negative, and $\mu \leq 1$; therefore

$$\kappa_o \leq \{\Sigma_T(E)\}_{Min} \equiv \kappa^* \qquad (3)$$

Corngold[5] has proved a maximum absorption theorem in which he states that there exists a maximum absorption concentration, N_a^*, such that for, $N_a > N_a^*$, no discrete eigenvalues exist. This means that, as the absorption concentration increases, the eigenvalue increases at a relatively faster rate than $\Sigma_T(E)$ and at some maximum absorption concentration even the fundamental eigenvalue exceeds the limit given in Equation 3. This implies that the flux decay in such systems becomes non-exponential even at large distances from the source.

Thus far, we have considered only a semi-infinite medium. It is interesting to find out the effect of leakage on the diffusion length in a finite block of moderator. This problem has been theoretically analyzed

by Williams[6,7,8] using the transport equation and taking into account the neutron leakage in the transverse directions. In his analysis of the existence of a fundamental mode decay as a function of both absorption and transverse dimensions, he finds that the limit on the existence of the discrete fundamental mode decay, in terms of a maximum transverse buckling, B^*, is given by

$$(B^*)^2 = \{\Sigma_T(E)\}^2_{Min} - \kappa_o^2 \tag{4}$$

where κ_o is the infinite medium fundamental decay constant which is equal to the inverse of the diffusion length. The maximum transverse buckling, B^*, of rectangular prisms of polycrystalline moderators with only natural absorption is found to be of the order of 10^{-3} cm^{-2} for beryllium and 1.5×10^{-3} cm^{-2} for graphite at 300°K.[9] However, it should be noted that, for poisoned and low-temperature crystalline moderators, these maximum bucklings will be even smaller because, for this case, an increase in absorption will increase the value of κ_o faster than $\Sigma_T(E)$ below the Bragg cut-off energy.

For a large class of moderators, like H_2O and D_2O, the minimum value of σ_t occurs at "high" energies, ~ 1 eV, and is the free-atom cross section value.[5] However, in the case of crystalline materials like beryllium, beryllium oxide, and graphite, σ_t displays sharp fluctuations because of the coherent Bragg scattering peaks. Figure 1 shows that σ_t drops at an energy just below the Bragg cut-off to a minimum which is much lower than the free atom value. As seen in Figure 1, the total cross

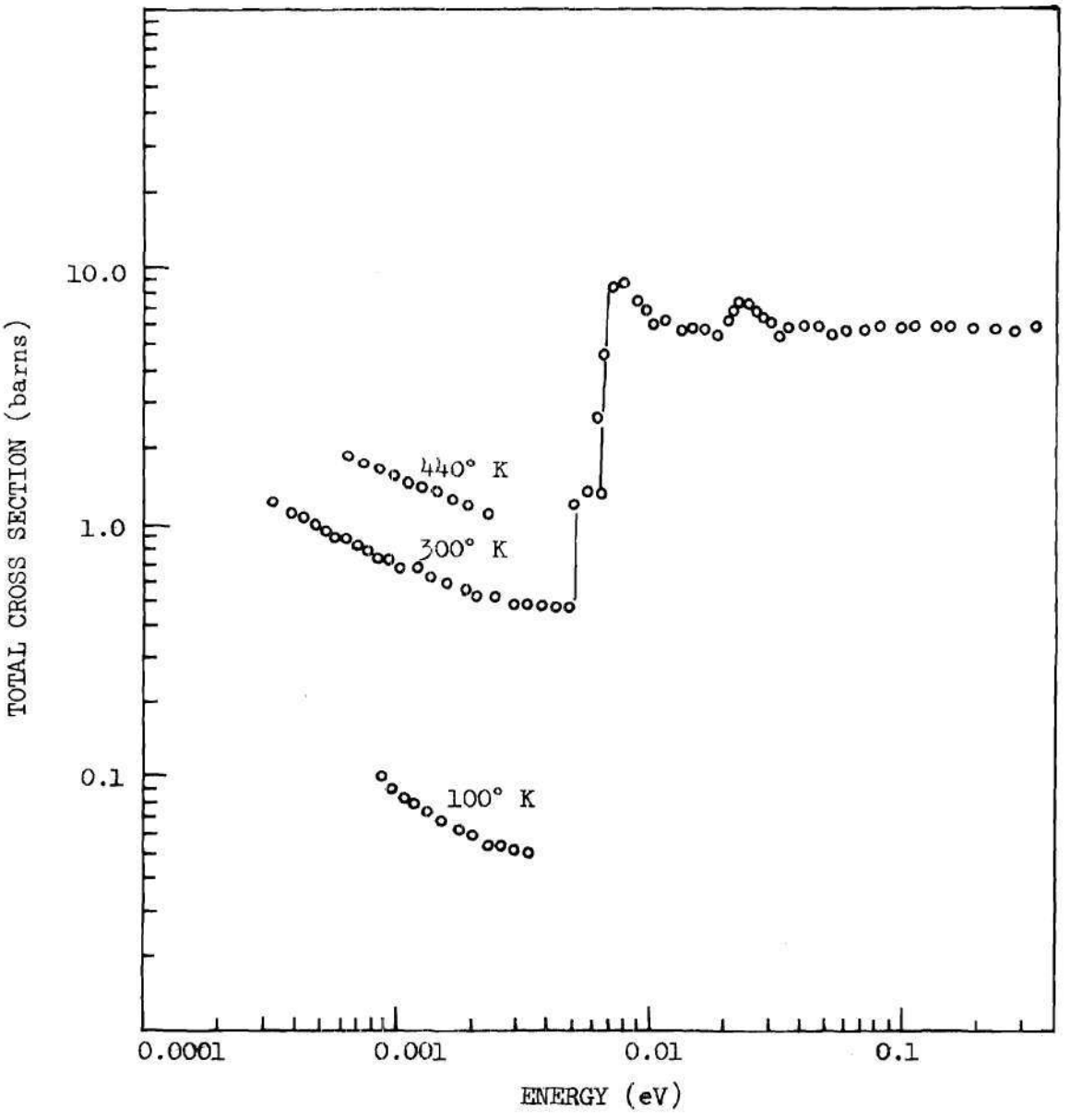

Figure 1. Total Microscopic Cross Section for Beryllium in the Thermal Energy Range[10]

section below the Bragg cut-off energy is very sensitive to the moderator temperature. We notice from Equations 3 and 4 that the critical absorption concentration or the critical transverse buckling is more restricted in crystalline systems than in common liquids like H_2O and D_2O.

The pulsed neutron problem is a study of the time behavior of an initial pulse of neutrons injected into a finite moderating system. For this case, the general proof for the existence of a fundamental time-eigenvalue using the transport equation has been given by Nelkin[11] and Corngold.[12] The limit on the existence of the discrete fundamental mode time-eigenvalue, λ_o, as predicted by transport theory analysis is given by

$$\lambda_o \leq \underset{v \to 0}{\text{Limit}} \{ v \Sigma_T(E) \} \equiv \lambda^* \tag{5}$$

where λ_o is the fundamental time decay constant and v is the neutron velocity.

Corngold[12] has proved a maximum buckling theorem in which he states that there exists a maximum value of buckling, $(B^*)^2$, such that, for B^2 greater than $(B^*)^2$, no discrete eigenvalues exist. This has been modified by a more recent theoretical analysis of this problem by Conn and Corngold.[13,14,15] The essence of their analysis is that, for systems with buckling less than $(B^*)^2$ true discrete modes exist, whereas for systems with buckling equal to and somewhat greater than $(B^*)^2$ psuedo-discrete modes exist. However, in systems with bucklings substantially greater than $(B^*)^2$, no discrete modes exist. Such a behavior has been experimentally observed by Ritchie and Rainbow[16,17] in a beryllium oxide moderator.

Current Experimental and Theoretical Situation

The behavior of the space, angle-dependent neutron energy spectrum in small beryllium moderator systems has been analyzed by Williams[6,7] by solving the transport equation for the case of a simple separable plus elastic kernel. This synthetic kernel is a crude approximation of the scattering kernel to describe the neutron scattering phenomenon in polycrystalline moderators and it is devised such that it satisfies the detailed balance equation and gives the correct total scattering cross section when integrated over the final energies. Williams[6] has shown that, in assemblies approaching the limit in Equation 4, the angular spectrum is strongly anisotropic as seen in Figure 2. The angular flux distribution has a marked forward (positive z direction) bias of neutrons possessing energies at and below the Bragg cut-off energy. As one moves away from the forward direction, the peak rapidly diminishes in intensity, becoming a depression in the negative z direction. When the moderator dimensions are small enough to exceed the limit in Equation 4, there is no asymptotic spatial decay and the angular flux distribution is governed by source and continuum transients. At some distance from the source, the source transients die away and the angular spectrum is totally governed by the continuum transients. In this region, the transient angular distribution has a forward bias of sub-Bragg neutrons; this bias progressively increases with the distance from the source and the buckling of the system.

As the size of the system is decreased, a point is reached when the angular spectrum would consist of a highly singular beam of neutrons of energies below the Bragg cut-off. This is the well known crystalline filtering effect.

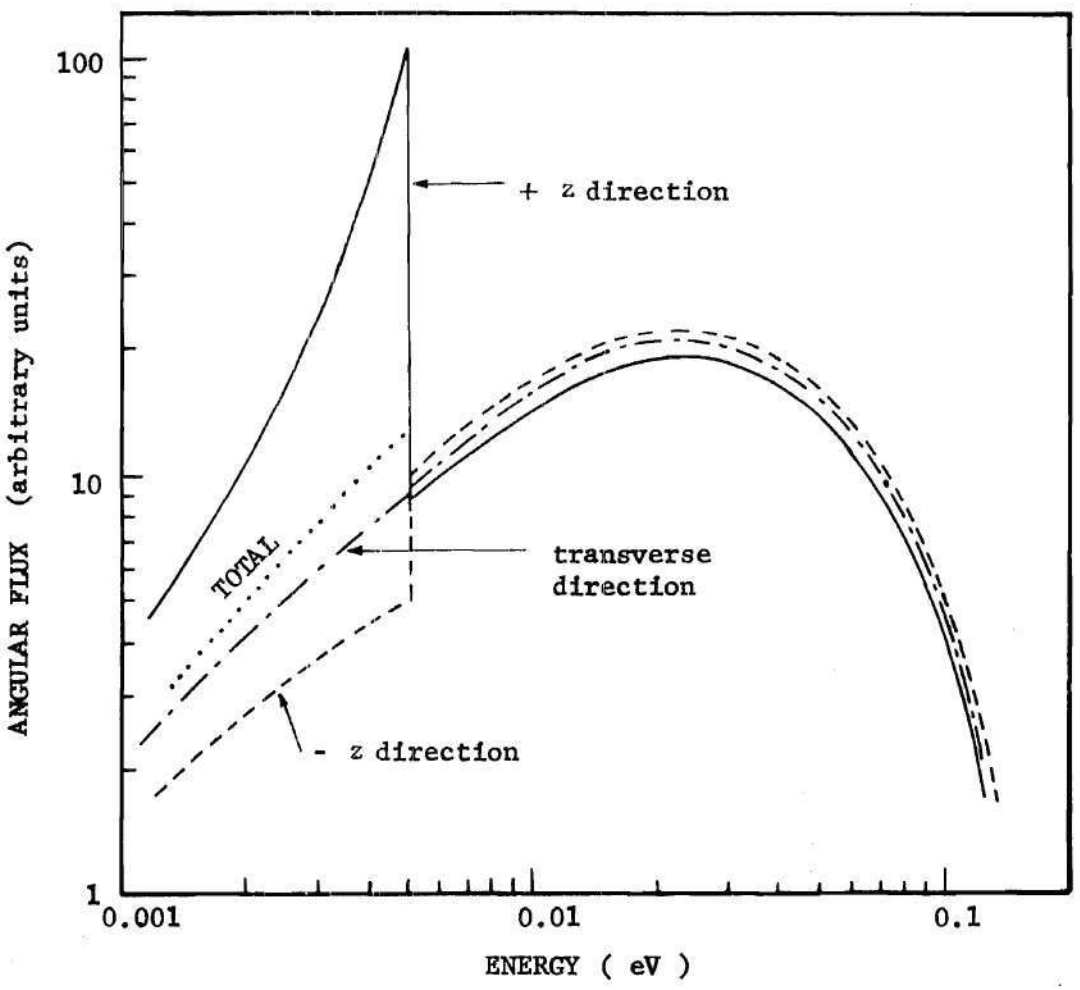

Figure 2. Theoretical, Steady-State, Asymptotic, Angular Neutron Energy Spectra in Beryllium Assembly with Transverse Buckling, $B^2 = 0.00035\ cm^{-2}$ (Calculations by Williams[6])

The behavior of the transverse flux distribution which changes progressively with distance from the source has been observed experimentally in graphite by DeJuren and Swanson.[18] They showed that, to fit a $\sin\{B(x + x_o)\}$ function (where x_o is the extrapolated end point) to the flux, it is necessary that x_o be an increasing function of z. Thus it was shown, at least by implication, that in sufficiently small steady state systems the flux is changing progressively even after large distances from the neutron source.

Recently Ahmed, Kothari, and Kumar[19] have analyzed the diffusion equation governing the spatial diffusion of neutrons in finite sizes of crystalline moderator systems by using diffusion theory and an energy-dependent buckling approximation. Their analysis predicted that the neutron distribution reaches an equilibrium condition in beryllium assemblies with transverse dimensions as low as 30 x 30 cm. They found that the equilibrium condition is not reached in assemblies of intermediate transverse dimensions between 20 x 20 cm and 30 x 30 cm; also that "pseudo-equilibrium" conditions are established in assemblies with transverse dimensions less than 20 x 20 cm. The critical dimension of 30 x 30 cm for polycrystalline beryllium is substantially lower than the critical dimensions of 127 x 127 cm, as predicted by the transport analysis of Williams.[9] Williams[20] has argued that the use of diffusion theory is not justifiable in such small systems and therefore the diffusion theory results of Ahmed et al. are highly questionable.

Lake and Kallfelz[21,22,23] have presented experimental results supporting the more restrictive limit, given in Equation 4, for the existence of the discrete fundamental mode decay. They have made a series of mea-

surements of space dependent angular neutron energy spectra in various rectangular configurations of polycrystalline beryllium. Figure 3 shows one set of measurements of the space dependence of neutron angular spectrum in the positive z direction along the longitudinal axis of the 35.6 x 35.6 x 50.8 cm beryllium assembly.

According to the Williams theory,[6,9] the buckling range used in this experiment should be well into the region governed by the continuum of eigenvalues, and thus the spectra should be strongly space dependent. But according to the aforementioned diffusion theory analysis of Ahmed et al.,[19] the transition from a discrete asymptotic mode to a continuum decay should occur for beryllium block sizes of 30 x 30 cm. As seen in Figure 3, the experimental results show that the relative flux peaking of sub-Bragg neutrons is a progressively increasing function of distance from the source. It shows no tendency to approach equilibrium distribution even at distances in excess of 40 cm from the source plane. Lake and Kallfelz concluded that their results are in qualitative agreement with Williams' transport theory predictions and in disagreement with Ahmed's diffusion theory analysis.

Importance of $\Sigma_T(E)_{Min}$

Theoretical study has shown that the upper limiting value of the discrete eigenvalue is determined by $\Sigma_T(E)_{Min}$ in the stationary diffusion length problem and by $(v\,\Sigma_T(E)_{Min})$ in the time dependent pulsed neutron problem as given in Equations 3, 4, and 5.

In the case of a strong coherent scatterer, like polycrystalline beryllium, beryllium oxide, and graphite, the total cross section shows

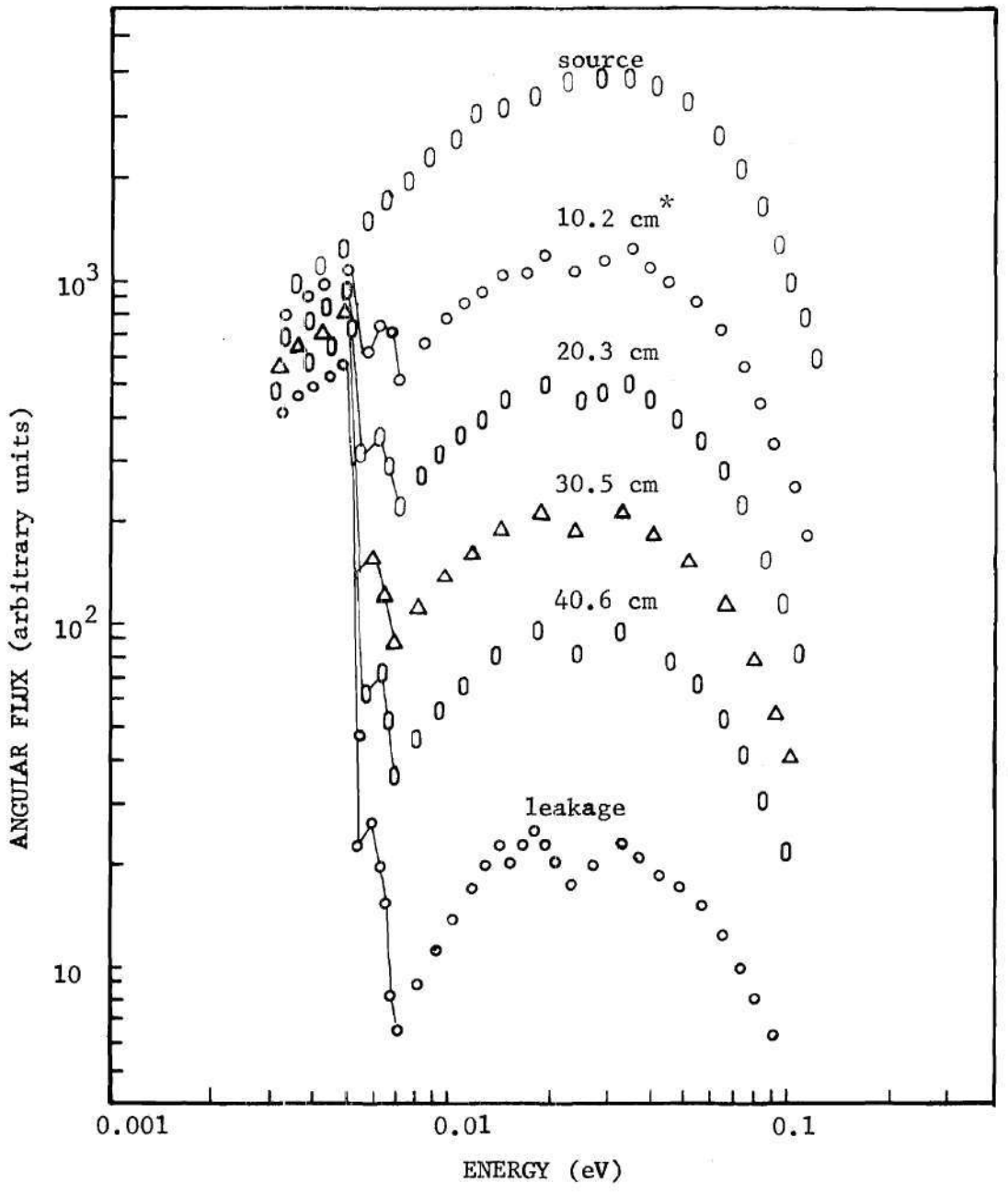

Figure 3. Space Dependence of the Angular Neutron Energy Spectrum in the Positive z Direction Along the Longitudinal Axis of the 35.6 x 35.6 x 50.8 cm Beryllium Assembly (Data from Lake[23]; * - distances from the source plane)

sharp fluctuations with energy in the vicinity of Bragg scattering peaks. At some Bragg cut-off energy the total cross section sharply drops down to a low value as seen in Figure 1. This is due to the fact that those neutrons whose wavelength is greater than twice the largest spacing between the crystal lattice planes cannot undergo coherent Bragg scattering.[25] At energies below the Bragg cut-off, $\Sigma_T(E)$ reaches its minimum value and has a smooth energy dependence. Here the total cross section is made up of the incoherent elastic, absorption, and thermal inelastic cross sections. In materials like beryllium, beryllium oxide, and graphite, the incoherent elastic cross section is negligibly small.[1] Since the absorption cross section is small, the total cross section is essentially equal to the inelastic cross section and is very sensitive to moderator temperature.

It is evident that, for any qualitative predictions of the value of the limits B^* and λ^*, an accurate knowledge of $\Sigma_T(E)_{Min}$ is necessary. Williams[6] has estimated the values of B^{*2} at 300°K for graphite and beryllium as 1.5×10^{-3} cm^{-2} and 10^{-3} cm^{-2}, respectively. In the time dependent case the usually accepted values of the upper limit of the time eigenvalue, λ^*, are 3800, 2600, and 2500 sec^{-1} for beryllium, graphite, and beryllium oxide, respectively. One might ask at this point how well established these values are. In general, discrepancies have been found in these critical values, particularly for graphite. Conn and Corngold[14] find that, for graphite, general agreement between theory and the experimental dispersion curve for the time dependent case seem to require a value of λ^* about half of the usually accepted value of 2600 sec^{-1}. For answers to such questions one should look at the reported

values of the total cross section below the Bragg cut-off energy for these crystalline materials. Discrepancies between the calculated and the experimental values have been reported[26,27] for all three materials.

Particularly for graphite, a glance at the reported values of the thermal inelastic cross section, σ_{inel}, indicates that experimental results seem to have limited accuracy. Both Hughes and Bacon[25] indicate a value of $\sigma_{inel} = 0.90$ barn for graphite at a neutron wavelength, λ, equal to 8 Å. On the other hand, Egelstaff[28] indicates $\sigma_{inel} = 0.56$ barn (BNL-325[10] data) and Palevsky's result reported in Reference 29 indicates $\sigma_{inel} = 0.28$ barn at 8 Å. Egelstaff[28] reports that the cross section measurement of polycrystalline materials, like graphite, is made difficult by the presence of a large small-angle scattering contribution. Small-angle scattering of neutrons[25,28,30,31] is a process similar to refraction where the neutrons are preferentially scattered through small angles as they pass through many air/solid interfaces in a porous sample such as graphite. The small-angle scattering contribution in an experimental evaluation of the thermal inelastic cross section depends on the presence of impurities, grain size, and the geometry of the experiment. It has been suggested[28] that the high cross section measurements, > 0.56 barn at 8 Å, may be due to small-angle scattering of neutrons by the graphite grains. However, this does not explain the difference of a factor of roughly two between the data of Egelstaff and Palevsky. The theoretical calculation of the thermal inelastic cross section in the incoherent approximation made by Ghatak[32] and Clendenin[33] gives a value which is a factor of two lower than the BNL-325 data.[10] It has been

suggested by several authors that, since graphite is a strong coherent scatterer, it may very well be that the discrepancies are caused by the breakdown of the incoherent approximation, especially at energies below the Bragg cut-off. Khubchandani et al.[34] have made a one phonon coherent calculation of the inelastic cross section using Krumhansl and Brooks'[35] model of the phonon frequency distribution in graphite. They find better agreement with the lower experimental results of Palevsky. Recently, Conn[36] has made a one phonon coherent calculation using his approximate model for the phonon frequency distribution of graphite. His results show good agreement with BNL-325 cross section data for graphite at 478°K but not at room temperature. On the whole, it is quite obvious that another careful measurement of the thermal inelastic cross section below the Bragg cut-off energy is desirable.

In the case of beryllium oxide there is only one reported value of the thermal inelastic cross section below the Bragg cut-off energy. This has been given by Zhezherun et al.,[37,38] who report a $\sigma_{inel} = 0.8$ barn below the Bragg cut-off energy. This figure has a large experimental error of the order of 50% or more, and, as stated by the authors, no attempt has been made to determine the effect of the small-angle scattering contribution. The theoretical incoherent calculation of the inelastic cross section below the Bragg cut-off energy, using the computer codes GASKET[39] and FLANGE[40], gives a value of σ_{inel} which is approximately half of that reported by Zhezherun et al. It should be noted here that, in the case of strong coherent scattering moderators, the incoherent calculation of the inelastic cross section has been reported to yield poor results,[34,36,41]

especially in the sub-Bragg energy region. The above discussion shows the desirability of an accurate measurement of the thermal inelastic cross section for beryllium oxide below the Bragg cut-off energy range.

Finally, for beryllium there is only one reported experimental result of the total cross section given in the BNL-325 cross section data. This measurement was done with the same technique and by the same group as the BNL-325 graphite measurement mentioned earlier, which still differs from theory and other measurements. Borgonovi and Sprevak[41] have made a one phonon coherent calculation of the thermal inelastic cross section in beryllium. Their result shows excellent agreement with the BNL-325 data as compared to an incoherent calculation which was a factor of two higher than the BNL-325 data. In view of the above discussion, it seemed desirable to have another measurement of σ_{inel} for beryllium, as a check on the previous experimental value.

Objectives

The objectives of this investigation are described in this section.

a) Perform a series of measurements at room temperature to determine the total cross section of beryllium, beryllium oxide, and graphite in the sub-Bragg energy range.

b) Measure the total cross section, in the above-Bragg energy range, at room temperature, for the beryllium moderator used in the experiments of Lake and Kallfelz[23] and compare the measured cross section with the BNL-325 data to determine the effects of extinction[25] on the cross section. The effect of extinction is to reduce the coherent Bragg peaks in the total cross section. The phenomenon of extinction is discussed in

detail in Chapter III.

c) Determine the space, angle-dependent neutron energy spectra in a small finite beryllium moderator using the adjoint Monte Carlo theoretical approach. From a comparison of the theoretical spectrum calculations with the experimental results of Lake and Kallfelz[21,22,23] one can obtain some information about the adequacy of various beryllium scattering kernels and about methods of solution of the transport equation.

d) Theoretically analyze the spatial behavior of the total, angle-integrated neutron energy spectra as a function of the transverse size of a beryllium moderating system. Both the S_N approximation and the diffusion theory approximation would be used in the theoretical analysis to determine whether the neutron distribution could reach an equilibrium condition in a 150 x 150 x 150 cm, 60 x 60 x 150 cm, and 35.56 x 35.56 x 150 cm long beryllium block. This analysis would provide an indication of whether the critical transverse size is closer to the Kothari[19] diffusion theory limit of 30 x 30 cm or the Williams[9] asymptotic transport theory limit of 127 x 127 cm. This in turn sheds light on the applicability of diffusion theory for small moderating systems.

CHAPTER II

MEASUREMENT OF TOTAL CROSS SECTION BELOW THE BRAGG CUT-OFF ENERGY

The total cross section was measured at room temperature in the sub-Bragg energy range for beryllium, beryllium oxide, and graphite. The method used was the simple transmission technique,[1,28,42] that is, the counting rate of neutrons at the detector was measured with and without the sample in the neutron beam. The ratio of these two counting rates is called the transmission of the sample and bears a direct relation to the total cross section of the sample. If I_o is the counting rate at the detector with no sample in the beam, then after insertion of a sample of thickness d, the counting rate is

$$I = I_o e^{-N\sigma_t d} \tag{6}$$

where σ_t is the microscopic total cross section and N is the atom density of the sample. If the transmission of the sample is defined as $T = I/I_o$, the total cross section σ_t can be expressed as

$$\sigma_t = \frac{1}{Nd} \text{Log}(T) \tag{7}$$

In order that this equation apply rigorously, scattered neutrons must not reach the detector, that is, the experiments must be carried out

with a "good geometry." Good geometry is best achieved by locating the detector as far away from the neutron source as possible and by making the detector and sample small.

The method used for the selection and measurement of the neutron energy, in the cross section measurement, was the slow neutron chopper and time-of-flight technique. The neutron beam from the thermal column of a reactor was chopped into short-time duration pulses by the rotating chopper. The neutrons of different energies in the pulse were allowed to traverse a flight path of 2 to 3 meters to a BF_3 detector where they were counted. The counting rate was recorded in a multi-channel analyzer as a function of time after the chopper burst. Knowing the flight time and path length, it was a straightforward procedure to arrive at the neutron velocities and hence the incident neutron energy spectrum. A synchronous motor was used to maintain a constant chopper speed while measuring the detector response with and without the sample in the neutron beam. This made it unnecessary to correct the cross section data for chopper transmission, detector efficiency, air scattering, and absorption corrections. As long as the chopper speed was maintained constant, these corrections were the same for the data taken both with and without the sample in the neutron beam and would eventually cancel out in the transmission ratio; hence it was unnecessary to correct the measured data for the above-mentioned factors. For the $\sigma_T(E)$ measurements, a chopper speed of 1800 RPM was selected which provided a reasonable compromise between acceptable energy resolution (which improves with increasing rotor speed) and good neutron transmission (which increases with decreasing rotor speed) in the

sub-Bragg energy range. This sub-Bragg energy range for beryllium, beryllium oxide, and graphite involved a region from 0.001 to 0.005 eV. As mentioned earlier, in this energy range the total cross section is made up of the incoherent elastic, absorption and both the coherent and incoherent thermal inelastic cross sections; however, the incoherent elastic cross section is negligibly small.[1,43] The absorption cross section in such moderators is relatively small, for example, in beryllium and beryllium oxide the absorption cross section, σ_a, is 10 mb at a neutron velocity of 2200 m/sec and in graphite σ_a is of the order of 4.5 mb. Thus, the inelastic cross section can be obtained by subtracting the 1/v absorption cross section from the measured total cross section in this energy range.

In a normal procedure to measure the total cross section, a good geometry must be maintained, such that the scattered neutrons cannot reach the detector. But in the case of materials like graphite and beryllium oxide, which are porous by nature, there is a large amount of small-angle scattering of neutrons. In such cases, maintaining a good geometry would mean that those neutrons which undergo small-angle scattering would not reach the detector, thus yielding an anomalously high total cross section. It was, therefore, necessary that the solid angle subtended by the detector at the sample be large enough for the detector to see all the small-angle scattered neutrons. However, in such a detector-sample geometry, those neutrons which are elastically and inelastically scattered through small angles, and also those that are multiple-scattered, can also reach the detector; from here on, these two contributions at the detector will

be referred to as "multiple-scattering" contributions. Such a measurement requires that the measured cross section data be corrected for the theoretically calculated "multiple-scattering" contribution. Such a theoretical calculation assumes a prior knowledge of the total cross section, which one wants to measure. Thus, one is required to develop an iterative scheme in the analysis of the total cross section measurement. This scheme is discussed in detail in a later section.

Instrumentation and Equipment

The total thermal neutron cross sections have been measured by the slow neutron chopper time-of-flight technique using the Georgia Tech Research Reactor (GTRR) thermal column as a neutron source. The instrumentation necessary to carry out such a cross section measurement consists of the neutron source, the neutron chopper, the neutron detection system, and the data processing and recording equipment. A detailed description of the instrumentation and equipment used in our experiments has been given by Lake.[23]

The neutron source was obtained from the end of the thermal column of the GTRR. During the work described here, the GTRR operated at one megawatt power and produced a peak thermal column neutron flux in excess of 10^{13} neutrons/cm^2/sec.

The neutron chopper[23] basically consists of a rotor with cadmium-plated stainless steel blades separated by narrow aluminum spacers. The drive is provided by a synchronous motor which maintains a constant speed of 1800 RPM. This speed was selected to provide a reasonable compromise between the acceptable energy resolution and good neutron transmission in the energy range of interest from 0.005 to 0.001 eV.

The neutron detector used in the measurements was a two inch diameter, aluminum cathode, Reuter-Stokes model RSN-44A, BF_3 proportional counter filled to a high gas pressure (90 cm of Hg) for improved neutron detection efficiency. A monitor detector, with a low efficiency of the order of a few tenths of a percent, was used to monitor the total number of neutrons incident on the chopper during the with- and without-sample measurements.

The data processing and recording equipment is basically a TMC multi-channel analyzer which measures and records the arrival time of neutrons at the BF_3 detector with respect to the zero reference time. This time is the instant at which the chopper blades are parallel to the neutron beam. The low level signals from the detectors are amplified in a solid state preamplifier and the leading and trailing edges are sharpened in a double-delay-line linear amplifier. Electronic and low voltage gamma ray noise pulses are blocked out in an integral discriminator prior to feeding the detector pulse to the TMC multi-channel analyzer unit. Figure 4 is a block diagram of the data collection system.

Experimental Procedure

A schematic diagram of a typical experimental set up is given in Figure 5. The 16 x 16 x 20 inch long cavity in the thermal column was used to house a 14 x 14 x 20 inch long Boral box tightly packed with beryllium blocks. The end of the box facing the thermal column was covered with a 1/8 inch thick aluminum plate and the opposite end was covered by a 1/4 inch Boral plate with a central 2 x 3 inch hole, to define the effective area of the neutron source. One of the purposes of using such a box was

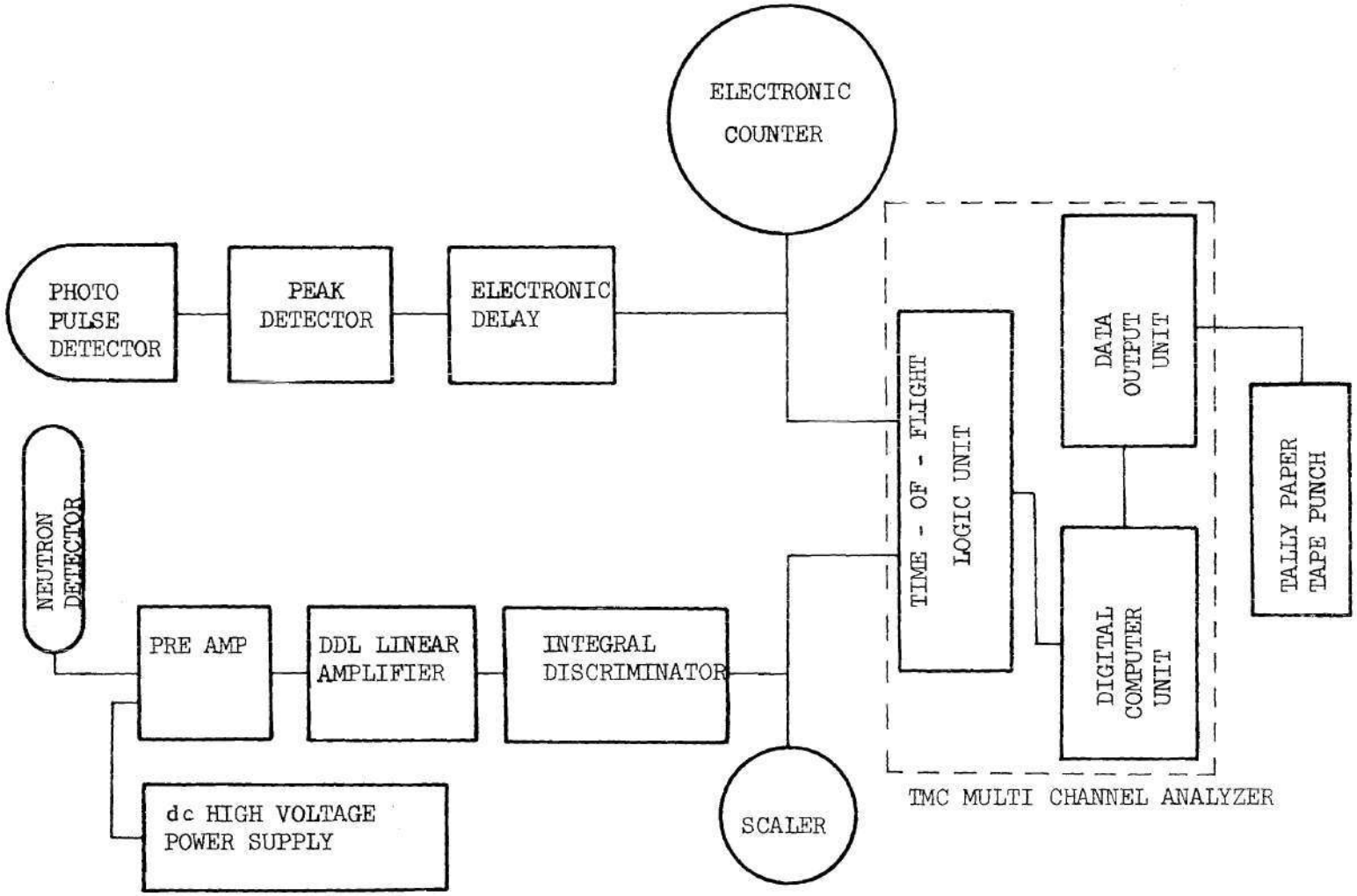

Figure 4. Block Diagram of the Time-of-Flight Data Acquisition System

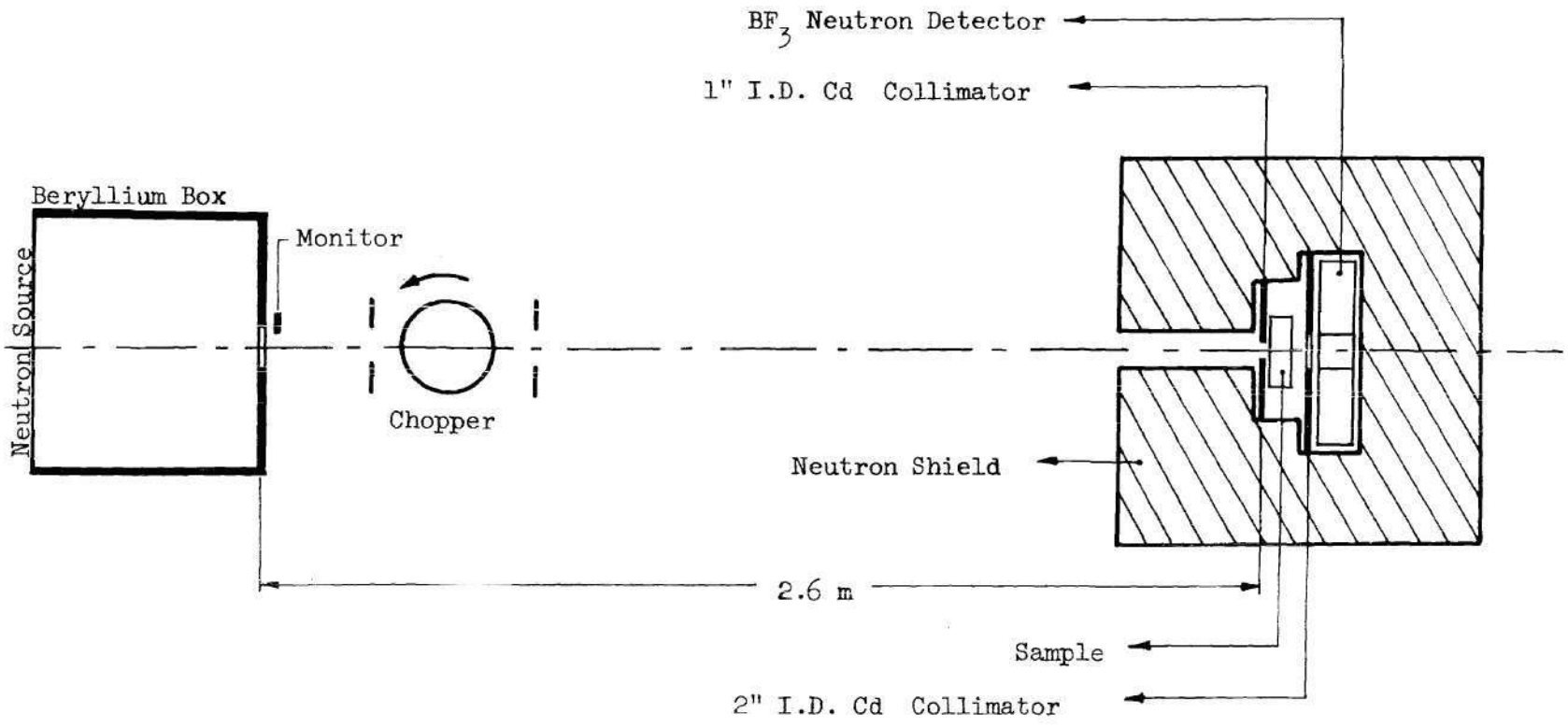

Figure 5. Schematic Diagram of a Typical Experimental Set Up to Measure Total Cross Section

to fill the cavity and thus to help reduce the neutron background. Also, the beryllium box conveniently served as a filter for beryllium cross section measurements. In the cross section measurement of graphite and beryllium oxide, a 1 x 1 inch hole running through the longitudinal axis of the box was provided to get the maximum primary neutron intensity.

The chopper with its zero timing device was positioned squarely in front of the GTRR thermal column, aligned with the center of the beam collimator, and leveled carefully. The monitor detector was placed between the collimator and the chopper. The BF_3 detector was set up and centered across the end of a typical 2.6 meter flight path.

In the beryllium cross section measurement, the BF_3 detector was surrounded by a 3 inch thick boron carbide shield, with only a 2 x 2 inch area of the detector exposed to the neutron beam. A sample holder, with its 2 x 2 inch cadmium plate collimator, was placed in front of the BF_3 detector on a table guide. The detector, the chopper, and the axis of the table guide were optically aligned to be on the central axis of the incident neutron beam.

In the cross section measurement of beryllium oxide and graphite it was required to have a sample-detector geometry in which the solid angle subtended by the detector at the sample was sufficient for the detector to see all the small-angle scattered neutrons. The experimental set up is shown schematically in Figure 5. The BF_3 detector was completely surrounded with a cylindrical cadmium shield exposing only the middle two inches of the detector. A two-inch diameter cadmium plate collimator was positioned close to and in front of the BF_3 detector. The

sample holder with a one-inch diameter cadmium plate collimator was placed on the bench guide, approximately 2 1/2 inches away from the 2 inch diameter collimator. As shown in Figure 5, a tight shield was formed around the BF_3 detector with boric acid filled boxes, coated with a layer of paraffin. A cavity was provided in the shield to house the sample holder. The distance of 2.6 meters between the 2 x 3 inch source collimator and the one-inch diameter collimator of the sample holder provided a well-defined incident neutron beam tightly collimated to less than 50 minutes of an arc. Details of the sample-detector geometry are given in Figure 6.

In order to average out the effects of any small variations in the thermal column neutron intensity, the cross section measurements with and without the sample were repeated with a convenient frequency of 600,000 TMC sweeps. For a typical chopper speed of 1800 RPM this corresponded to a time duration of one hour and twenty-four minutes per run. This repetitive data collection with and without the sample was continued until the accumulated neutron counts were sufficient to yield good statistical accuracy. A count of incident neutrons on the sample over the duration of each measurement was recorded by the monitor detector. This also reflects the small fluctuations in the incident neutron intensity. Thus, normalizing the with and without the sample data for the same total number of incident neutrons would also average out the influence of small fluctuations in the incident neutron intensity.

A preliminary measurement of the total cross section of beryllium below the Bragg cut-off energy range was made for two 1/2 inch thick beryllium samples. One was a new sample of Brush Wellman, N - 50 - C,

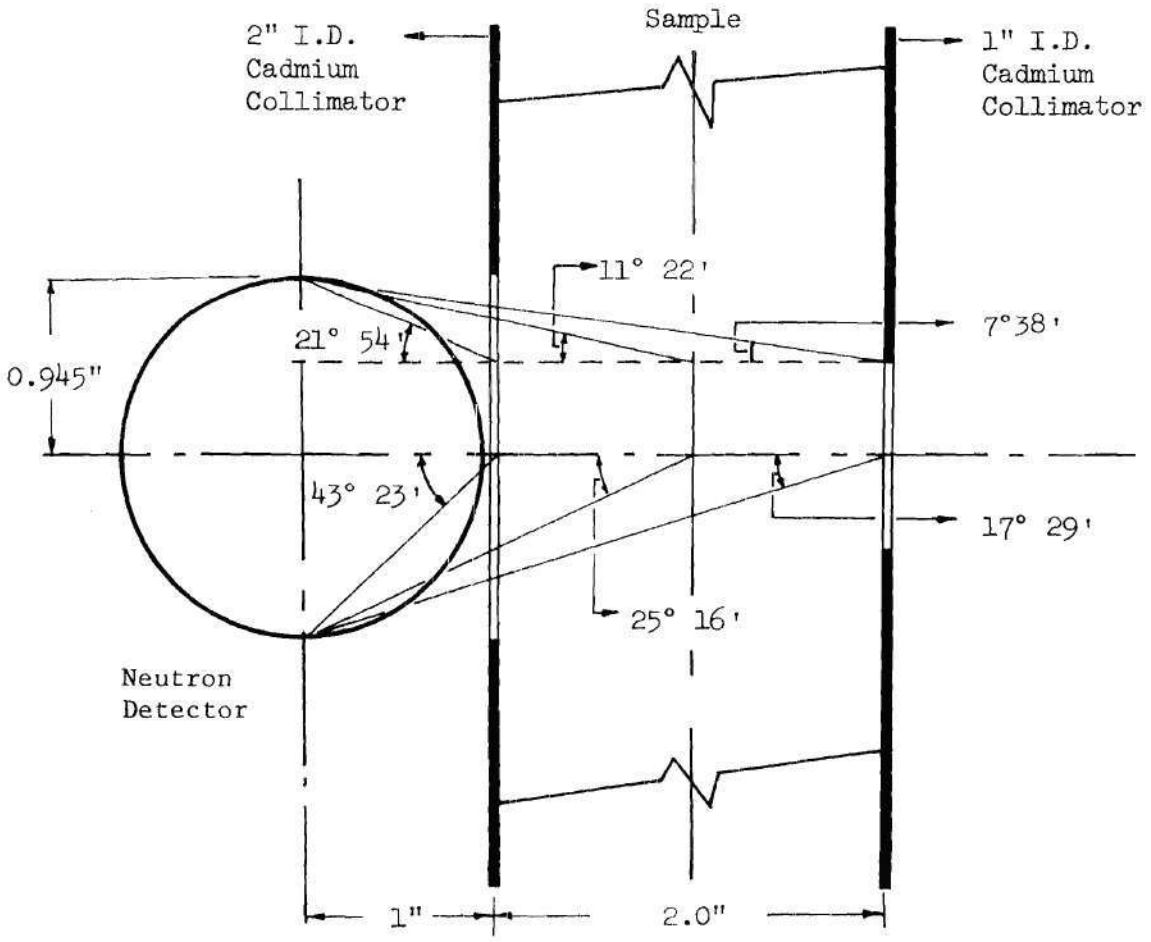

Figure 6. Sample-Detector Geometry Used in Cross Section Measurement (to take into account the small-angle scattering contribution)

high-purity grade beryllium, for which a detailed chemical analysis was available and the other sample was selected from an older lot of Brush reactor grade beryllium blocks borrowed from Argonne National Laboratory, where the blocks were last used as a part of a mock up of the beryllium reflector for the Argonne Advanced Research Reactor (A^2R^2). It was found that the two measurements yielded the same value for total cross section below the Bragg cut-off energy. The two beryllium samples were then put together to form a one inch thick sample and this was used in the subsequent experiments, primarily, because of the reduced experimental time and improved statistical accuracy. The chemical composition of the "new" sample of beryllium is given in Table 1. The density of the beryllium samples has been determined to be 1.85 gm/cm^3, indicating that the samples were practically pore-free. Measurement of the total cross section of beryllium below the Bragg cut-off energy was made with the sample at 64.75, 52.75, 46.75, and 2.0 inches from the BF_3 detector. The first three measurements were made to ensure that the experimental geometry was good, that is, the detector did not see the neutrons that are scattered in the sample. The last experiment was made to find out the influence of small-angle scattering, if any, on the measured total cross section and also as a check on the accuracy of the theoretical calculation of the "multiple-scattering" contribution.

In the total cross section measurement of graphite below the Bragg cut-off energy, two 2 inch thick Union Carbide, AGOT, reactor grade graphite samples were used. One of the graphite samples had the extrusion direction perpendicular and the other parallel to the thickness of the sample.

Table 1. Chemical Composition of the Brush Wellman, N - 50 - C, Reactor Grade Beryllium[44]
(Average grain size - 11.3 microns)

Element	% Weight
Beryllium	99.17
Beryllium oxide	0.9
Silicon	0.018
Nitrogen	0.016
Nickel	0.011
Calcium	< 0.01
Zinc	< 0.01
Magnesium	0.007
Chromium	0.006
Titanium	0.006
Aluminum	0.004
Manganese	0.004
Copper	0.003
Molybdenum	< 0.001
Lead	< 0.0006
Cobalt	0.0004
Silver	0.0003
Lithium	< 0.0003
Cadmium	< 0.0001
Boron	0.00008

The density of the graphite samples was measured to be 1.695 gm/cm^3. A partial chemical composition of the graphite sample is given in Table 2.

Table 2. Chemical Composition of the Union Carbide, AGOT, Reactor Grade Graphite[45] (Maximum grain size - 30 μ)

Boron content (ppm)	0.4
Ash content (%)	0.07

(Half of the ash content is (supposedly) iron and the rest is made up of trace amounts of calcium, silicon, vanadium, titanium, etc.)[45]

Two measurements of the total cross section for graphite, below the Bragg cut-off energy, were made with the center of the sample 2 and 2.5 inches away from the center of the detector. When the sample was moved 1/2 inch away from the previous position, the solid angle subtended by the detector at the sample was reduced by 56%, which was a substantial change at this close range. A comparison of the results of these two measurements gives an indication of whether the solid angle subtended by the detector at the sample was large enough that all the small-angle scattered neutrons reached the detector. If the results of these two measurements, corrected for the "multiple-scattered" neutrons, are the same within the experimental accuracy, then for this sample-detector geometry, the detector was seeing all the small-angle scattered neutrons. To find the influence of the extrusion direction on the total cross section below the Bragg cut-off energy, another cross section measurement of graphite was made in which the extrusion

direction of the graphite sample was at right angles to the incident neutron beam.

The basic principle behind the total cross section measurement of beryllium oxide, below the Bragg cut-off energy, is very similar to that of graphite and has been discussed in detail in the above paragraphs. The BeO sample was 1.837 inch thick; its density was measured to be 2.886 gm/cm^3. The theoretical density of beryllium oxide is 2.96 gm/cm^3, indicating that the sample was slightly porous. The chemical composition of the beryllium oxide sample obtained from the Ventron Corporation is given in Table 3. The beryllium oxide sample was prepared at the Oak Ridge Y-12 Plant by hot pressed powder fabrication techniques, wherein a fine mesh beryllium oxide powder is pressure-compacted at elevated temperatures in a graphite die. This method yields a fine grained structure which is randomly oriented to give an essentially isotropic polycrystalline material.

Procedure of Data Analysis

Detector Analyzer Dead-time

An experiment was performed by Lake[22] to determine the magnitude of the combined BF_3 detector plus multi-channel analyzer dead time losses as a function of measured count rate. The detector count rate as a function of reactor power level was measured with the time-of-flight analyzer by repeatedly triggering the analyzer with an electronic pulser. Since the neutron intensity incident on the detector was directly proportional to the reactor power level, the measured count rate should change in a linear relationship with the reactor power level if the dead time is negligible. Thus, any deviation from such a simple linear relationship is

Table 3. Chemical Composition of the Nuclear Grade Beryllium Oxide (Ventron Corporation Stock No. 16100)[45] (Average grain size - 1-2 μ)

Element	Parts per Million
Beryllium oxide	99%
Sulphur	770
Phosphorus	< 50
Sodium	20
Calcium	20
Silicon	20
Iron	17
Aluminum	10
Copper	10
Fluorine	10
Zinc	< 10
Nickel	< 10
Chromium	< 10
Manganese	< 10
Magnesium	< 10
Titanium	< 10
Barium	< 10
Molybdenum	< 10
Strontium	< 10
Cobalt	< 1
Tin	< 1
Lead	< 1
Silver	< 1
Boron	< 0.5
Cadmium	< 0.5
Lithium	< 0.4

indicative of the magnitude of the dead time as a function of measured count rate. An empirical relationship for the percent live time was given by Lake as

$$\% \text{ Live Time} = (Ax + B) \tag{8}$$

where x is the measured count rate and A = -1.665 ± 0.03 %/unit count rate. The intercept, B = 99.6 ± 0.7 %, at zero count rate was obtained by least squares fit to the experimental data.[22] Equation 8 has been used to correct for the detector dead time losses.

Obviously, the logic of the situation requires that the live-time be 100% for zero count rate, i.e., B should be equal to 100%. This, however, has insignificant influence on the measured cross section because of the reasons given below. In all the total cross section measurements below the Bragg cut-off energy, the dead time corrections were always less than 2% in the case of beryllium oxide and graphite measurements and less than 4% in the case of the beryllium measurements. Also the dead time corrections for the with- and without-the sample data were different by a factor less than 0.8%. However, to test the accuracy of the live time correction, two measurements of beryllium total cross section were made by us in the energy region around 0.06 eV. The total cross section for beryllium reaches a fairly constant value of 6.0 barns near this energy region. In the first experiment the detector live time corrections were of the order of 82 to 99%, compared to 57 to 97% live time correction of the second experiment. The two measurements yielded the same value of total cross section of beryllium within the experimental accuracy of ± 2%.

From this relatively severe test it can be concluded that dead time correction did not have any significant errors.

The experiment to determine the detector dead time, described in the earlier paragraph, was repeated by us for the low efficiency monitor detector. Figure 7 shows the measured count rate versus the reactor power level. The linear relationship of the curve indicates that the dead time of the monitor detector was negligible over the count rate of interest.

Neutron Background

The measured time spectrum in a cross section measurement invariably includes a background of neutrons that were not chopped by the chopper and also those that were scattered into the detector from the surroundings. In the calculation of cross section one must correct the measured data for the neutron background and, therefore, one should have an accurate knowledge of the magnitude and the nature of this neutron background. The measured time spectrum had a region in which the spectrum was made up of only the background neutrons and this region of the spectrum was indicative of the actual background present during the cross section measurement. At a normal chopper speed of 1800 RPM and a channel width of 64 μ sec, this region of background started after the 200th channel, corresponding to a chopper cut-off velocity of 213 meters per second. An average background for each experiment was calculated by averaging the neutron counts from channel 200 to 230 in the tail end of the measured spectrum. This method of determining an average background was preferred against making individual, separate background measurements, which had to be done at a time other than the main cross section measurements. Such separate background measurements might very well have a background level other than the main

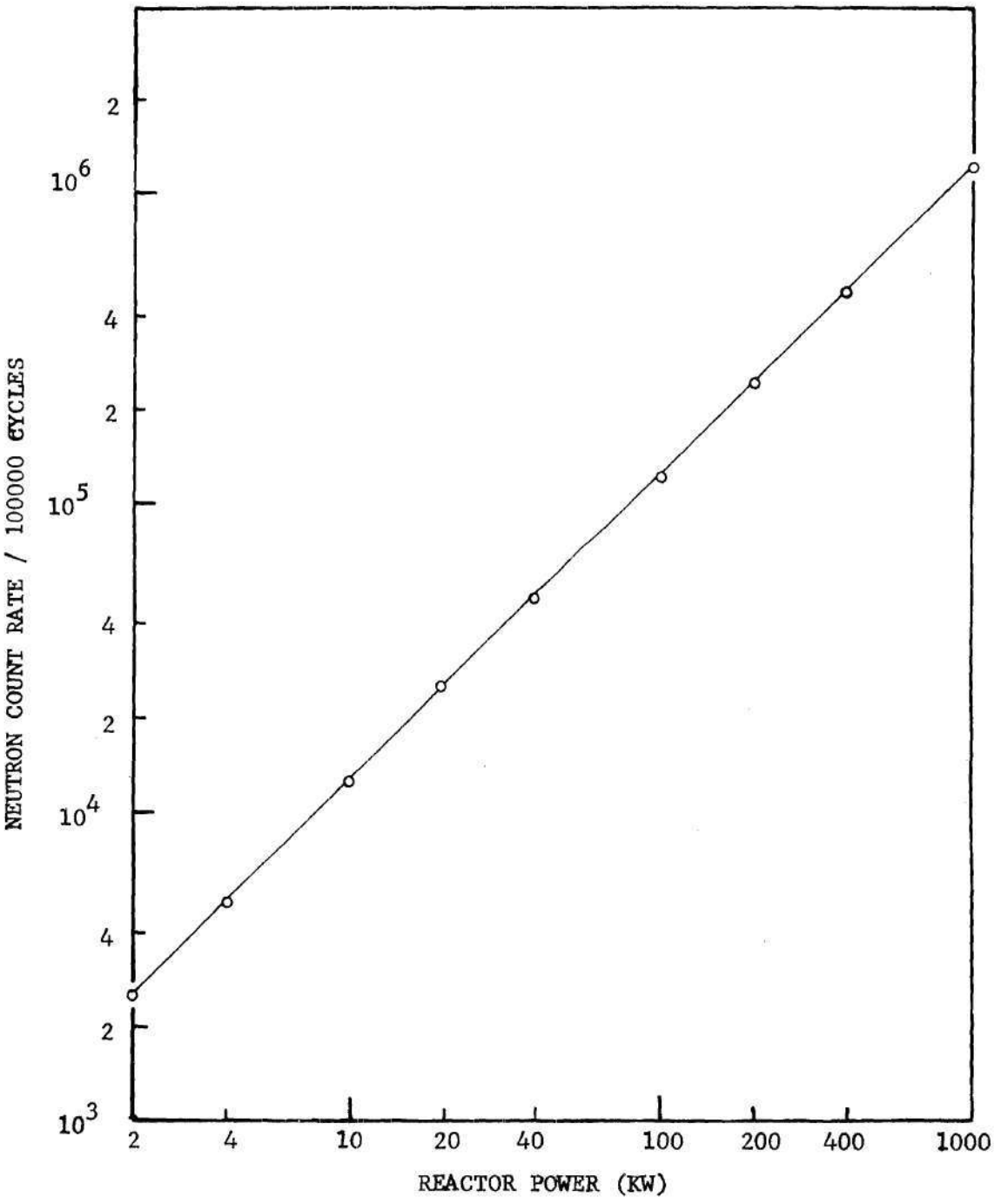

Figure 7. Monitor Neutron Count Rate as a Function of Reactor Power Level

experiment. The validity of using such an average background requires that the background be independent of energy and thus have essentially the same average value everywhere. In order to check this point, a neutron background measurement was made in which the primary neutron beam was blocked by a cadmium shield placed midway between the chopper and the detector. This arrangement permits the detector to see some of the epithermal neutrons that were not chopped by the neutron chopper and also the neutrons that were scattered from the surroundings into the detector. The result of this experiment showed that the measured background had no energy dependence except in the very first few channels corresponding to the epithermal neutron energy region, which was far removed from the energy region of interest. The peak-to-background ratio, in any experiment, was always greater than 6:1.

Conversion of Time Scale to Energy Scale

The time spectrum measured in a cross section experiment is the time distribution of neutrons arriving at the detector with respect to the middle of the chopper burst. In order to find the average energy of the neutrons in a given analyzer channel, one needs to know the time of arrival of neutrons with respect to the zero reference time, which is the middle of the chopper burst; that is, the time when the chopper slits are exactly parallel to the neutron beam. The time duration from the zero reference time to the middle of the first analysis channel, F_T, consists of the following[23]:

1. The time duration between the center of the chopper burst and of the photo-transistor pulse caused by the reflected light beam from one of the mirrors on the rotor shaft.

The zero timing unit on the chopper was set at an angle 9.4° from the vertical axis of the chopper. Thus, the beam reflected from the mirror would initiate the photo-transistor pulse 9.4° earlier than the moment when the chopper blades were parallel to the neutron beam (this corresponds to the middle of the chopper burst). This time duration is given by

$$T_1 = \frac{9.4^\circ}{6(\text{RPM})} \text{ (seconds)} \tag{9}$$

where RPM is the chopper rotation speed in units of rotations per minute.

2. The time duration between the peak of the photo-transistor pulse to the output trigger pulse to the analyzer gate. This time has been measured, with a calibrated-time-base oscilloscope,[23] to be 82 μ sec.

3. The time delay between the arrival of the trigger pulse and the time at which the time-of-flight analyzer sweep sequence was initiated. This has been measured to be equal to 15 μ sec.

4. The time from the initiation of the sweep to the middle of the first channel is just half the channel width, DE.

Putting all these factors together, the time F_T is given as

$$F_T = \frac{-9.4^\circ}{6(\text{RPM})} + \{82 - 15 + (DE/2)\} \times 10^{-6} \text{ (seconds)} \tag{10}$$

Now the average values of time, velocity and energy of neutrons in the Nth channel, are given in the following equations.

$$t = F_T + (N-1)DE \times 10^{-6} \text{ (seconds)} \tag{11}$$

$$v = \frac{\text{Flight Path}}{t} \quad \text{(meters/sec)} \tag{12}$$

$$E = 5.2161 \times 10^{-9} \times V^2 \quad \text{(eV)} \tag{13}$$

In order to check the accuracy of the parameter, F_T, given by Equation 10, the following experiment was conducted. Two pyrolytic graphite crystals, having a "d" spacing of 3.355 Å, were positioned properly in a double diffraction spectrometer. The two crystals were oriented at a diffraction angle of approximately 40° and the detector was roughly positioned to receive the diffracted neutron beam from the second crystal. In this position, first the 2θ-scan was made, that is, the detector was moved in increments of half a degree and the neutron counts were recorded at each position of the detector. The detector was then positioned at an angle corresponding to the peak of the observed neutron intensity. Now, with the detector fixed in this position, an ω-scan was made, that is, the second crystal was rotated in increments of 1/4° and the neutron intensity was recorded as a function of the orientation of the second crystal. With the help of this observed neutron intensity distribution, the second crystal was set at an angle corresponding to the peak in the neutron intensity. The 2θ-scan and the ω-scan were repeated alternately until the second crystal was set at the exact diffraction angle.

Now the secondary crystal was moved through an angle 2θ from the previous position and correspondingly the detector was moved through an angle of 4θ. In this position, the 2θ-scan and the ω-scan were conducted alternately to fix the exact diffraction angle. This gives accurately

the angle $2\theta_o$ through which the secondary crystal was rotated from one diffraction position to the other position. This value of $2\theta_o$ was measured to be equal to 82.9°, that is, the diffraction angle is 41.45°. Knowing the "d" spacing and the diffraction angle θ_o, one can easily calculate the neutron wavelength, λ, from the Bragg relation.

$$n\lambda = 2d \sin\theta_o \tag{14}$$

where n = 1,2,3 . . ., is the order of Bragg reflections. Using Equation 14, the wavelength of neutrons in the diffracted beam, for three orders of reflection, was calculated to be $\lambda_1 = 4.442$, $\lambda_2 = 2.221$, and $\lambda_3 = 1.48$ Å.

The energy distribution of neutrons in the diffracted neutron beam from the second crystal was measured with the time-of-flight apparatus. Here a channel length of 16 μ sec, a chopper speed of 1800 RPM, and a flight path of 3.24 meters were used. The measured time spectrum of the incident neutron beam indicated that there were three peaks in the measured spectrum. The three peaks in the measured spectrum occurred in the 278, 128, and 165 channels of the time-of-flight analyzer. Using Equations 10, 11, 12, and 13, it was calculated that the three channels, #278, 128, and 165, corresponded to neutron wavelengths of 4.442, 2.16, and 1.48 Å, respectively. This experiment showed that the parameter, F_T, given in Equation 10 was quite accurate. The accuracy of this equation had also been checked earlier by Lake.[23]

Iterative Scheme for Cross Section Evaluation

In the total cross section measurement of materials like beryllium oxide and graphite, one has to take into account the effects of large small-angle scattering of neutrons in these materials. In the sample-detector geometry described, all the small-angle scattered neutrons, as well as some fraction of the elastically and inelastically scattered neutrons, would enter the detector. Thus, in such experiments, the measured data with the sample in the neutron beam had to be corrected for the theoretically calculated "multiple-scattered" neutron contributions. Such a correction required that the total cross section, which was to be measured, be known for making the theoretical calculation of the "multiple-scattering" contribution. To circumvent this situation, a simple iterative scheme for cross section evaluation was developed.

Let $P_o(E)$ and $P_1(E)$ be the observed neutron counts in a given analysis channel, for "without and with the sample" in the neutron beam experiment, respectively. The total cross section, σ_u, uncorrected for the "multiple-scattering" contribution is given by

$$\sigma_u(E) = \frac{1}{Nd} \ell n\{P_o(E)/P_1(E)\} \tag{15}$$

where N is the atom density and d is the sample thickness. Use this total cross section, σ_u, as an initial guess in calculating the "multiple-scattering" contribution. Let $I_m(E')$ be the calculated "multiple-scattered" neutron contribution as seen by the detector per incident neutron on the sample. Here E' is used as a subscript of I_m, since the "multiple-scattered" neutrons may have changed their energy during the

scattering collisions. The distance between the sample and the detector is very small so that the neutrons, even though their energy is changed in the scattering collisions, almost always end up in the same channel as those neutrons which did not interact in the sample. The number of neutrons that is "multiple-scattered" and is deflected into the detector is given by

$$I_d(E) = I_m(E') \; P_o(E)/\epsilon(E) \tag{16}$$

where $\epsilon(E)$ is the efficiency of the detector for the neutrons of energy E, and $P_o(E)/\epsilon(E)$ are the number of neutrons incident on the sample. Here the negligibly small effect of the loss of neutrons scattered and absorbed in the air present in the short distance between the sample and the detector is not considered. $P_1(E)$ consists of the uncollided neutrons, all the small-angle scattered neutrons, and a neutron fraction that is "multiple-scattered" into the detector. Now,

$$P_c(E) = P_1(E) - I_d(E) \tag{17}$$

where $P_c(E)$ is the neutron counts consisting of only the uncollided neutrons and all the small-angle scattered neutrons. Therefore, the corrected total cross section is given by

$$\sigma_c(E) = \frac{1}{Nd} \ell n\{P_o(E)/P_c(E)\} \tag{18}$$

To make the convergence faster, assume a cross section which is an average of $\sigma_c(E)$ and $\sigma_u(E)$ and use this to calculate a new value of $I_m(E)$. This new value of $I_m(E)$ is used to calculate the new corrected cross section $\sigma_c(E)$ by using Equation 18. This procedure is repeated until the assumed cross section $\sigma_u(E)$ and the calculated cross section $\sigma_c(E)$ converge to the same value. It has been found that the calculated cross section converges in less than ten iterations. This procedure has been used in cross section evaluations for graphite and beryllium oxide. A detailed description of the Monte Carlo program to theoretically calculate the "multiple-scattering" contribution is given in Appendix A.

CHAPTER III

MEASUREMENT OF THE TOTAL CROSS SECTION IN BERYLLIUM

As mentioned earlier in the introduction, Lake and Kallfelz[21,22,23] have made a series of measurements of the space, angle-dependent, neutron energy spectra in various parallelepiped configurations of polycrystalline beryllium.

A theoretical analysis of this particular problem was made by us using the Monte Carlo method, a detailed description of which is given in the next chapter. In this analysis, the total cross section of beryllium moderator, above the Bragg cut-off energy region, was taken from the BNL-325 cross section data.[10] The result of this theoretical analysis of the angle-dependent energy spectrum did not agree with the measured spectrum of Lake and Kallfelz.

It was suggested by Ritchie[47] that this discrepancy between our theoretical work and the experimental spectrum might be due to the effects of extinction on the coherent elastic cross section of the beryllium blocks used in the experiments of Lake and Kallfelz. Ritchie et al.[48] have made a diffusion theory calculation of the behavior of the time eigenvalues in finite blocks of polycrystalline beryllium oxide moderator. They have found that their calculated time eigenvalues, as a function of the buckling of the system, agreed better with the measured time eigenvalues of Ritchie and Rainbow,[16,17] when the beryllium oxide cross section used in their analysis was modified to take into account the extinction effects.

Also, Zhezherun et al.[37,38] have observed experimentally the effect of extinction on the measured total cross section of beryllium oxide by varying the grain size in the beryllium oxide sample. Fermi et al.[42] have suggested that, for perfect crystallites of linear dimensions smaller than a micron, the reduction in the measured total cross section, due to extinction effects, would not be significant.

The conventional theoretical analysis[25] to calculate the coherent elastic cross section of polycrystalline materials assumes that the diffracting region is so small that this region can be considered to be uniformly bathed by the incident radiation. In practice, the diffracting domains are sufficiently large that they can no longer be considered to be uniformly bathed by the incident radiation. The incident radiation becomes progressively weaker as it penetrates deeper into the diffracting domain due to extinction effects, and results in a diffracted intensity which is smaller than the results of the conventional theoretical analysis. The effect of extinction is to reduce the Bragg peaks in the coherent elastic cross section. This reduction is most pronounced for the intense reflections and at the Bragg cut-off energy. The quantitative theory to calculate the diffracted intensity is distinctly different from the conventional theory and the intensity and cross sections are correspondingly different.

The extinction effect is subdivided into primary and secondary extinction. These effects may be qualitatively understood as follows. In the process of a Bragg reflection, each successive lattice plane in a perfect region of a crystal reflects a fraction of the incident radiation,

with the result that it becomes progressively weaker as it penetrates to lower planes.[25,42] Also, the reflected radiation is reflected back into the crystal in a direction parallel to the incident radiation. Because a $\pi/2$ phase change occurs on reflection, the twice reflected radiation has a phase difference of π with respect to the incident radiation and interferes to cause an additional decrease of the penetrating radiation. The combined effect is known as primary extinction. The intensity of a reflected radiation suffers through primary extinction, not only because the incident radiation is weakened, but also because multiply reflected rays, traveling in the reflection direction, may interfere.

In practice, the crystals do not have a perfectly regular sequence of atomic planes throughout the whole volume of the crystal. They are permeated by imperfections which have the effect of dividing the crystal into much smaller sub-regions of the order of 0.1 μ in size. These mosaic sub-regions are more or less perfect, but are misoriented from parallel alignment by less than one degree. At any Bragg diffraction setting a large number of these mosaic blocks are precisely oriented to reflect the incident beam. Each block reflects away a fraction of the incident radiation as it passes to greater depths; hence, the intensity of the reflected radiation is less than if all the blocks received the full benefit of the incident radiation. This effect is known as secondary extinction.

As mentioned earlier, it was suspected that the total cross section of beryllium moderator, used in the experiments of Lake and Kallfelz, might be different than the BNL-325 values due to extinction effects.

The spectrum measurements of Lake and Kallfelz can be a complete set as a benchmark test-case only with the knowledge of the total cross section of the beryllium moderator used in their experiment. Also, we were not able to explain the discrepancy between our calculated spectra and the measured spectra of Lake and Kallfelz by any other factors influencing the theoretical calculation.

For these reasons, a series of measurements of the total cross section, in the energy range above the Bragg cut-off energy, were made for a beryllium sample taken from the lot of Brush reactor grade beryllium blocks which were used by Kallfelz and Lake[21,22,23] in their steady-state experiments. The time-of-flight technique was used for these cross section measurements in which a chopper speed of 1800 RPM, a channel width of 16 μ sec, and a flight path of 2.6 meters were used. The details of this time-of-flight technique and the instruments required have already been described. In the following description of the series of cross section measurements, the beryllium sample selected from the lot of beryllium blocks used by Kallfelz and Lake in their experiments will be referred to as the Lake-beryllium sample.

In the first set of experiments to measure the total cross section, above the Bragg cut-off energy range, two Lake-beryllium samples were used (1/8 inch and 1/4 inch thick, respectively). This experiment was intended to show the effect of multiple-scattered neutrons at the detector, if any, on the measured total cross section. If the measured total cross sections of these two samples were the same, then it meant that only a negligible number of neutrons scattered in the beryllium samples had been able to reach the detector.

The second set of experiments to measure the total cross section was made for a 1/4 inch thick Lake-beryllium sample with two chopper speeds of 1800 and 3954 RPM. The contention here was that, if the two values of the measured cross sections averaged over a certain energy range were found to be the same within the experimental accuracy, then the measured cross section was not affected by the energy resolution of the experiment. That is, any difference found between this measured total cross section and the BNL-325 beryllium cross section[10] would be attributable to the extinction effects in the Lake-beryllium sample due to the presence of large crystallites.

A 1/2 inch thick Brush-Wellman, N - 50 - C, high-purity grade polycrystalline sample having an average grain size of 11.3 microns was available. The chemical composition of this sample has been given in Table 1. An experiment to measure the total cross section of this beryllium sample was made covering the energy range above the Bragg cut-off. A comparison of the total cross section of this sample and the Lake-beryllium sample should give an idea of the effect of impurities and the average grain size of the Lake-beryllium sample.

The results of the measurements described in the above paragraphs will be presented in Chapter V.

CHAPTER IV

THEORETICAL SPECTRUM ANALYSIS

This chapter describes in detail the theoretical methods and the procedure used in calculating the spatial behavior of the neutron energy spectra in small beryllium systems. In brief, the adjoint Monte Carlo method has been used to calculate the energy spectrum in the positive z direction along the longitudinal axis of a beryllium assembly using several scattering kernels. Comparing this calculation with the experimental results of Lake and Kallfelz[23] would shed light on the nature of the neutron thermalization in such small beryllium systems and on the adequacy of the theoretical scattering kernels to describe the thermal neutron scattering phenomenon in beryllium.

The S_N method[49] has been used to calculate the spatial behavior of the total flux as a function of the transverse dimensions of the beryllium assembly. This study would enable one to resolve the debate over the applicability of diffusion theory for the steady-state diffusion length problem in small beryllium systems with severe transverse leakage.

A rigorous analytical or numerical solution of the space, angle, and energy-dependent neutron transport equation describing the transport of neutrons in a finite medium is a very difficult task, unless one makes simplifying assumptions such as the diffusion approximation, space-energy separability, buckling approximation, etc. We have used two types of

theoretical methods to study the spatial decay of the thermal neutron distribution in small beryllium systems with a planar steady-state thermal neutron source.

One of the theoretical methods used was the Monte Carlo technique, which provides a very satisfactory means of solution, wherein the geometry of the experiment and the transition probability of neutrons going from one phase space to the other can be treated exactly. This method is also free of some of the usual simplifying assumptions used in other methods. However, the Monte Carlo method will always have a statistical error associated with it due to the practical limitations on the number of neutron histories followed. It was found that, for this problem with an extended area source and a point detector, the adjoint Monte Carlo method is very advantageous in comparison to the forward Monte Carlo procedure. In the adjoint Monte Carlo procedure the "adjunctons" (pseudo-particles) are started at the "small" point detector and are scored (counted) at the "large" area source. This reduces significantly the variance on the statistical estimation of the flux in comparison to the forward Monte Carlo scheme, where the neutrons would be scored at the "small" point detector. It was sufficient for this problem to calculate the flux at several energy points to characterize the shape of the energy spectrum and this reduces the required computational time. A computer program was written using the adjoint Monte Carlo method. The basic theory and the adjuncton random walk procedure behind the computer program are described in the latter part of this chapter.

The other method of solution used was the method of discrete ordinates (S_N method), where the transport equation is reduced to a system of

linear differential equations by replacing the integration over the angles by a summation over a discrete number of directions. This method is advantageous in being able to obtain solutions at large distances from the source plane. A one-dimensional transport computer code, ANISN,[49] was used, where the effect of transverse leakage was introduced by the energy-dependent transverse buckling concept. A description of the theory of the S_N method and the simplifying assumptions used is given in a later section.

The S_N method is often preferred for deep penetration problems with a simple geometry, whereas the Monte Carlo method is preferred for complicated geometries. However, the Monte Carlo method can easily treat a three-dimensional problem in comparison to the S_N method. The available S_N computer codes are limited to one- and two-dimensional problems. The 2-D, S_N method can suffer from the ray effects when there is a strong anisotropic scattering, a highly absorbing medium with a strong anisotropic source, and when the angular domain is represented by an insufficient number of discrete directions. The use of a set of discrete directions to represent the angular domain could cause distortions in the calculated spectrum due to the preferential movement of the neutrons along the discrete directions. This is known as the ray effects.

Forward and Adjoint Monte Carlo Methods

The basic equations used in the Monte Carlo method will be developed in this section. Many of the equations presented here for the sake of completeness have been taken from Reference 50. The derivations of some of the equations are given in detail in References 50 and 51 and they will not be reproduced here. We are interested only in a homogeneous medium

made up of a single nuclide and, therefore, the neutron cross sections are independent of spatial variable.

The steady-state, group form of the neutron transport equation for the angle, space, energy-dependent neutron flux, $\varphi(\bar{r},E,\bar{\Omega})$, is given by

$$\bar{\Omega} \cdot \nabla\varphi_g(\bar{r},\bar{\Omega}) + \Sigma_t^g \varphi_g(\bar{r},\bar{\Omega}) \tag{19}$$

$$= S_g(\bar{r},\bar{\Omega}) + \sum_{g'} \int_{4\pi} d\bar{\Omega}' \Sigma_S^{g'\to g}(\bar{\Omega}'\to \bar{\Omega}) \varphi_{g'}(\bar{r},\bar{\Omega}')$$

where the group flux is

$$\varphi_g(\bar{r},\bar{\Omega}) = \int_{\Delta E_g} \varphi(\bar{r},E,\bar{\Omega})dE \tag{20}$$

and ΔE_g is the energy interval of group g.

The group source is

$$S_g(\bar{r},\bar{\Omega}) = \int_{\Delta E_g} S(\bar{r},E,\bar{\Omega})dE \tag{21}$$

The group total macroscopic cross section is

$$\Sigma_t^g = \frac{1}{\varphi_g(\bar{r},\bar{\Omega})} \int_{\Delta E_g} \Sigma_t(E) \varphi(\bar{r},E,\bar{\Omega})dE \tag{22}$$

The group-to-group cross section is

$$\Sigma_S^{g'\to g}(\bar{\Omega}'\to\bar{\Omega}) = \frac{1}{\varphi_{g'}(\bar{r},\bar{\Omega}')}\int_{\Delta E_{g'}}\int_{\Delta E_g}\Sigma_S(E'\to E,\bar{\Omega}'\to\bar{\Omega}) \tag{23}$$

$$\times\,\varphi(\bar{r},E',\bar{\Omega}')\,dE\,dE'$$

The integral form of Equation 19 is given by

$$\varphi_g(\bar{r},\bar{\Omega}) = \int_o^\infty dR\; e^{-\Sigma_t^g R}\left\{S_g(\bar{r}-R\bar{\Omega},\bar{\Omega})\right. \tag{24}$$

$$\left. + \sum_{g'}\int d\bar{\Omega}'\;\Sigma_S^{g'\to g}(\bar{\Omega}'\to\bar{\Omega})\;\varphi_{g'}(\bar{r}-R\bar{\Omega},\bar{\Omega}')\right\}$$

The neutron collision density $\psi_g(\bar{r},\bar{\Omega})$ is defined as

$$\psi_g(\bar{r},\bar{\Omega}) = \Sigma_t^g\,\varphi_g(\bar{r},\bar{\Omega}) \tag{25}$$

Multiplying Equation 24 by Σ_t^g and using Equation 25, we have

$$\psi_g(\bar{r},\bar{\Omega}) = \int_o^\infty dR\;\Sigma_t^g\,e^{-\Sigma_t^g R}\left\{S_g(\bar{r}-R\bar{\Omega},\bar{\Omega}) + \sum_{g'}\int d\bar{\Omega}'\;\frac{\Sigma_S^{g'\to g}(\bar{\Omega}'\to\bar{\Omega})}{\Sigma_t^{g'}}\right. \tag{26}$$

$$\left.\times\,\psi_{g'}(\bar{r}-R\bar{\Omega},\bar{\Omega}')\right\}$$

Define the emergent neutron density as

$$X_g(\bar{r},\bar{\Omega}) = S_g(\bar{r},\bar{\Omega}) + \sum_{g'}\int d\bar{\Omega}'\;\frac{\Sigma_S^{g'\to g}(\bar{\Omega}'\to\bar{\Omega})}{\Sigma_t^{g'}}\,\psi_{g'}(\bar{r},\bar{\Omega}') \tag{27}$$

From Equations 26 and 27, it is easy to show that

$$X_g(\bar{r},\bar{\Omega}) = S_g(\bar{r},\bar{\Omega}) + \sum_{g'} \int d\bar{\Omega}' \frac{\Sigma_S^{g'\to g}(\bar{\Omega}'\to \bar{\Omega})}{\Sigma_t^{g'}} \int_0^\infty dR\, \Sigma_t^{g'}\, e^{-\Sigma_t^{g'} R}\, X_{g'}(\bar{r}-R\bar{\Omega}',\bar{\Omega}') \tag{28}$$

For use in the adjoint Monte Carlo method, the group adjoint equation which is adjoint to the group form of the transport equation (19) is given by

$$-\nabla\cdot\bar{\Omega}\, \varphi_g^*(\bar{r},\bar{\Omega}) + \Sigma_t^g\, \varphi_g^*(\bar{r},\bar{\Omega}) = P_g(\bar{r},\bar{\Omega}) + \sum_{g'} \int d\bar{\Omega}'\, \Sigma_S^{g\to g'}(\bar{\Omega}\to \bar{\Omega}')\, \varphi_{g'}^*(\bar{r},\bar{\Omega}') \tag{29}$$

where Σ_t^g is the forward weighted group total cross section given in Equation 22 and $\Sigma_S^{g\to g'}(\bar{\Omega}\to \bar{\Omega}')$ is simply the transposition of the forward weighted group to group differential scattering matrix and

$$P_g(\bar{r},\bar{\Omega}) = \frac{1}{\varphi_g(\bar{r},\bar{\Omega})} \int_{\Delta E_g} P(\bar{r},E,\bar{\Omega})\, \varphi(\bar{r},E,\bar{\Omega})\, dE \tag{30}$$

where $P(\bar{r},E,\bar{\Omega})$ is the detector response function.

The integral form of Equation 29 is given by

$$\varphi_g^*(\bar{r},\bar{\Omega}) = \int_0^\infty dR\, e^{-\Sigma_t^g R} \Big\{ P_g(\bar{r}+R\bar{\Omega},\bar{\Omega}) + \sum_{g'} \int d\bar{\Omega}'\, \Sigma_S^{g\to g'}(\bar{\Omega}\to \bar{\Omega}') \times \varphi_{g'}^*(\bar{r}+R\bar{\Omega},\bar{\Omega}') \Big\} \tag{31}$$

Equation 31 which defines the adjoint flux is rather inconvenient to use as a basis for the adjuncton walk procedure, since the transport of adjunctons from $\bar{r}+R\bar{\Omega}$ to $\bar{r}$ is in the direction opposite to the direction vector, $\bar{\Omega}$. This can be overcome by defining a new function

$$H_g(\bar{r},\bar{\Omega}) = \Sigma_t^g \varphi_g^*(\bar{r},-\bar{\Omega}) \tag{32}$$

and

$$H_g(\bar{r},\bar{\Omega}) = \int_o^\infty dR\, \Sigma_t^g\, e^{-\Sigma_t^g R}\, G_g(\bar{r}-R\bar{\Omega},\bar{\Omega}) \tag{33}$$

where $H_g(\bar{r},\bar{\Omega})$ is referred to as "adjuncton event density" and $G_g(\bar{r},\bar{\Omega})$ is the "emergent adjuncton density."

Using Equation (32) in Equation (31) we get, after some readjustment,

$$H_g(\bar{r},\bar{\Omega}) = \int_o^\infty dR\, \Sigma_t^g\, e^{-\Sigma_t^g R}\left\{P_g(\bar{r}-R\bar{\Omega},-\bar{\Omega}) + \sum_{g'}\int d\bar{\Omega}'\, \frac{\Sigma_S^{g\to g'}(-\bar{\Omega}\to\bar{\Omega}')}{\Sigma_t^{g'}}\right. \tag{34}$$

$$\left.\times\, H_{g'}(\bar{r}-R\bar{\Omega},-\bar{\Omega}')\right\}$$

Letting $\bar{\Omega}'' = -\bar{\Omega}'$ and noting that $\Sigma_S(-\bar{\Omega}\to-\bar{\Omega}'') = \Sigma_S(\bar{\Omega}\to\bar{\Omega}'')$, we have

$$H_g(\bar{r},\bar{\Omega}) = \int_o^\infty dR\, \Sigma_t^g\, e^{-\Sigma_t^g R}\left\{P_g(\bar{r}-R\bar{\Omega},-\bar{\Omega}) + \sum_{g'}\int d\bar{\Omega}''\, \frac{\Sigma_S^{g\to g'}(\bar{\Omega}\to\bar{\Omega}'')}{\Sigma_t^{g'}}\right. \tag{35}$$

$$\left.\times\, H_{g'}(\bar{r}-R\bar{\Omega},\bar{\Omega}'')\right\}$$

Using Equations 33 and 35, it is easy to show that

$$G_g(\bar{r},\bar{\Omega}) = P_g(\bar{r},-\bar{\Omega}) + \sum_{g'} \int d\bar{\Omega}'' \frac{\Sigma_s^{g\to g'}(\bar{\Omega}\to\bar{\Omega}'')}{\Sigma_t^{g'}} \int_o^\infty dR\, \Sigma_t^{g'}\, e^{-\Sigma_t^{g'}R} \times G_{g'}(\bar{r}-R\bar{\Omega}'',\bar{\Omega}'') \tag{36}$$

The quantity of interest is given by

$$\lambda \equiv \sum_g \int\int \frac{S_g(\bar{r},-\bar{\Omega})}{\Sigma_t^g} \int_o^\infty dR\, \Sigma_t^g\, e^{-\Sigma_t^g R} G_g(\bar{r}-R\bar{\Omega},\bar{\Omega})\, d\bar{r}\, d\bar{\Omega} \tag{37}$$

Equation 36 is identical to Equation 28, which defines the forward emergent particle density, $x_g(\bar{r},\bar{\Omega})$, and serves as the formal basis for the forward random walk procedure. Equation 36, which defines the adjuncton emergent density function, is convenient to use as a basis for the adjuncton walk procedure. However, one must take into account the reversal of direction between the adjunctons and real particles. For example, if in the forward problem particles entering the detector in the forward direction are scored, the corresponding source adjunctons would be introduced in the backward direction. Likewise, adjunctons would be scored for entering a volume from which the source particles in the forward problem would be emitted.

Problem Description

The details of the steady state diffusion length problem, to be solved by the adjoint Monte Carlo method, are described in the following. The beryllium moderating medium was a 14 x 14 x 20 inch long rectangular block with a 14 x 14 inch planar thermal neutron source located at one end of the beryllium block. As mentioned earlier, Lake and Kallfelz[21,22,23]

have measured the energy distribution of neutrons in the positive z direction and at several distances from the neutron source. It was concluded by them that the size of the beryllium moderator is less than the "critical" size and there exists no fundamental mode decay, as supported by Figure 3.

A theoretical analysis of this problem was made using the adjoint Monte Carlo method; in particular, the solution we sought was the energy distribution 4 inches (10.2 cm) away from the neutron source on the longitudinal, z-axis of those neutrons whose motion was directed in the positive z direction. This analysis included the exact geometry of the experiment and the exact treatment of the coherent elastic scattering of thermal neutrons in the polycrystalline beryllium moderator. The analysis had the flexibility to accept different scattering kernels to describe the thermal inelastic neutron collisions.

The Thermal Neutron Source

The experimental geometry of Lake and Kallfelz[21,22,23] consisted of a 60 x 60 x 36 inch long graphite thermal column against which the 14 x 14 x 20 inch long beryllium assembly was positioned. The side of the beryllium assembly, facing the thermal column, had a 14 x 14 x 1/4 inch thick Plexiglass sheet to smooth out the small Bragg perturbations in the graphite thermal column spectrum. Therefore, for our geometry, in the Monte Carlo analysis, the moderator is a 14 x 14 x 20 inch long block with a planar source of thermal neutrons coming into the beryllium block. In this analysis, we are interested in calculating the spectrum in the positive direction along the longitudinal axis (z-axis) at 10.2 cm from the source plane.

Lake[23] has measured the energy spectrum of the source at the center of the source plane in the positive z direction, which is shown in Figure 8. This energy distribution has been used in our Monte Carlo analysis. The spatial distribution of the source neutrons integrated over all angles and energies has been measured by Unus.[52] This spatial distribution from the center of the source plane to the edge along one of the axes of the plane is shown in Figure 9. Because of symmetry, this distribution will be the same along the other axis also. We have used this spatial distribution in our Monte Carlo theoretical analysis.

The angular distribution of the planar source has been assumed to have a "cosine angle distribution," a distribution proportional to the cosine of the angle measured from the z-axis. This is based on the assumption that the thermal column flux is isotropic. Also, the source distribution is taken to be separable in energy, space, and angle.

To investigate the validity of the assumptions made about the energy and angle dependence of the planar source, a one-dimensional transport theory calculation of the space and angle-dependent energy spectrum was made using the true graphite, Plexiglass, beryllium geometry along the z-direction. This one-dimensional calculation should give good results for the energy and angle dependence of the source distribution near the middle of the block, which is of most interest due to a large (~ 70%) uncollided flux contribution for the below-Bragg energies. The effect of the finite transverse dimensions of the three regions was introduced by means of an energy-dependent buckling approximation. The calculated source flux at the center of the block is not very sensitive to this approximation as the

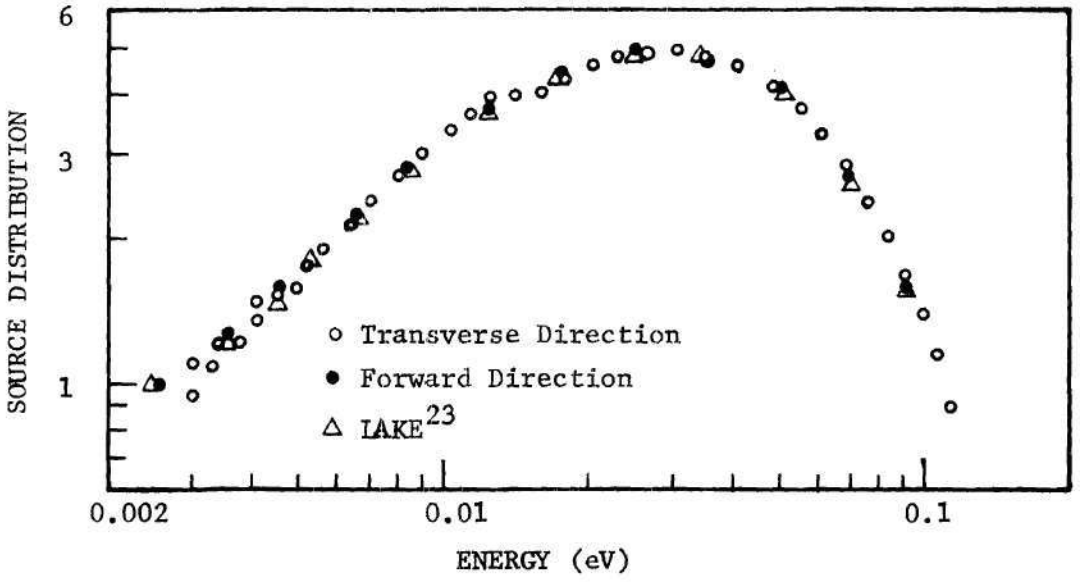

Figure 8. Theoretical and Experimental Source Energy Distribution at the Center of the Source Plane

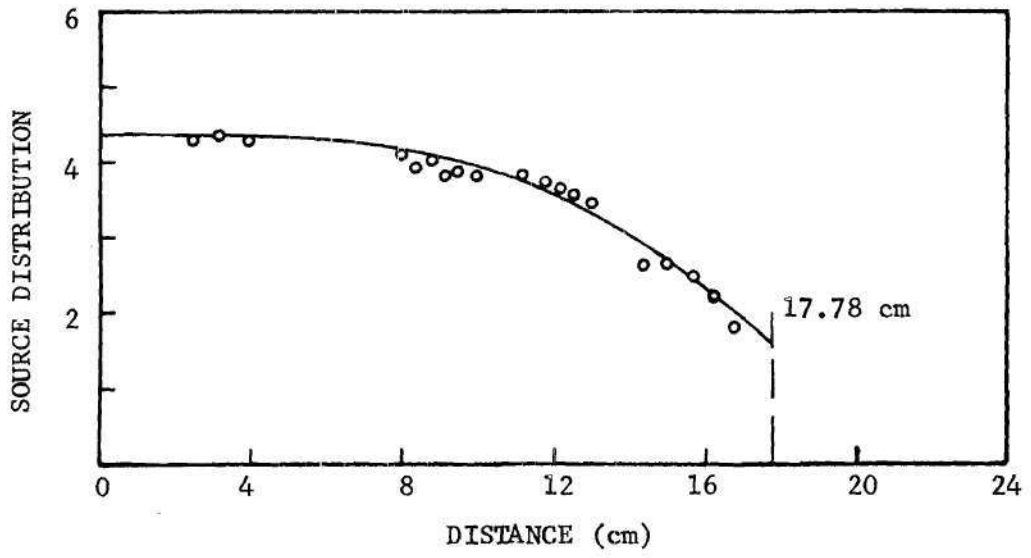

Figure 9. Measured Source Transverse Spatial Distribution Along x and y Axes Lying on the Source Plane (Experimental data from Unus[52])

transverse leakage is small in graphite and Plexiglass. To do this calculation, a one-dimensional, S_N transport computer code, ANISN,[49] was used. Henceforth, this calculation will be referred to as the ANISN-calculation. The scattering kernels for graphite and beryllium were calculated using the computer codes HEXSCAT,[53] GASKET,[39] and FLANGE.[40] The anisotropy of scattering collisions was represented by the P_3 Legendre expansion of the differential scattering cross sections. The frequency distributions for graphite, beryllium, and hydrogen have been taken from Reference 54. The scattering kernel for hydrogen has been used to approximate the scattering properties of Plexiglass. To simulate the presence of carbon and oxygen in Plexiglass, a constant cross section (free atom-value) has been added to the diagonal terms of the hydrogen scattering kernel. The correct number densities of hydrogen, carbon, and oxygen in Plexiglass ($C_5H_8O_2$, density 1.18 gm/cc) have been used.

Figure 8 shows the results of the ANISN-calculation of the source energy distribution for the forward and the transverse directions. The calculated source energy spectrum in the forward direction is in good agreement with the experimental result. Also, the similarity of the energy distribution in the forward and the transverse directions supports our assumption of energy and angle separability, at least at the block center.

Figure 10 shows the ratio of ANISN-calculated, normalized source angular distribution to the normalized source "cosine angle distribution" for 0.09, 0.025 (above-Bragg), and 0.0045 eV (below-Bragg) neutrons. Both

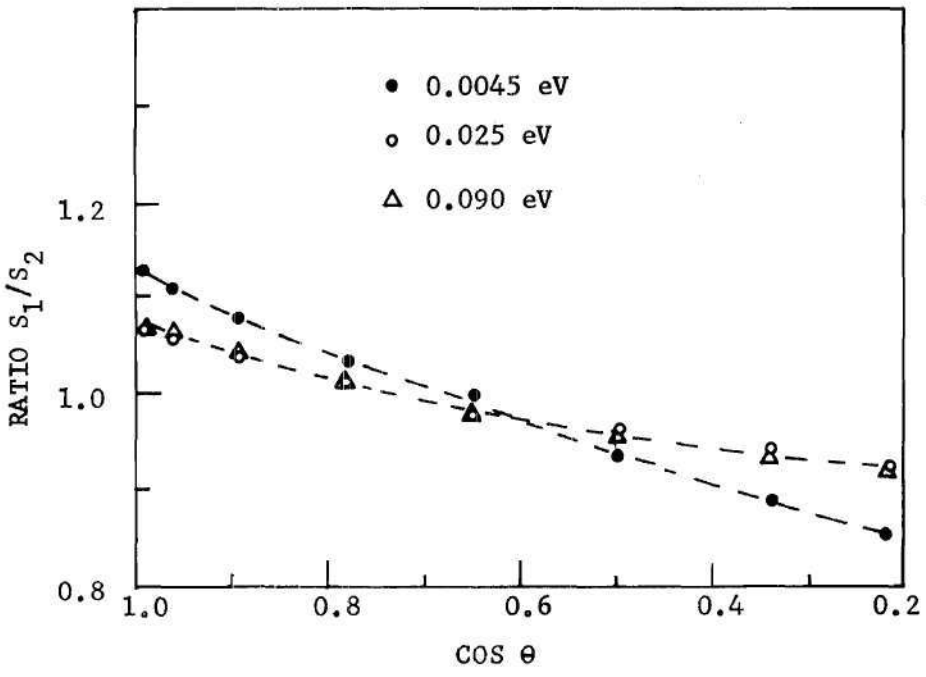

Figure 10. The Ratio of ANISN-Calculated Anisotropic Normalized Source Distribution to a Normalized Cosine Source Distribution for Various Average Neutron Energies

the distributions have been normalized so that the area under the distributions is unity. We notice that, for directions in the positive z direction ($\cos\theta = 1.0$) there are, relatively, 13% more sub-Bragg neutrons for ANISN-calculated distribution than for the "cosine distribution." The uncollided neutron contribution to the forward spectrum at 10.2 cm from the source is negligible for the above-Bragg region and is of the order of 70% for the sub-Bragg region. Thus, the use of the ANISN-calculated source distribution in the Monte Carlo analysis would result in a sub-Bragg flux which is higher by approximately 10% than if the "cosine angle distribution" had been used. The above-Bragg neutrons in the spectrum at 10.2 cm are relatively less sensitive to the source angular distribution since they have to have many collisions before they reach the detector at 10.2 cm and would have forgotten their initial angular distribution.

The source spatial distribution shown in Figure 9 is for the total angle and energy integrated flux. The source spatial distribution for the Monte Carlo analysis should be for the neutrons coming into the beryllium block from the thermal column. This spatial distribution of neutrons coming into the block would have a somewhat flatter distribution than that given in Figure 9; i.e., the distribution for neutrons moving in the positive direction would not drop as rapidly near the transverse edges of the block as for neutrons moving in the negative direction. Thus, we are introducing relatively more neutrons at the center of the source plane by using the distribution shown in Figure 9. This has a direct influence on the calculated spectrum at 10.2 cm below the Bragg cut-off energy due to the direct streaming of sub-Bragg source neutrons. The systematic error

due to this effect has been estimated to result in a 10-20% higher relative peaking of the sub-Bragg neutrons over the above-Bragg neutrons in the calculated spectrum at 10.2 cm, whereas the systematic error due to the use of the "cosine angle distribution" for the source distribution results in a 10% lower relative peaking of the sub-Bragg neutrons. Thus the net uncertainty of the calculated relative peaking of sub-Bragg neutrons in the spectrum at 10.2 cm from the source plane is of the order of 10%. A rough estimation of the source spatial distribution is made in Appendix D.

Thermal Neutron Scattering

This section gives a brief description of the phenomenon of the thermal neutron scattering in polycrystalline beryllium and the scattering kernels used in the adjoint Monte Carlo calculations. Also, we have developed a procedure to treat the coherent elastic scattering collisions in a Monte Carlo method using a continuous energy variable. However, this procedure has not been used in our adjoint Monte Carlo analysis, as this procedure is not applicable when the energy variable is treated by the energy-group method. A detailed discussion on this procedure is given later.

The neutron-nucleus elastic scattering collisions, for neutrons of energy larger than the binding energy of atoms in a crystalline moderator, are billiard ball type collisions. When the neutron energy is in the thermal energy range, the chemical binding plays an important role and the scattering properties of the crystalline moderator are completely altered.

A thermal neutron in beryllium can undergo three major types of

interactions with the moderating medium.[1,25,43] It can have coherent elastic collisions with the beryllium atoms in which the incident neutron changes its direction, whereas the neutron energy remains the same. The second type of interaction is the thermal inelastic collision where the neutron can gain or lose energy from the thermal vibrations of the chemically bound beryllium atoms. The third type of collision is an absorption event for which the probability is relatively small in beryllium moderators. As a result of the periodic arrangement of nuclei in a lattice, the scattering of neutron waves from one nucleus may interfere with the scattering from others. This interference phenomenon of the scattering is called the "coherent" scattering and this effect occurs in both the elastic and inelastic scattering processes. The scattering process, in which the nuclei scatter independently, is known as "incoherent" scattering and part of both elastic and inelastic scatterings is incoherent. Beryllium predominantly scatters neutrons coherently; that is, the elastic and inelastic collisions are strongly coherent.

Coherent Elastic Scattering

A computer program has been written by us to calculate the beryllium coherent elastic scattering kernel for the adjoint Monte Carlo analysis. The theory and methods used to calculate this kernel are described here.

Beryllium has a hexagonal close-packed lattice structure with two atoms per unit cell, which has lattice parameters, a = 2.2854 Å and c = 3.5841 Å. The differential elastic scattering cross section per nucleus for polycrystalline beryllium is[25,43]

$$\frac{d\sigma_{el}}{d\mu} = \frac{\sigma_b}{8\pi V} \frac{e^{-2\omega_\tau}}{\tau^2} \left(\frac{1 + \cos\psi}{2}\right)_\tau M_\tau \tag{38}$$

This expression holds for only those directions which satisfy the relation

$$2\pi\tau = 2K_o \sin(\theta/2) \tag{39}$$

where σ_b, the bound scattering cross section, is 7.54 b, V, the volume of a unit cell, is 8.0027×10^{-24} cm^3, $e^{-2\omega_\tau}$ is the familiar Debye-Waller factor, τ is the magnitude of the reciprocal lattice vector and is inversely proportional to the lattice spacing d, $(1 + \cos\psi)_\tau$ is the structure factor term, M_τ is the multiplicity of planes for a given τ, K_o is the magnitude of the neutron wave vector, θ is the angle of scattering, and $\mu = \cos\theta$.

The length of the $\bar{\tau}$ vector in terms of the Miller indices h, κ, and ℓ is given by

$$\tau = \frac{1}{a}\left[\frac{4}{3}(h^2 + h\kappa + \ell^2) + \ell^2 \frac{a^2}{c^2}\right]^{\frac{1}{2}} \tag{40}$$

and ψ as a function of h, κ, and ℓ is

$$\psi = 2\pi\left(\frac{h+2\kappa}{2} + \frac{\ell}{2}\right)_\tau \tag{41}$$

Assuming a Debye frequency distribution for the lattice vibrational modes

$$\rho(\omega) = 3\left(\frac{\hbar}{K_B\theta_D}\right)^3 \omega^2 \qquad 0 \le \omega \le K_B\theta_D \tag{42}$$

where θ_D, the Debye temperature, is 1000°K for beryllium.

ω_τ is given by

$$\omega_\tau = (6\pi^2\hbar^2\tau^2/mK_B\theta_D)\left\{\frac{1}{4} + \left(\frac{T}{\theta_D}\right)^2 Q\left(\frac{\theta_D}{T}\right)\right\} \tag{43}$$

and the function

$$Q(y) = \int_o^y \left\{g/(e^g - 1)\right\} dg \tag{44}$$

where $\hbar$ is the Planck's constant divided by 2π, K_B is Boltzmann's constant, m is the mass of the moderating atom, and T is the moderator temperature.

Equation 38 describes the transition probability of a neutron undergoing a coherent elastic collision with a set of Bragg planes, characterized by the reciprocal vector $\bar{\tau}$, in which the neutron is scattered through an angle θ.

In the adjoint Monte Carlo analysis, neutron energies ranging up to 0.3 eV were of interest, hence lattice planes with Miller indices varying from -12 to +12 were considered for the calculations of the elastic scattering kernel. A computer program was written to calculate the magnitude of $\bar{\tau}$ vectors, the structure factor, and the Debye-Waller factor. The program generated the Miller indices from -12 to +12 and using Equation 40 the corresponding magnitude of $\bar{\tau}$ vectors was calculated. Those planes, defined by their Miller indices, that have the same magnitude of the $\bar{\tau}$ vectors, were collected together. This gives the value of M_τ, the multiplicity of planes which have the same magnitude of the $\bar{\tau}$ vector. The

structure factor $(1 + \cos\psi)/2$, for a given τ, was calculated by using Equation 41. The Debye-Waller factor, $e^{-2\omega_\tau}$, was calculated using Equations 43 and 44.

From Equation 39, one notices that the maximum value of the τ vector is given by $\tau_{max} = (K_o/2\pi)$, where τ_{max} corresponds to the minimum value of the distance between lattice planes d_{min}. In other words, a neutron with a given initial energy can be diffracted by all those lattice planes whose lattice spacing, d, is greater than or equal to d_{min}. The angle through which the neutrons are diffracted from these planes is determined by Equation 39 and the probability for neutron diffraction from these planes is given by Equation 38.

A simple procedure to treat the anisotropy of elastic scattering in a Monte Carlo method using a continuous energy variable is given here. It is required to input only an array of the magnitude of $\bar{\tau}$ vectors and a corresponding array of the probability of neutrons interacting with the respective $\bar{\tau}$ vectors. Knowing the neutron initial energy, one determines the set of $\bar{\tau}$ vectors ($\tau \leq \tau_{max}$) from which the neutron can be diffracted. The specific τ, i.e., the d spacing of the lattice planes from which the neutron is diffracted, can be chosen by random sampling from the corresponding normalized probability distribution table obtained from Equation 38. After selecting this d spacing or τ, the angle θ through which the neutron of given energy is scattered can be obtained from Equation 39.

In our Monte Carlo program, the energy variable is treated in the multi-group method in which a neutron is assigned the average energy of the energy-group; therefore, the above mentioned procedure to describe the anisotropy of the elastic scattering is not feasible.

An alternative procedure is given here. Consider an energy group from 0.007 to 0.01 eV for beryllium at room temperature. Table 4 shows the lattice vector, cosθ values, and the probability of diffraction for neutron energies of 0.007 and 0.01 eV.

Table 4. Differential Coherent Elastic Cross Section and the Corresponding cosθ Values

Energy (eV)	$\tau = 1/d$ (1/Å)	$\frac{d\sigma_{el}}{d\mu}$	cosθ
0.007	0.50525	1.3024	- 0.4923
	0.55802	1.40188	- 0.8203
	0.57717	5.86549	- 0.9473
0.01	0.50525	1.3024	- 0.0446
	0.55802	1.40188	- 0.2742
	0.57717	5.86549	- 0.3631

These energies correspond to the bounds of the energy group considered here. From Table 4 we notice that neutrons, at these two energies, can be diffracted from one set of lattice planes with the same probability but are scattered through different angles. As the neutron energy increases from 0.007 to 0.01 eV, for a given $\tau = 0.50525$ Å, the neutrons are scattered through angles from $\cos\theta = - 0.4923$ to $\cos\theta = - 0.0446$. Likewise, considering also the values given for other τ's, neutrons are scattered through the angular range from $\cos\theta = - 0.2742$ to $\cos\theta = - 0.0446$ with a probability of 1.3024 and from $\cos\theta = - 0.3631$ to $\cos\theta = - 0.2742$ with a probability of 2.70212. Using the above procedure, the probability distribution for the entire angular range can be evaluated.

Table 5 shows the anisotropy of elastic scattering collisions for neutrons belonging to the 0.007 - 0.01 eV energy group. Such a distribution describing the anisotropy can be evaluated for all the energy groups and the distribution is normalized so that the area under the curve is unity. These normalized distributions, as a function of $\cos\theta$, for all energy groups, are used in the Monte Carlo program to describe accurately the anisotropy of elastic scattering collisions in beryllium.

Table 5. The Anisotropy of the Coherent Elastic Scattering of Neutrons in an Energy Group from 0.007 to 0.01 eV

Energy Width (eV)	$\frac{d\sigma_{el}}{d\mu}$	Upper $\cos\theta$	Lower $\cos\theta$
	0.0	- 1.0	- 0.9473
	5.86549	- 0.9473	- 0.8203
0.007	7.26737	- 0.8203	- 0.4923
to	8.56761	- 0.4923	- 0.3631
0.01	2.70212	- 0.3631	- 0.2742
	1.30024	- 0.2742	- 0.0446
	0.0	- 0.0446	0.0
	0.0	0.0	+ 1.0

Thermal Inelastic Scattering

The two thermal inelastic scattering kernels for beryllium, which were used in our Monte Carlo analysis, are described in this section. One of the scattering kernels used in the analysis was the Placzek[1,43] expansion of the differential thermal inelastic cross section. This kernel assumes a Debye phonon frequency distribution (Equation 42) and is made in the incoherent approximation. The first term of the Placzek expansion is given as

$$\sigma_{inel}(E'\to E,\mu) = \frac{S}{2}\left(\frac{E}{E'}\right)^{\frac{1}{2}}\left\{\frac{3\chi^2\hbar^2}{2m(K_B\theta_D)^3}\left[\frac{(E'-E)}{1-\exp(-(E'-E)/K_BT)}\right]\right\} \qquad (45)$$

$$\text{for } |E-E'| < K_B\theta_D \ ;$$

$$= 0 \quad \text{otherwise}$$

and

$$\sigma_{inel}(E'\to E) = \frac{3S}{m}\left(\frac{E}{E'}\right)\frac{(E'+E)}{(K_B\theta_D)^3}\,\frac{(E'-E)}{(1-\exp(-(E'-E)/K_BT))} \qquad (46)$$

$$\text{for } |E'-E| \le K_B\theta_D \ ;$$

$$= 0 \quad \text{otherwise}$$

where E' and E are the initial and final neutron energies, respectively, and χ is the momentum transfer.

The second scattering kernel which is relatively more sophisticated was obtained from the computer codes GASKET[39] and FLANGE.[40] The differential scattering cross section is expressed in terms of a scattering law, $S(\alpha,\beta)$, which is a function of only two variables, α and β.

$$\sigma_{inel}(E'\to E,\mu) = \frac{S}{4\pi T}\left(\frac{E}{E'}\right)^{\frac{1}{2}} e^{-\beta/2} S(\alpha,\beta) \qquad (47)$$

where the energy exchange β is given by

$$\beta = (E-E')/T \qquad (48)$$

and the momentum transfer α by

$$\alpha = \frac{1}{AT} \left(E+E' - 2\mu \sqrt{E\ E'}\right) \tag{49}$$

where S is the bound-atom cross section, T is the moderator temperature, A is the moderator mass, μ is the cosine of the scattering angle, E' and E are the initial and final neutron energies. The value of $S(\alpha,\beta)$ for beryllium was calculated by the computer code GASKET [39] using a more realistic frequency distribution[54] than the simple Debye model. The computer code FLANGE[40] uses these values of $S(\alpha,\beta)$ to calculate the differential scattering cross sections $\sigma_{inel}(E'\rightarrow E)$ and $\sigma_{inel}(E'\rightarrow E,\mu)$ in the incoherent approximation. From now on this kernel will be referred to as the Gulf kernel.

A computer program was written for the Georgia Tech Univac-1108 computer to calculate the group-to-group inelastic scattering matrix, $\Sigma_{inel}^{g'\rightarrow g}(\mu)$, by using Equations 45 and 23, where a Maxwellian energy distribution was used for flux weighting. The forward matrix was transposed to obtain the adjoint inelastic scattering matrix and was normalized so that the area under the curve is unity. Another computer program was written to calculate the $\Sigma_{inel}^{g'\rightarrow g}$ matrix by using Equation 46.

In the sub-Bragg energy region both the Gulf kernel and the Placzek kernel calculate a value of $\sigma_{inel}(E')$ which differs from that given in BNL-325 data (which were the same as our experimental data). Therefore, for the Gulf kernel, $\sigma_{inel}(E'\rightarrow E)$ has been normalized so that the evaluated value of $\sigma_{inel}(E')$ is equal to the $\sigma_{inel}(E')$ data of the BNL-325 cross section set, in the energy range below the Bragg cut-off energy. Above

the Bragg cut-off energy, the calculated shape of $\sigma_{inel}(E')$ has been maintained, but normalized to the experimental value at the Bragg cut-off energy. Similarly, the Placzek kernel has also been normalized so that the calculated values of $\sigma_{inel}(E')$ are the same as those given by the normalized Gulf kernel. This, in effect, means that both these normalized kernels give the same value of $\sigma_{inel}(E')$, but will have their own individual shape of the energy exchange probability curve.

Adjoint Random Walk Procedure

The random walk procedure in our adjoint Monte Carlo computer program, to calculate the neutron spectrum in finite beryllium assemblies, is based on Equation 36. This adjoint random walk procedure is described in the following steps.

Step 1:

The adjuncton source coordinates g_o, $\bar{\Omega}_o$ (i.e., A_o,B_o, and C_o), and $\bar{r}_o$ (i.e., x_o, y_o, and z_o) were chosen from the detector response function $P_g(\bar{r},-\bar{\Omega})$. The initial adjuncton weight, W_o, was set to unity.

The detector was assumed to be a 5 x 5 cm area detector perpendicular to the z axis located at 10.2 cm from the source plane, which corresponds to the base of the 5 x 5 cm extraction channel used by Lake and Kallfelz[23] for their experiment. Thus the spatial coordinates x_o and y_o were chosen from a uniform distribution over the 5 x 5 cm area. Since we were interested in the flux of neutrons with neutron directions lying in the cone of 1° polar angle about the positive z direction, the adjuncton angular coordinates were chosen from an isotropic distribution over a cone of 1° polar angle about the negative z axis. The experimental spectrum

results of Kallfelz and Lake[23] have been corrected for the energy-dependent detector efficiency. Thus the energy of the adjuncton, E_o, was chosen from a uniform distribution in energy.

Step 2:

The distance to the next collision site, R, was chosen from the distribution, $\Sigma_t^{g_o} e^{-\Sigma_t^{g_o} R'}$, along the direction $\bar{\Omega}_o$. It should be noted here that the moderating medium is made of a homogeneous beryllium moderator and hence the cross sections do not depend on the spatial variable. Knowing the parameters R, $\bar{\Omega}_o$, and r_o, it is easy to obtain the spatial coordinates x_1, y_1, and z_1 of the next collision site.

The adjuncton history was terminated if the selected collision site fell outside the geometry of the problem.

Step 3:

The type of neutron collision at the new collision site was decided by the ratio

$$R^* = \frac{\sum_g \int d\bar{\Omega}\, \Sigma_{el}^{g \to g_o}(\bar{\Omega} \to \bar{\Omega}_o)}{\sum_g \int d\Omega\, \Sigma_S^{g \to g_o}(\bar{\Omega} \to \bar{\Omega}_o)} \qquad (50)$$

If the random number selected from a uniform distribution, varying from 0 to 1, was less than or equal to R^*, then the collision was taken to be elastic. Otherwise, the collision was taken to be an inelastic collision.

In an elastic collision the neutron does not change its energy;

Page missing from thesis

in the Russian roulette, the history was continued from Step 2 onwards.

Adjunctons were scored at the beginning of Step 2 according to Equation 37 to obtain the effect of interest.

Test Cases

This section describes several test-case problems that were used to determine any errors in our Monte Carlo computer programs.

A test-case problem was solved by using both the forward and the adjoint Monte Carlo programs in order to find out whether there were any errors in these two programs. Since these two programs were written independently, calculating the same results by both methods would enhance one's confidence in them. The test-case problem chosen for this purpose was a steady-state diffusion length problem in which thermal neutrons from an isotropic planar source were diffusing into a 14 x 14 x 20 inch long block of moderator. The source consisted of neutrons belonging to two energy groups, where 40 percent of the source neutrons were born in the first group and a remaining 60 percent were born in the second group. The moderator consisted of a material with a macroscopic total cross section of $\Sigma_t^1 = 0.2$ and $\Sigma_t^2 = 0.3$ cm^{-1} and a macroscopic scattering cross section of $\Sigma_S^1 = 0.18$ and $\Sigma_S^2 = 0.29$ cm^{-1}, where the superscripts 1 and 2 refer to the first and second energy groups, respectively. The thermal elastic cross section for the second energy group was equal to 0.19 cm^{-1} and zero for the first energy group. The effect of interest to be calculated was the neutron flux at 6 cm from the source plane, on the z axis, with neutron directions lying in the positive z direction with a polar angular spread from 0 to 20°. This particular problem was made up to check on the method

Page missing from thesis

be totally suppressed. A macroscopic total cross section, 0.55 cm^{-1}, and a macroscopic scattering cross section, 0.5 cm^{-1}, were chosen for this moderator. The block of 30 x 30 cm is quite large in comparison to the mean free path of 1.82 cm for the monoenergetic neutrons considered here. Also, the absorption cross section was chosen to be very small in comparison to the scattering cross section. Thus, for regions sufficiently distant from the source and along the central axis of the block, the diffusion equation could be used to analytically calculate the spatial dependence of the total flux and hence the relaxation length of the neutron decay. The analytically calculated inverse relaxation length was found to be equal to 0.308 cm^{-1} as compared to the adjoint Monte Carlo result equal to 0.294 cm^{-1}. This particular calculational check on the adjoint Monte Carlo program instills a reasonable confidence in the calculational procedure.

The uncollided flux as a function of distance from the source plane was calculated and it was found that the Monte Carlo results were the same as the analytical result. Checks were also made to find the value of the minimum weight to terminate the particle history and to find the initial number of particles necessary to yield reasonable statistical accuracy on the calculated results. The Monte Carlo program was so written that a complete print-out of the step-by-step details of the particle random walk procedure could be obtained. Hand calculations for these details for several particles were made to check the detailed calculation of the Monte Carlo programs.

The Discrete S_N Approximation

This section describes the S_N method used in calculating the spatial behavior of the total energy spectrum in finite sizes of beryllium moderator to investigate the applicability of the diffusion theory for small systems with strong transverse leakage.

The neutron transport equation in the rectangular geometry is given by

$$\left\{\mu \frac{\partial}{\partial z} + \eta \frac{\partial}{\partial x} + \xi \frac{\partial}{\partial y} + \Sigma_t(E)\right\} \varphi(\bar{r},E,\bar{\Omega}) = Q(\bar{r},E,\bar{\Omega}) \tag{54}$$

where $\varphi(\bar{r},E,\bar{\Omega})$ is the neutron flux at $\bar{r}$ having energies in dE about E and directions in $d\Omega$ about $\bar{\Omega}$; $\Sigma_t(E)$ is the total macroscopic cross section; μ, η, and ξ are the direction cosines as shown in Figure 11, and $Q(\bar{r},E,\bar{\Omega})$ is the external boundary source, $S(\bar{r},E,\bar{\Omega})$, plus the inscattering source.

$$Q(\bar{r},E,\bar{\Omega}) = S(\bar{r},E,\bar{\Omega}) + \int d\bar{\Omega}' \int dE' \, \Sigma_S(E'\rightarrow E,\bar{\Omega}'\rightarrow \bar{\Omega}) \, \varphi(\bar{r},E',\bar{\Omega}') \tag{55}$$

For a one-dimensional geometry in z, Equation 54 reduces to

$$\left\{\mu \frac{\partial}{\partial z} + \Sigma_t(E)\right\} \varphi(z,E,\bar{\Omega}) = Q(z,E,\bar{\Omega}) \tag{56}$$

Expanding the scattering kernel $\Sigma_S(E'\rightarrow E,\bar{\Omega}'\rightarrow \bar{\Omega})$ in Legendre polynomials and truncating after LT terms, we have[49]

$$\Sigma_S(E'\rightarrow E,\bar{\Omega}'\rightarrow \bar{\Omega}) = \sum_{\ell=0}^{LT} \frac{2\ell+1}{2} \Sigma_{S\ell}(E'\rightarrow E) \, P_\ell(\bar{\Omega}'\cdot\bar{\Omega}) \tag{57}$$

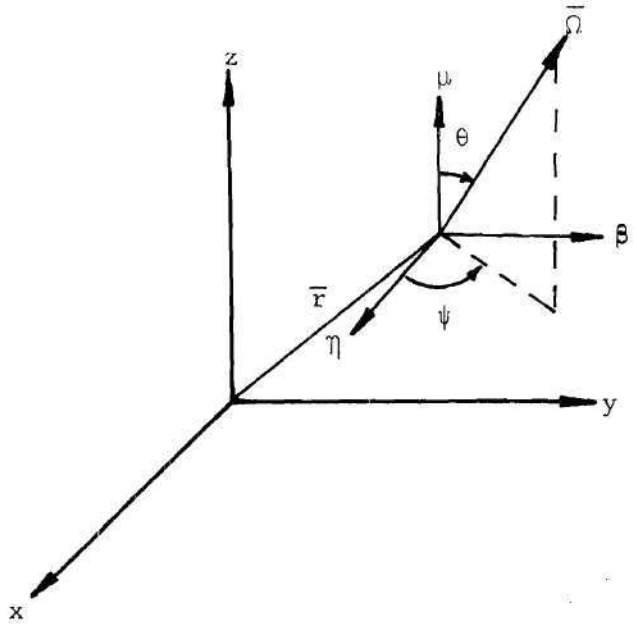

Figure 11. Geometric and Angular Coordinate System

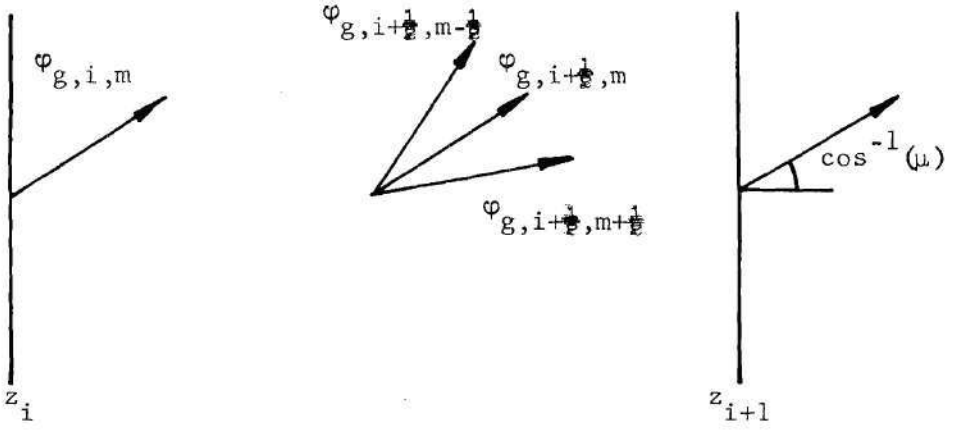

Figure 12. Spatial and Angular Mesh Interval for Any Energy Group g

where

$$\Sigma_{S\ell}(E'\to E) = \frac{1}{2\pi}\int d\mu\ \Sigma_S(E'\to E,\bar{\Omega}'\to\bar{\Omega})\ P_m(\bar{\Omega}'\cdot\bar{\Omega}) \tag{58}$$

According to the addition theorem for the Legendre polynomials[1]

$$P_\ell(\bar{\Omega}'\cdot\bar{\Omega}) = P_\ell(\mu)\ P_\ell(\mu') + 2\sum_{m=1}^{\ell}\frac{(\ell-m)!}{(\ell+m)!}\ P_\ell^m(\mu)\ P_\ell^m(\mu')\ \mathrm{cosm}(\psi'-\psi) \tag{59}$$

Define

$$\varphi(z,E,\mu) = \int_0^{2\pi} d\psi\ \varphi(z,E,\bar{\Omega}) \tag{60}$$

$$S(z,E,\mu) = \int_0^{2\pi} d\psi\ S(z,E,\bar{\Omega}) \tag{61}$$

Inserting Equations 59 and 57 into Equation 55, and integrating over ψ, we have[55]

$$Q(z,E,\mu) = S(z,E,\mu) \tag{62}$$

$$+\int dE'\sum_{\ell=0}^{LT}\frac{(2\ell+1)}{2}\ P_\ell(\mu)\ \Sigma_{S\ell}(E'\to E)\int_{-1}^{+1} d\mu'\ P_\ell(\mu')\ \varphi(z,E,\mu')$$

Integrating Equation 56 over ψ and using Equations 60, 61, and 62, we have

$$\left\{\mu\frac{\partial}{\partial z}+\Sigma_t(E)\right\}\varphi(z,E,\mu) = S(z,E,\mu) + \sum_{\ell=0}^{LT}\frac{2\ell+1}{2}\ P_\ell(\mu) \tag{63}$$

$$\times\int dE'\ \Sigma_{S\ell}(E'\to E)\int_{-1}^{+1} d\mu'\ P_\ell(\mu')\ \varphi(z,E,\mu')$$

In the discrete S_N approximation to the transport equation (63), the distance from the origin is measured by Z_i, i=1 to IZ+1; that is, the system is divided into IZ spatial intervals. The areas, A_i, of the orthogonal surfaces at any Z_i are taken to be unity and the volume, $V_{i+\frac{1}{2}}$, between Z_i and Z_{i+1}, is equal to ΔZ_i.

Discrete directions $\bar{\Omega}_m$, m=1, to MM are chosen and a solid angle W_m is associated with each direction.

The energy range is subdivided into ΔE_g intervals with g=1 to IE, with the first group, g=1, being the highest energy group.

The discrete ordinate form of Equation 63 can be written as[55]

$$\frac{\mu}{V}\left(\varphi_{i+1} - \varphi_i\right) + \Sigma_t \varphi = S + \sum_{\ell=o}^{LT} \frac{2\ell+1}{2} P_\ell(\mu_m) \sum_{h=1}^{IE} \Sigma_{S\ell}^{h\to g} \times \sum_{m'=1}^{MM} W_{m'} P_\ell(\mu_{m'}) \varphi_{h,i+\frac{1}{2},m'} \tag{64}$$

The description of the mesh interval is given in Figure 12 (page 78). The centered subscripts, $i+\frac{1}{2}$ in the spatial mesh and m in the angular mesh, and the energy group subscript, g, have been omitted in the equation but are shown in Figure 12.

The computer code ANISN[49] uses Equation 64 to solve the one-dimensional transport equation (63) by the method of discrete S_N approximation. Using this method, we are interested in investigating the behavior of $\varphi(r,E,\bar{\Omega})$, in finite sizes of beryllium moderator along the z axis, as a function of the transverse dimension of the system. This study is intended to show whether the critical transverse size of the beryllium moderator, below which the neutron distribution fails to reach an equilib-

rium condition, is closer to 30 x 30 cm (diffusion theory limit[19]) or to 127 x 127 cm (asymptotic transport theory limit[9]). This investigation will have conclusive bearing on the applicability of diffusion theory in small systems with strong transverse leakage.

To conduct this investigation, we have solved the one-dimensional transport equation by using the computer code ANISN[49] in which the effect of the additional loss term, due to the transverse leakage, was introduced by using an effective total removal cross section, Σ_{ef}, instead of Σ_t in Equation 64. The total removal cross section is given by

$$\Sigma_{ef} = \Sigma_t(E) + D(E)B^2(E) \tag{65}$$

The diffusion coefficient, D(E), is defined as

$$D(E) = 1{\cdot}0/3\ (\Sigma_a(E) + \Sigma_{tr}(E)) \tag{66}$$

where $\Sigma_a(E)$ and $\Sigma_{tr}(E)$ are the macroscopic absorption and transport cross sections.

The transverse buckling, B(E) is given by

$$B^2(E) = 2\left\{\frac{\pi}{D_T + 1{\cdot}42\ \lambda_{tr}(E)}\right\}^2 \tag{67}$$

where D_T is the transverse dimension of the square block of moderator and λ_{tr} is the transport mean-free-path.

It should be noted that the loss term due to transverse leakage

given by the second two terms of Equation 54 is dependent on the direction $\bar{\Omega}$, and it is zero for the positive and the negative z directions; whereas, by using a DB^2 approximation to the transverse leakage loss, we will be introducing a loss term which is a constant in all directions. A detailed discussion on the implications of this approximation is given in Appendix C as well as in Chapter V.

Calculations were made to evaluate $\varphi(z,E,\mu)$ in beryllium blocks with transverse dimensions of 35.56 x 35.56 cm, 60 x 60 cm, and 150 x 150 cm. The planar thermal neutron source at z=0 was assumed to be isotropic with a Maxwellian energy distribution at 300°K. The anisotropy of the scattering collisions was described by going up to P_4 terms in the Legendre expansion of the differential scattering cross section. This scattering matrix was calculated by using the computer codes HEXSCAT,[53] GASKET,[39] and FLANGE.[40]

The differential neutron density, $n(\bar{r},E)dVdE$, which is the number of neutrons in an elemental volume dV whose energy lies between E and E+dE, is defined as

$$n(\bar{r},E)dV\ dE = \frac{\Phi(\bar{r},E)}{v}\ dV\ dE \tag{68}$$

where v is the neutron velocity and

$$\Phi(\bar{r},E) = \int d\bar{\Omega}\ \varphi(\bar{r},E,\bar{\Omega}) \tag{69}$$

The average energy, $\bar{E}_n$, is defined as

$$\bar{E}_n = \frac{\int E\ n(\bar{r},E)dE}{\int n(\bar{r},E)dE} \tag{70}$$

CHAPTER V

RESULTS AND DISCUSSION

In this chapter, the results of the various cross section measurements and the theoretical spectrum analysis in finite beryllium systems are presented.

Measured Cross Section Results

This section presents the results of the measured total cross section of polycrystalline beryllium, beryllium oxide, and graphite. All the cross section measurements have been made at room temperature, 299 ± 2°K. The Bragg cut-off energies for beryllium, beryllium oxide, and graphite are 0.0052, 0.0037, and 0.0018 eV, respectively.

In all the figures presenting the experimental results of the total cross section, the bars on the experimental points indicate the accuracy of the measured result and the triangle shown on the axis represents the energy resolution of the experiment. The calculated error bar on the experimental points includes not only the statistical nature of the neutron counts at the detector, but also the inaccuracy in the determination of sample thickness, sample number density, the detector efficiency, and the "multiple-scattering" contribution. The indicated energy resolution was calculated taking into account the uncertainties in the duration of the chopper burst, the detector thickness and the analyzer channel width, as well as the inaccuracy in the determination of the

the average energy caused by all the relevant errors in evaluating the time from the middle of the chopper burst to the middle of the first analyzer channel, the detector flight path, the chopper speed, etc. A detailed discussion on the error analysis and energy resolution is given in Appendix B.

Beryllium Cross Section

Figure 13 shows the total cross section of beryllium below the Bragg cut-off energy, measured with the beryllium sample at distances of 64.75, 52.75, and 46.75 inches from the detector. As seen from Figure 13, the results of these measurements agree within the statistical accuracy of the experiment. This shows that the geometry of the experiment was good in the sense that the neutrons scattered in the beryllium sample did not reach the detector.

Figure 14 shows the total cross section of beryllium below the Bragg cut-off energy, measured with the sample at distances of 64.75 and 2.0 inches from the detector. The result of the cross section measurement with the sample at 2.0 inches from the detector has been corrected for the "multiple-scattering" contribution. As seen from Figure 14, the results of the two measurements yield the same value of the total cross section within the experimental accuracy, indicating that the small-angle scattering of neutrons in the beryllium sample, if any, has little effect on the measured total cross section.

Figure 15 shows the measured total cross section of beryllium below the Bragg cut-off energy, compared with the BNL-325 cross section data. It is seen that the measured beryllium cross section is in good agreement

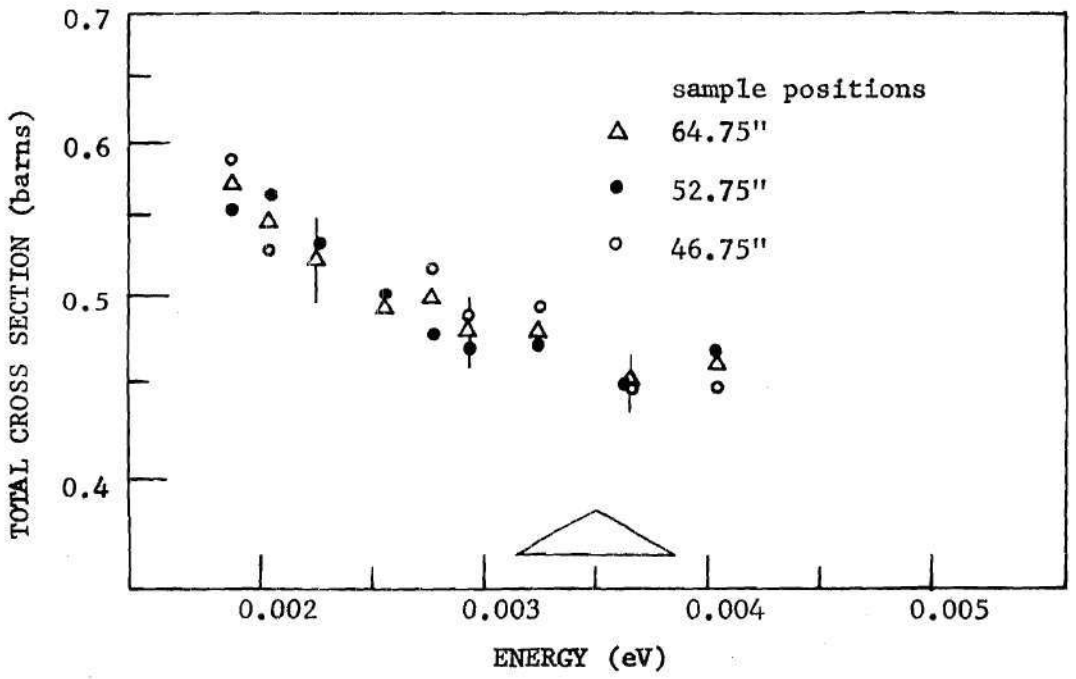

Figure 13. Total Cross Section of Beryllium for Various Sample Positions

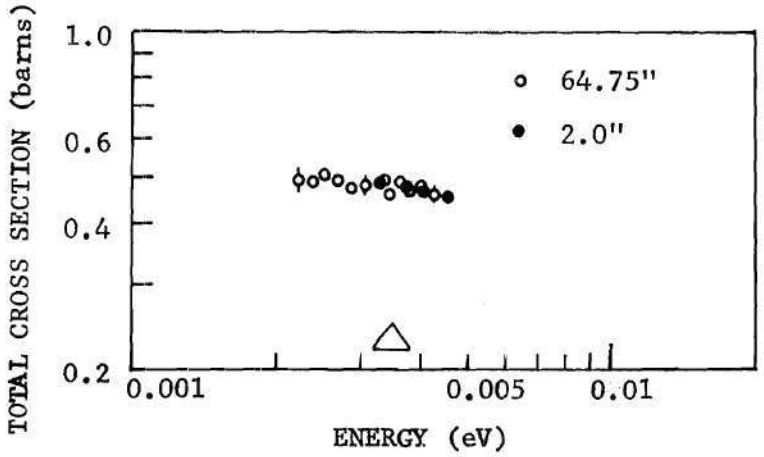

Figure 14. Total Cross Section of Beryllium with Sample at 64.75 Inches and 2.0 Inches

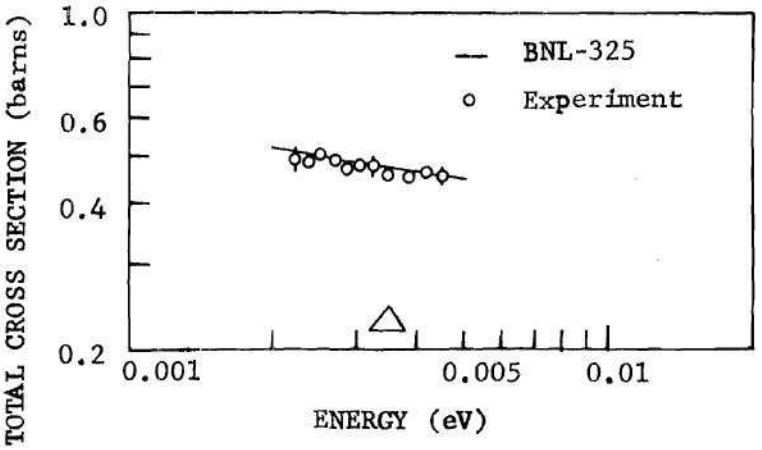

Figure 15. Measured Total Cross Section of Beryllium Compared with BNL-325 Data Below 0.005 eV

with the BNL-325 cross section data. As mentioned earlier, the one-phonon coherent calculation of the beryllium total cross section by Borgonovi and Sprevak[41] is in good agreement with both the BNL-325 data and our results. Therefore, it can be said that the total cross section of beryllium below the Bragg cut-off energy has been established quite accurately.

The total cross section measurements were made in the energy range above the Bragg cut-off energy for a typical beryllium sample selected from the lot of beryllium blocks used by Lake and Kallfelz[21,22,23] in their space-angular dependent, steady-state, energy spectrum measurements. This beryllium sample has been referred to as the "Lake sample." The primary purpose of this measurement was to find out whether there are any extinction effects in the beryllium samples used in their experiments. The measured energy spectrum of Lake and Kallfelz will depend on the nature of the beryllium moderator and any theoretical analysis of this particular problem should have an accurate knowledge of the scattering properties of the Lake-beryllium sample in order to make a comparison with their experimental spectrum results.

Figure 16 shows the measured total cross section above the Bragg cut-off energy for two beryllium samples, 1/8 and 1/4 inch in thickness, at 2.5 meters from the detector. The measurement of cross section for two different thicknesses of sample should indicate the presence of a "multiple-scattered" neutron contribution, if it is significant. As seen in Figure 16, the results indicate that the "multiple-scattering" contribution at the detector is negligible.

Another measurement of the total cross section of beryllium, above

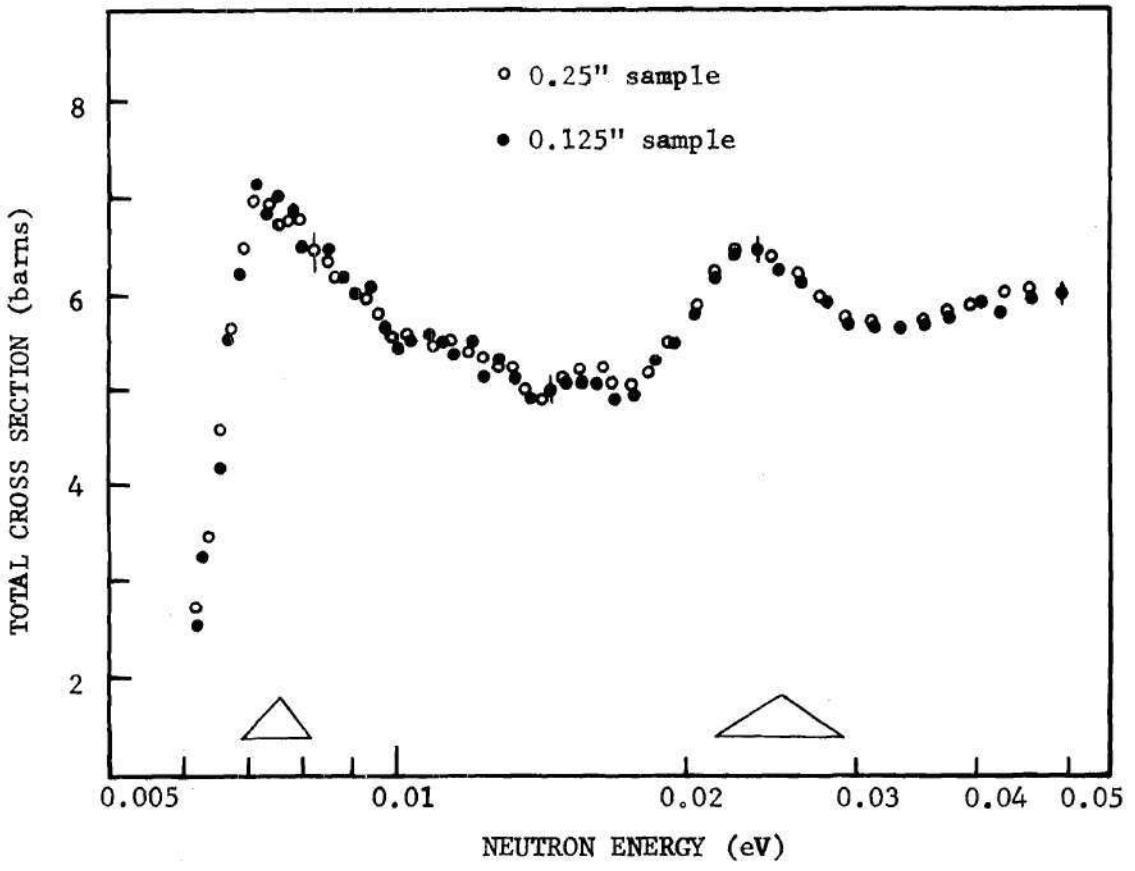

Figure 16. Total Cross Section of Lake-Beryllium Measured for 1/8 Inch and 1/4 Inch Thick Samples, with a Chopper Speed of 1800 RPM

the Bragg cut-off energy, was made keeping the thickness of the sample the same, while using two different chopper speeds, 1800 and 3954 RPM. The effect of doubling the chopper speed is to improve significantly the energy resolution of the experiment, particularly at higher energies. Thus comparison of these two measurements should indicate any influence of the energy resolution on the measured cross section. Figure 17 shows the two measured total cross sections of beryllium with chopper speeds of 1800 and 3954 RPM. The results indicate that any differences in the two cross sections are not significantly greater than the probable error of the measured results.

Figure 18 shows the total cross section of the Lake-beryllium sample above the Bragg cut-off energy, as compared to the BNL-325 cross section data. This clearly shows that the total cross section values for the Lake-beryllium sample are consistently smaller than the BNL-325 cross section up to 0.05 eV. This difference in the cross section is clearly due to the extinction effects in the Lake-beryllium sample. This means that the average beryllium crystallite size in the Lake sample was large enough to cause such an extinction effect.

To gain an approximate knowledge of the average size of crystallites in the Lake-beryllium sample, another cross section measurement with a Brush-Wellman, N - 50 - C, high-purity grade beryllium sample was made. The chemical composition and the average grain size of this sample have been given in Table 1. Figure 19 shows the total cross section of both the Lake-beryllium sample and the N - 50 - C beryllium sample. The results indicate that the two measured cross sections were almost the same, indicating that the average grain size in the Lake-beryllium sample was in

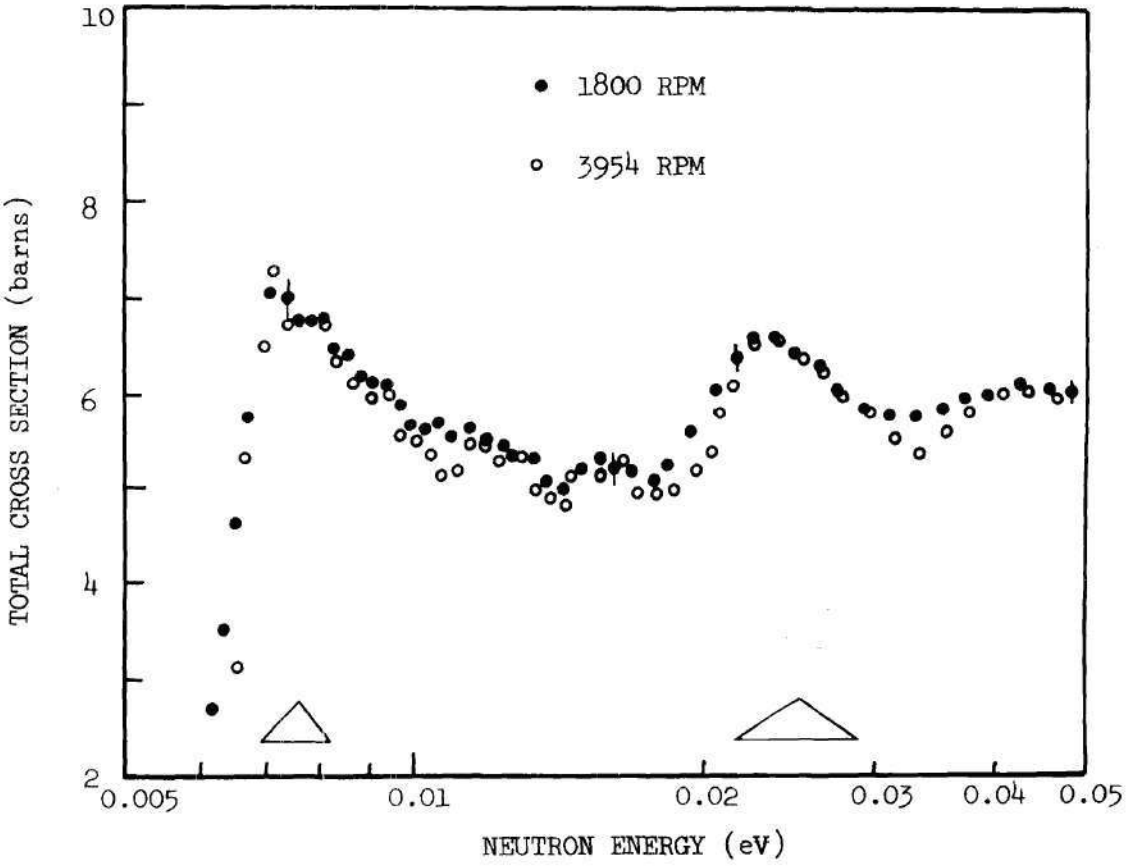

Figure 17. Total Cross Section of Lake-Beryllium Measured with 1800 and 3954 RPM, Chopper Rotational Speeds

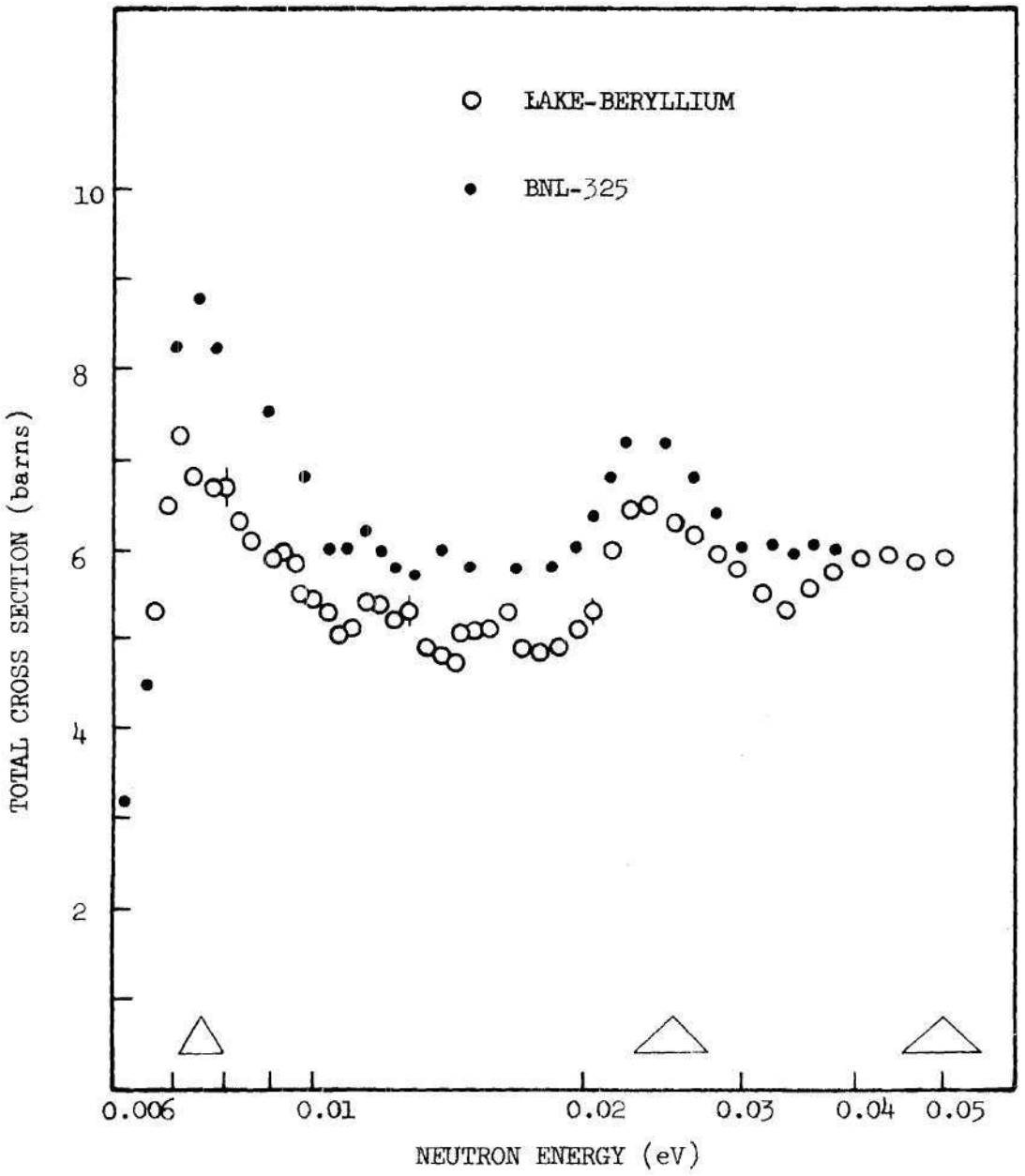

Figure 18. Comparison of Total Cross Section of Lake-Beryllium Sample with the BNL-325 Cross Section Data

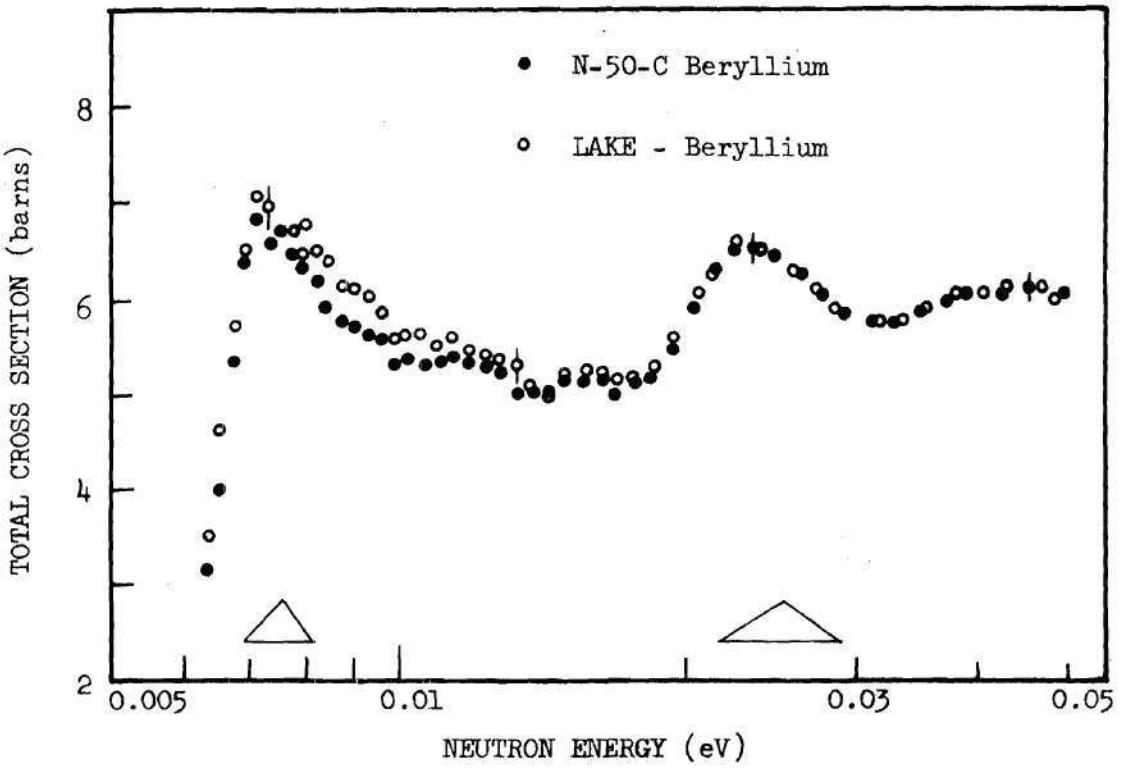

Figure 19. Comparison of Total Cross Sections of Lake-Beryllium and N-50-C Beryllium Samples

the vicinity of 11 microns.

Beryllium Oxide Cross Section

Figure 20 shows the measured total cross section of beryllium oxide below the Bragg cut-off energy with the sample at 2.15 and 2.78 inches from the detector. The distances given here are measured from the face of the sample to the center of the detector. Moving the sample away from the detector at this close range causes a significant reduction in the angle subtended by the detector at the sample, as seen in Figure 6. Figure 20 shows that the cross sections agree quite well within the experimental error. This indicates that the detector-sample geometry was such that all the small-angle scattered neutrons were counted in the detector.

Figure 21 shows a comparison of the experimental results for the beryllium oxide total cross section with the theoretical incoherent calculational results. This calculation was performed using the computer codes GASKET[39] and FLANGE.[40] We note that the theoretical results are higher than the measured results. This may be caused by the use of the incoherent approximation in the theory. It has been mentioned earlier that, in the case of beryllium also, the incoherent calculations were higher than the measured total cross section below the Bragg cut-off energy and this discrepancy was removed by the one-phonon coherent calculation of Borgonovi and Sprevak.[41] At present there are no reported results of the coherent calculation of the thermal inelastic section for beryllium oxide known to the author. Experimental results of Zhezherun et al.[37,38] indicate a value of about 0.8 b for the total cross section of beryllium oxide in comparison to our value of 0.445 b at 0.003 eV. The main purpose of

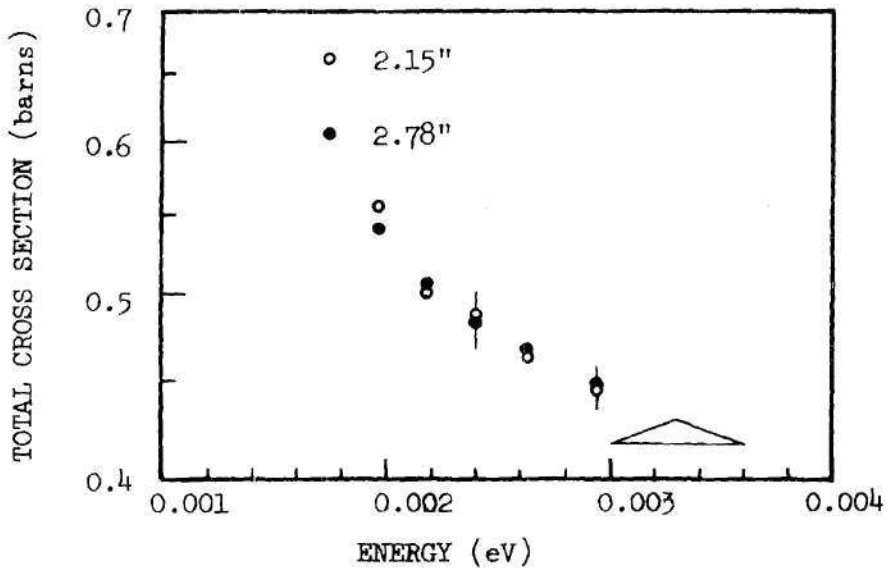

Figure 20. Total Cross Section of BeO with Samples at 2.15 and 2.78 Inches

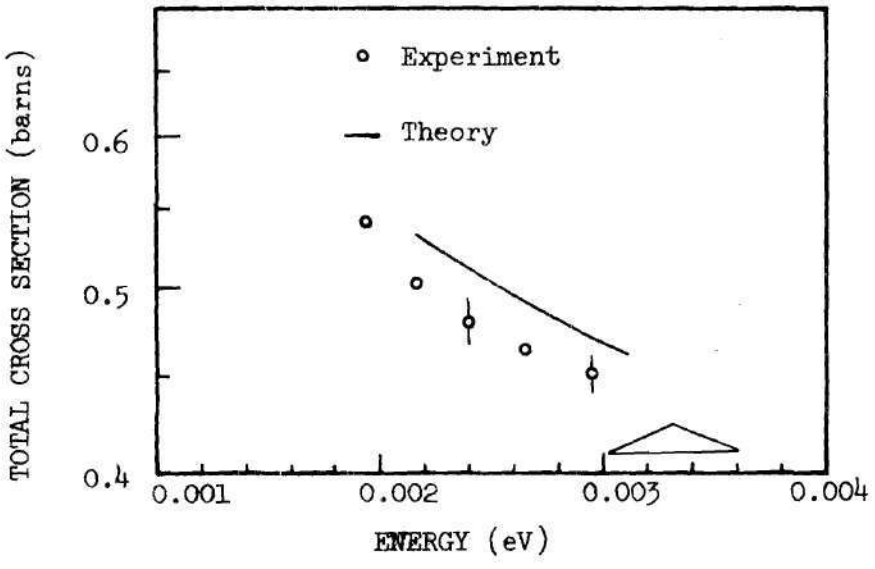

Figure 21. Total Cross Section of BeO Compared with Theoretical Results of GASKET and FLANGE

their investigation was to measure the total cross section in the above-Bragg region. Their experimental values of the total cross section, below the Bragg cut-off energy, have poor statistical accuracy and have not been corrected for the small-angle scattering effects.

Graphite Cross Section

Figure 22 shows the results of the total cross section measurements for graphite below the Bragg cut-off energy with the sample at 2.0 and 2.5 inches from the detector. Here the extrusion direction of the sample was in a direction parallel to the incident neutron beam. The results of these two measurements agree within the experimental accuracy, indicating that the geometry of the experiment was such that all the neutrons that were small-angle scattered in the sample were seen by the detector.

Figure 23 shows the results of the total cross section of graphite measured with the extrusion direction of the sample perpendicular and parallel to the incident neutron beam. The results indicate that the influence of the orientation of the sample extrusion direction with respect to the direction of the incident neutron beam is negligible for energies below the Bragg cut-off energy. For the energy range just above the Bragg cut-off energy, the total cross section has relatively stronger dependence on the extrusion direction, as reported by Egelstaff.[28]

Figure 24 shows the experimental result of the total cross section of graphite in comparison to the BNL-325 data. Our results are lower than the BNL-325 cross section values and the energy dependence of our results seems to be relatively flatter. It is difficult to pin-point the exact reason for this discrepancy between our results and the BNL-325 data, particularly in view of the fact that, as stated by Egelstaff,[28] the BNL-325

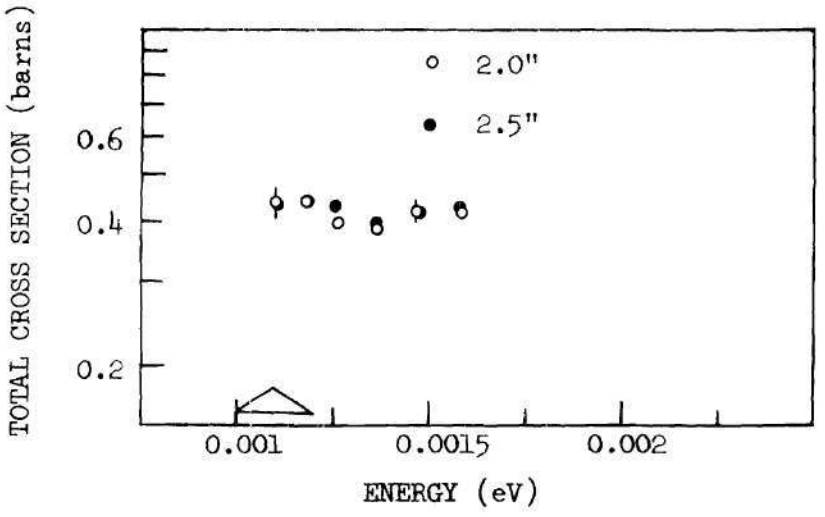

Figure 22. Total Cross Section of Graphite Measured with the Sample at 2.0 and 2.5 Inches

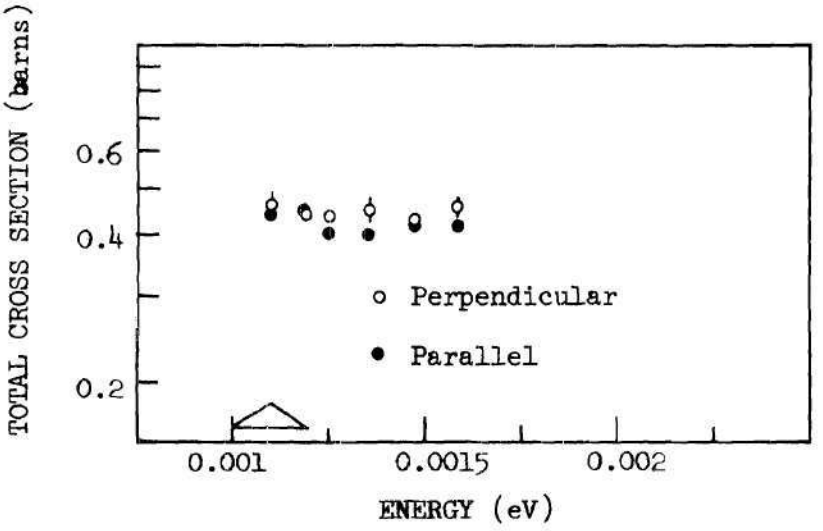

Figure 23. Total Cross Section of Graphite Measured with the Sample Extrusion Direction Parallel and Perpendicular to Neutron Beam

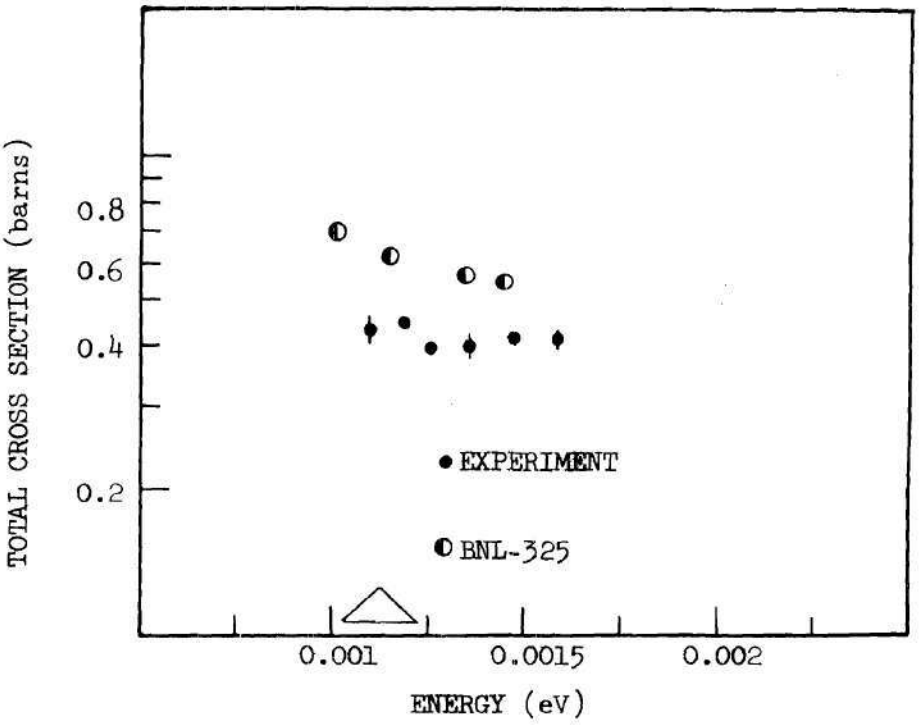

Figure 24. Comparison of Measured Total Cross Section of Graphite with the BNL-325 Data

data also take into account the effect of small-angle scattering in a manner similar to our measurement. However, no details are given there on how they have corrected for the "multiple-scattering" contribution except to state that this contribution is small. In a sense this is true; for example, in graphite the "multiple-scattering" contribution is of the order of 0.9% of the intensity of neutrons incident on a sample of thickness of 2.0 inches. But we also find that for our case this seemingly small contribution can make a correction in the total cross section of the order of 8%, since this contribution is significant in comparison to the fraction of the neutrons which are scattered in the sample. Thus, this "multiple-scattering" correction is quite important and an accurate knowledge of this correction is necessary. However, this does not explain why the BNL-325 data are higher than our measured total cross section for graphite.

Figure 25 shows our graphite cross section results in comparison to several other reported values. The theoretical results reported by Ghatak and Honeck[32] have been calculated using the incoherent approximation. Graphite is a strong coherent scatterer[1] and the use of the incoherent approximation in calculating the total cross section is not a valid approximation.

The experimental results of Palevsky as reported by Khubchandani et al.[34] are shown in Figure 25. The details of this experiment have not been published.

Figure 25 also shows the theoretical results of Conn[36] in comparison to the BNL-325 data and our experimental results. Conn has made a one-phonon calculation of the total cross section of graphite for sub-Bragg

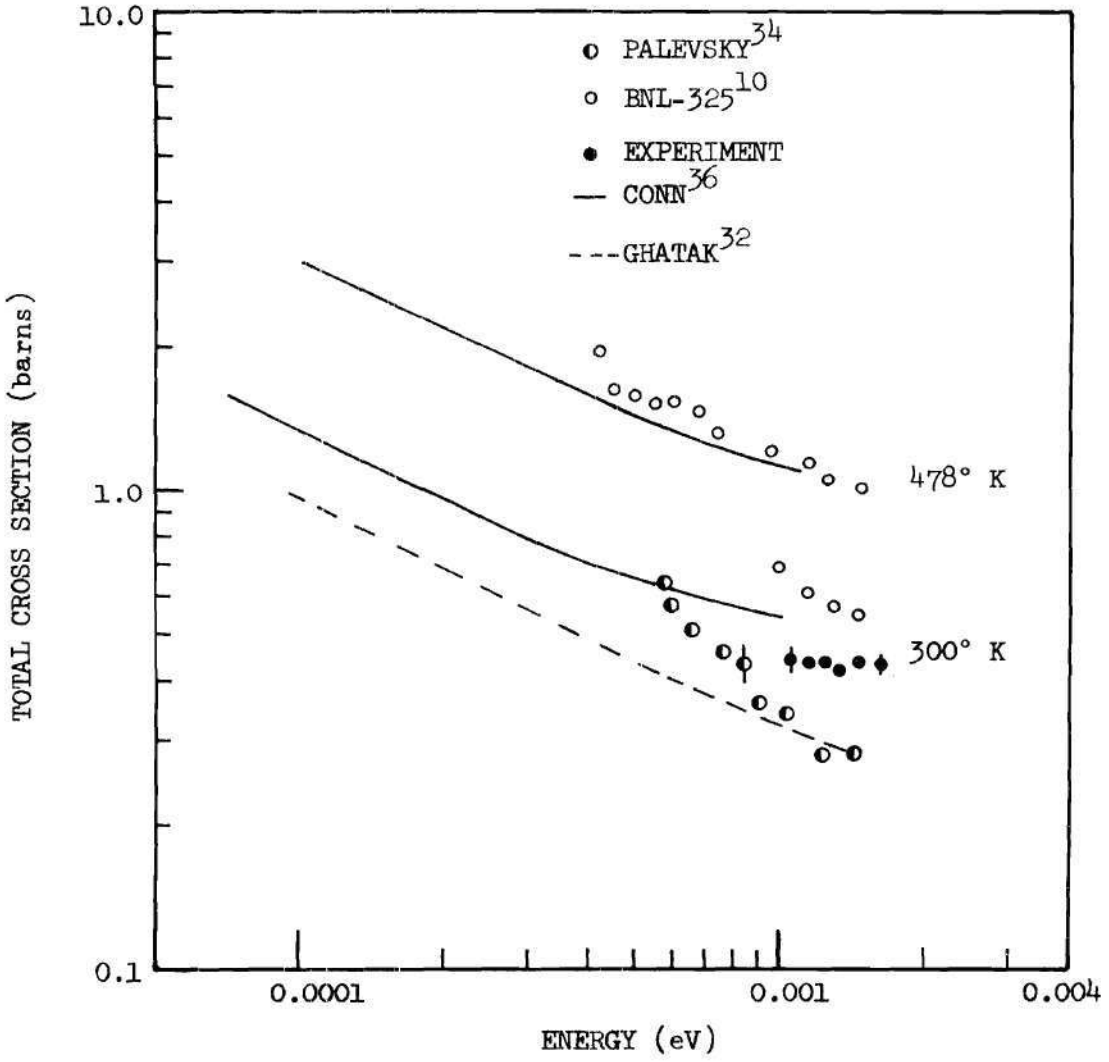

Figure 25. Comparison of Measured Total Cross Section for Graphite with Various Theoretical and Experimental Results

energies using an approximate and relatively better model for the graphite phonon frequency distribution. As seen in Figure 25, his results for the graphite total cross section at 478°K are in good agreement with the BNL-325 data, whereas at room temperature his results do not seem to compare very well with the BNL-325 data. This discrepancy between Conn's theoretical results and the BNL-325 data at room temperature can be seen in both the magnitude and the slope of the total cross section. Conn has not attempted to calculate the total cross section of graphite at other temperatures; thus, from his results at 478°K and at room temperature, we note that his calculation may not be predicting the temperature dependence of the total cross section properly. All the reported theoretical calculations of the total cross section of graphite have either been made with the incoherent approximation or with a one-phonon coherent calculation using crude approximations for the graphite phonon frequency distributions.

Measured sub-Bragg total cross sections of beryllium, beryllium oxide, and graphite at several energies are given in Table 7.

Results of the Theoretical Spectrum

The theoretical results of the adjoint Monte Carlo and the S_N calculations of the neutron energy spectra in finite beryllium systems are described in this section.

Results of Adjoint Monte Carlo Method

This section presents the results of the adjoint Monte Carlo calculation of the steady-state angle-dependent neutron energy spectrum in the positive z direction, at 10.2 cm from the source plane in a 14 x 14 x 20 inch long beryllium moderator at room temperature.

Table 7. Measured Sub-Bragg Total Cross Section of Beryllium, Beryllium Oxide, and Graphite at Room Temperature

	Energy (eV)	Total Cross Section (barns)	% Error
Beryllium Oxide	0.00296	0.4460	± 2.8
	0.00270	0.466	
	0.00240	0.485	± 3.6
	0.00220	0.505	
	0.00199	0.555	± 4.8
Beryllium	0.00446	0.448	± 2.3
	0.00355	0.451	
	0.00289	0.471	± 3.2
	0.00240	0.484	
	0.00202	0.560	± 4.2
Graphite	0.00147	0.427	± 3.5
	0.00136	0.420	
	0.00126	0.447	± 4.5
	0.00118	0.439	
	0.00110	0.440	± 6.5

These theoretical calculations have been made using the Placzek and the Gulf kernels to describe the thermal inelastic neutron scattering phenomena.

Figures 26 and 27 compare the energy transition probability distribution of the Placzek and Gulf scattering kernels for beryllium at room temperature for initial neutron energies of 0.0045, 0.035, and 0.0945 eV. We notice that the energy transfer from the above-Bragg to the sub-Bragg energy range is relatively small for the two kernels. Figure 28

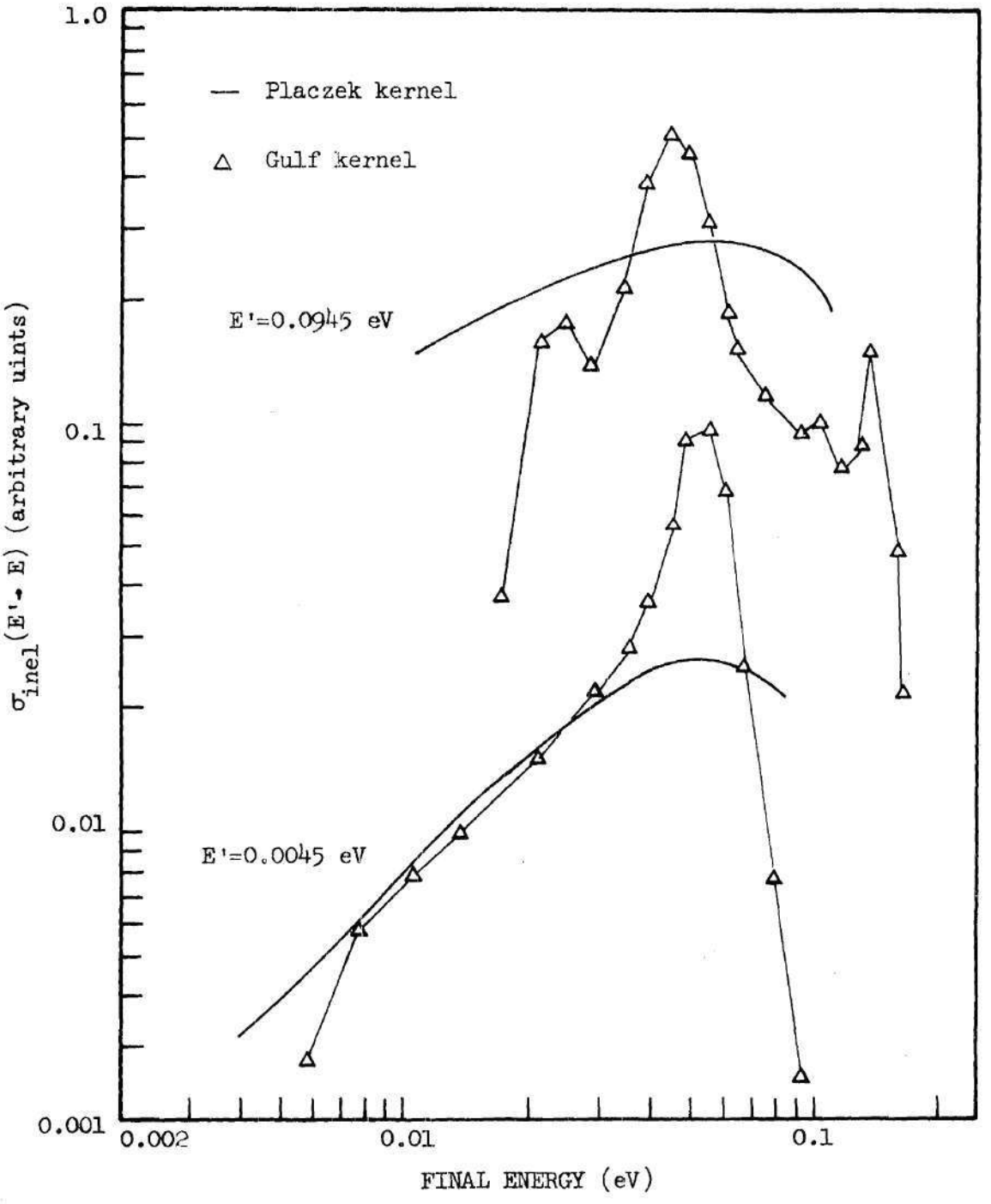

Figure 26. Energy Transition Probability Distribution of the Placzek and the Gulf Kernels of Beryllium for Initial Neutron Energies, 0.0045 and 0.0945 eV

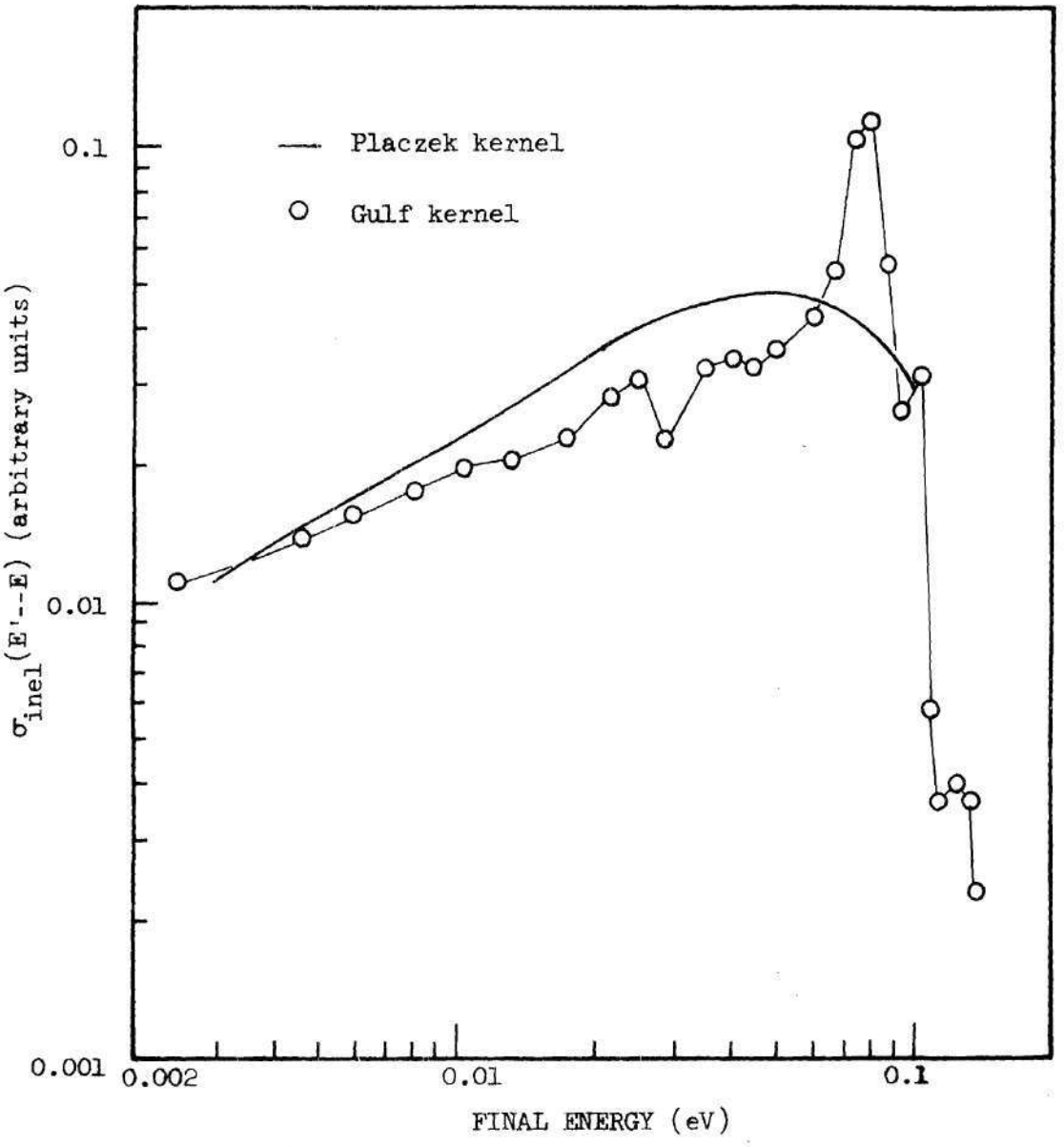

Figure 27. Energy Transition Probability Distribution of the Placzek and the Gulf Kernels for an Initial Neutron Energy of 0.035 eV

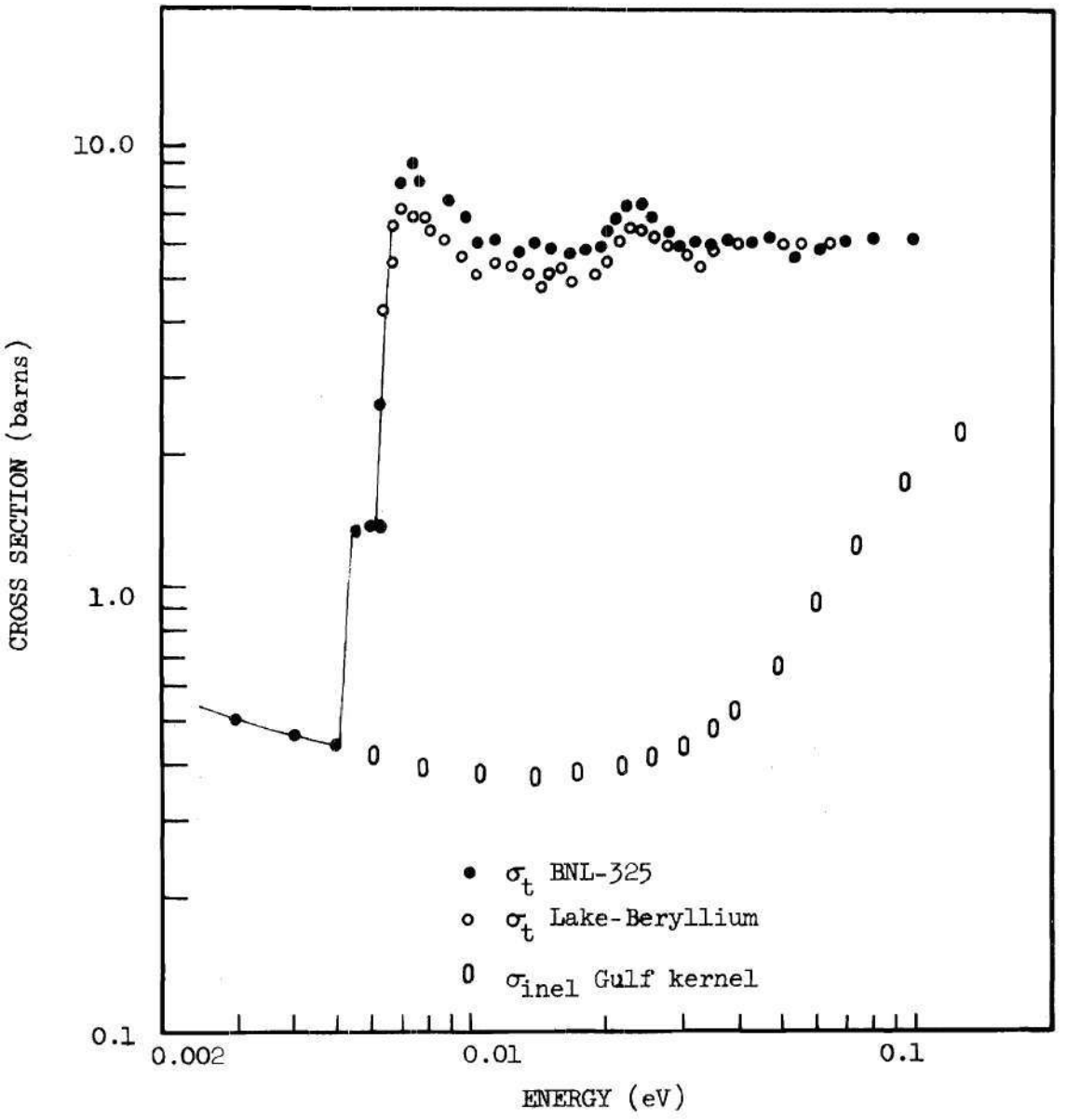

Figure 28. Measured and Calculated Microscopic Total and Inelastic Cross Sections of Lake-Beryllium at Room Temperature

shows the microscopic total and the inelastic cross section of Lake-beryllium at room temperature. Here the total cross section for Lake-beryllium, above the Bragg cut-off energy, has been taken from our measurement given in Figure 18 and the sub-Bragg total cross section is from Figure 15. Figure 28 also shows the total cross section of beryllium at room temperature obtained from BNL-325 cross section data.

The coherent elastic cross section of Lake-beryllium was influenced by the extinction effects due to the presence of large crystallite sizes. This effect can be clearly noted by comparing the BNL-325 data with our experimental results of the Lake-beryllium total cross section in Figure 28. In our Monte Carlo analysis of the neutron spectrum, we have used the measured cross section of Lake-beryllium, shown in Figure 28. We also note from Figure 28 that the inelastic cross section is relatively small over a wide range of energies. This and the shape of the inelastic scattering kernel, shown in Figures 26 and 27, indicate that, at room temperature, the energy transfer mechanism across the Bragg cut-off energy is rather weak in beryllium.

The adjoint Monte Carlo results of the neutron energy spectrum calculated with the Placzek kernel are shown in Figure 29 together with the experimental results of Lake and Kallfelz.[20,22,23] Figure 30 shows the same comparison for the calculation using the Gulf kernel. We notice from Figures 29 and 30 that our adjoint Monte Carlo theoretical analysis has been able to predict the significant spectrum distortion at the Bragg cut-off energy, which is about 0.0052 eV for beryllium. The theoretical spectrum calculated by using both the Placzek and the Gulf kernels yields essentially the same results, within the accuracy of the calculation, and

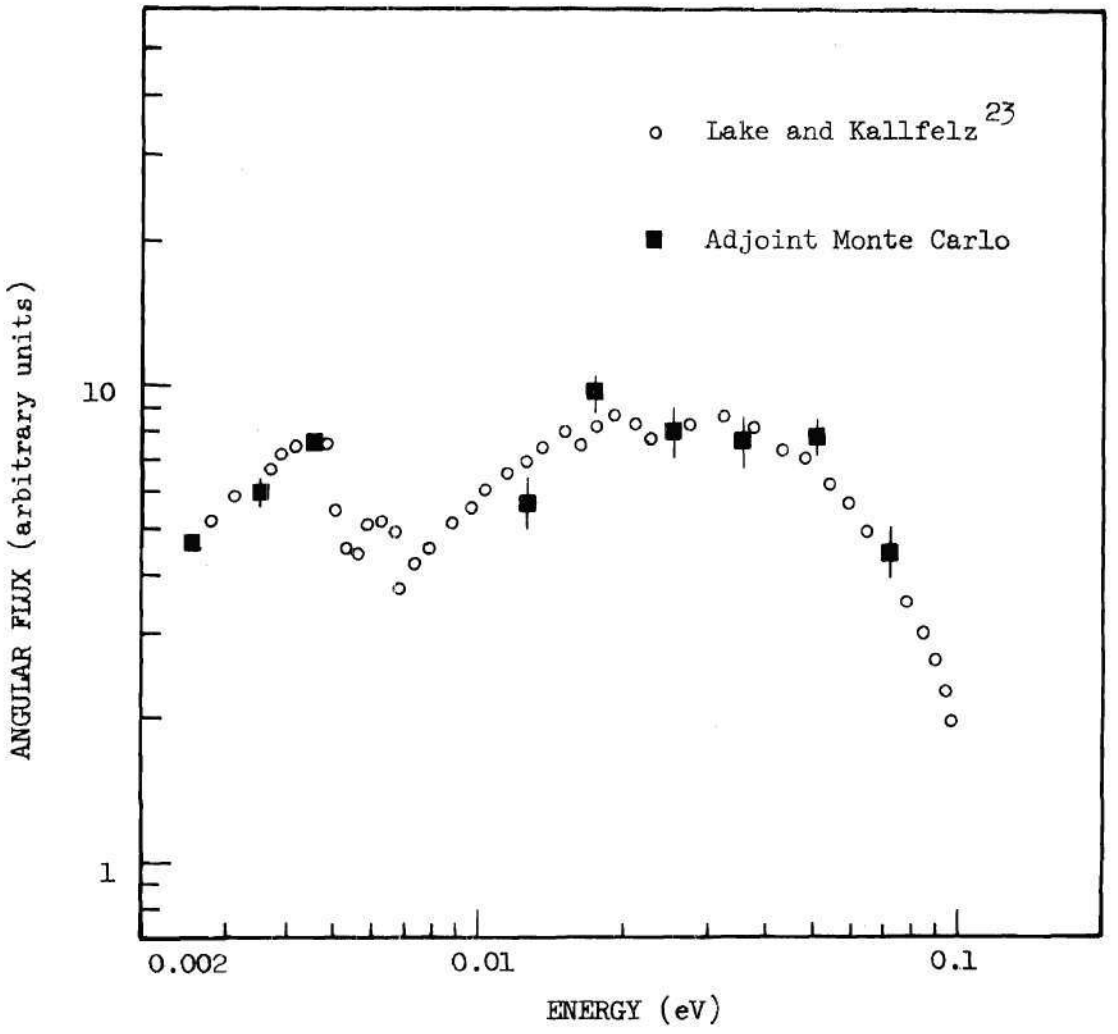

Figure 29. Adjoint Monte Carlo Results of the Spectrum in the Positive z Direction at 10.2 cm from the Source Plane in a 14 x 14 x 20 Inch Long Beryllium Block (Placzek Kernel)

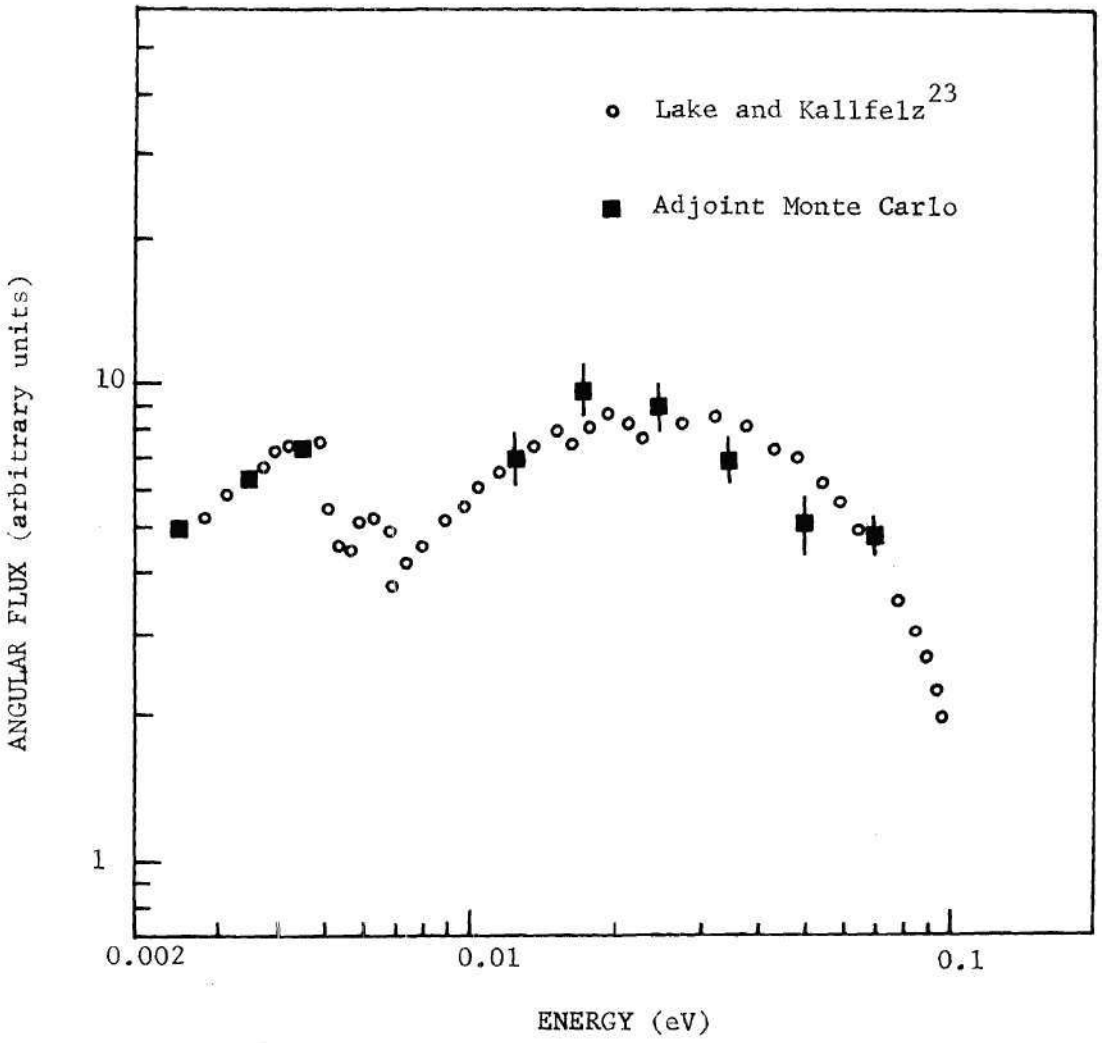

Figure 30. Adjoint Monte Carlo Results of the Energy Spectrum in the Positive z Direction at 10.2 cm from the Source Plane in a 14 x 14 x 20 Inch Long Beryllium Block (Gulf Kernel)

both are in good agreement with the experimental spectrum results. This indicates that, in beryllium at room temperature, because of the weak energy transfer, the experimental spectrum at 10.2 cm from the source plane is insensitive to the detailed description of the shape of the energy transfer probability distribution curve of the inelastic scattering kernel as long as the kernel can predict, on the average, the energy transfer across the Bragg cut-off energy. Because of the limit in the statistical accuracy of the adjoint Monte Carlo calculation and the use of a coarse energy structure, our calculation has been unable to bring out the small distortions in the above-Bragg region.

Even though the Placzek kernel is known to yield incorrect values for the inelastic cross section at higher energies, the shape of the normalized energy exchange probability distribution is quite comparable to the normalized Gulf kernel as seen in Figures 26 and 27. As we have seen, the normalized Placzek kernel does a good job of predicting the major features of the spectrum; refer to Figure 29.

If the spatial and angular dependence of the spectrum are treated accurately, then to theoretically predict the significant spectrum distortion at the Bragg cut-off energy in small beryllium systems at room temperature, it seems sufficient for the theoretical inelastic scattering kernel to predict accurately the average energy transfer across the Bragg cut-off energy.

Results of S_N Method

This section presents the results of the S_N theoretical analysis of the spatial behavior of the total energy spectrum in small beryllium systems with strong transverse leakage. This investigation was conducted to

check whether the critical size of the beryllium moderator is closer to 30 x 30 cm (diffusion theory limit[19]) or to 127 x 127 cm (asymptotic transport theory limit[9]) and to determine the applicability of diffusion theory for this case. The cross sections shown in Figure 28 for Lake-beryllium have been used in this analysis.

The neutron density weighted average energy is shown in Figure 31, as a function of the distance from the source plane in 150 cm long beryllium assemblies with transverse dimensions of 150 x 150 cm, 60 x 60 cm, and 35.56 x 35.56 cm. As seen from Figure 31, the average energy decreases as one moves away from the source plane and reaches a constant value at about 40 cm, indicating that the neutron distribution has reached an asymptotic condition. This means that the shape of the neutron energy distribution is not changing as a function of the distance from the source plane. However, in the other two beryllium assemblies the average energy progressively decreases even after 100 cm from the source plane, indicating a progressive build up of the sub-Bragg neutrons relative to the above-Bragg neutrons. This shows that, for these two assemblies, the transverse dimensions are below the critical size and that the neutron distribution fails to reach an asymptotic condition. This means that the critical dimensions for the beryllium moderator are definitely larger than 60 x 60 cm. This is in direct contradiction to the Ahmed et al.[19] diffusion theory analysis which predicts a critical size of 30 x 30 cm. Our analysis predicts that the critical size is somewhere between 60 x 60 cm and 150 x 150 cm, which agrees qualitatively with Williams' asymptotic transport theory predictions.[9]

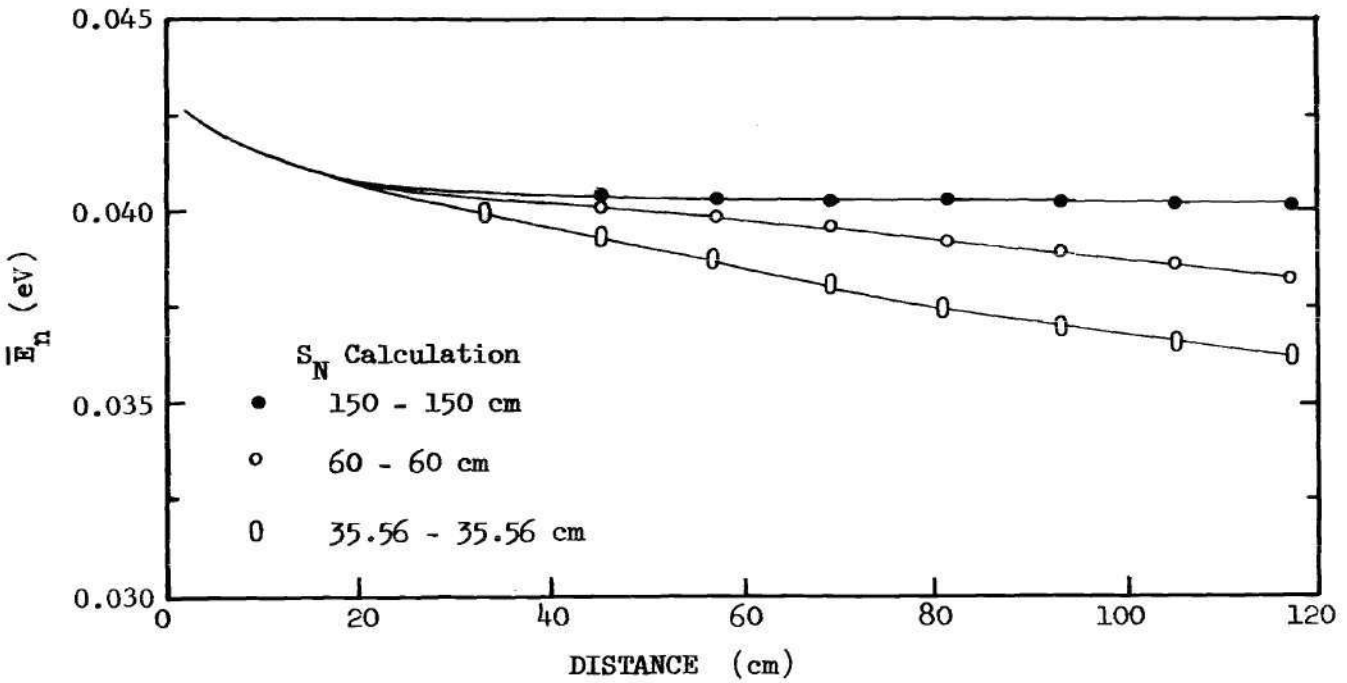

Figure 31. Behavior of the Average Energy with Distance from the Source Plane for the Total Energy Spectra in Beryllium Systems for Several Transverse Sizes

As discussed by Lake,[23] integral parameters, such as the average energy, are sometimes not sensitive enough to reflect small changes in the neutron energy spectrum. The spatial behavior of the neutron energy spectra is a more sensitive indicator in determining the establishment of an equilibrium condition. Therefore, the results of the spatial behavior of the total energy spectra are presented here.

Figure 32 shows the ratio of the angle integrated flux at 0.0045 eV to that at 0.035 eV ($\varphi_{cold}/\varphi_{th}$) as a function of the distance from the source plane in beryllium assemblies for several transverse dimensions. These calculations were made using the S_N method. We notice that, in the 150 x 150 cm beryllium assembly, the relative build up of the sub-Bragg neutrons in the spectrum reaches a constant value at about 55 cm from the source plane. In contrast, the relative build up of sub-Bragg neutrons in the other two beryllium assemblies increases in almost a linear fashion even after a distance of 120 cm from the source plane, showing no tendency to reach an asymptotic condition. This linear behavior seems to indicate that the cold and the thermal neutrons are decaying in space effectively as if they were independent of each other, a phenomenon also observed experimentally for the forward spectrum by Lake and Kallfelz.[23]

The ratio $\varphi_{cold}/\varphi_{th}$ for the 150 x 150 cm beryllium assembly has a gradual slope after a distance of 55 cm and is not noticeable in Figure 32. The ratio increases by 2% from 55 to 103 cm, i.e., in a distance of 48 cm. This is because the ANISN-solution has not converged completely even after a computational time of two and one-half hours. The increase of 2% in the ratio over a distance of 48 cm is small and we have assumed that the spectrum has reached an asymptotic condition. We did not continue

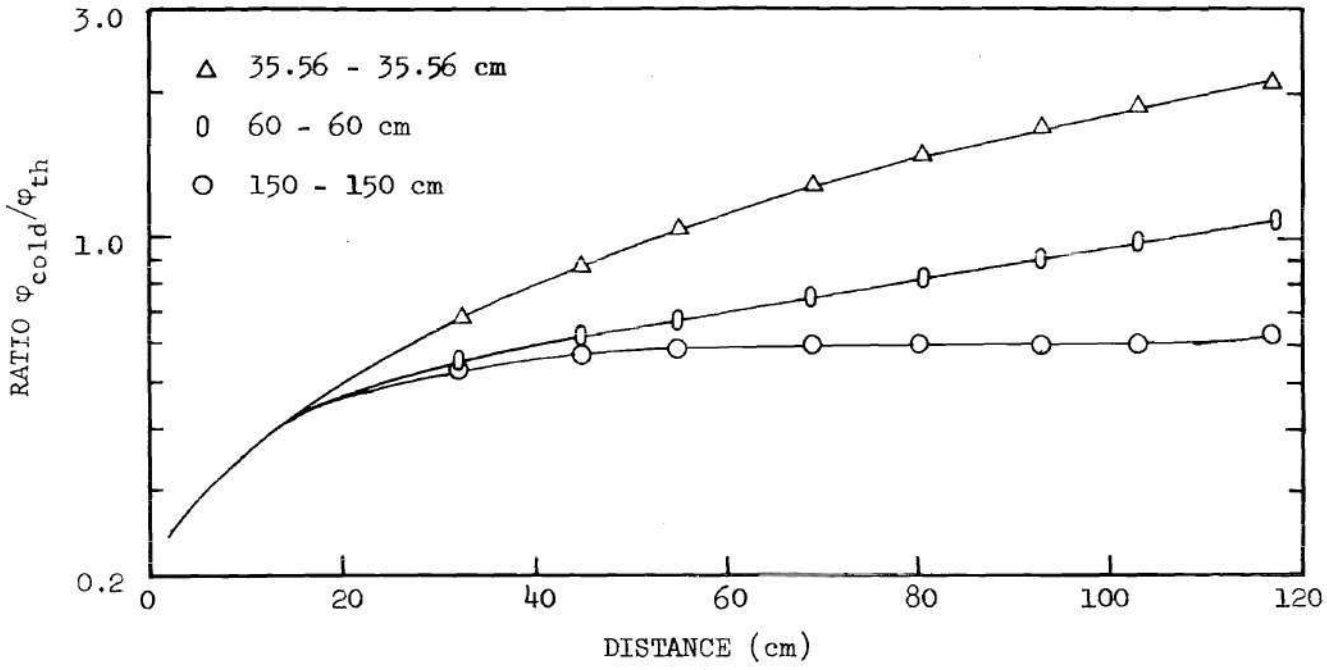

Figure 32. Spatial Behavior of the Ratio $\varphi_{cold}/\varphi_{th}$ in Beryllium Assemblies for Various Transverse Dimensions (S_N Calculation)

the ANISN calculation to obtain a completely converged solution since the rate of convergence was extremely slow.

Figure 33 shows the ratio, $\varphi_{cold}/\varphi_{th}$, as a function of distance from the source plane in beryllium assemblies with transverse dimensions of 150 x 150 cm, 60 x 60 cm, and 35.56 x 35.56 cm. This calculation was made using the diffusion theory option of the computer code ANISN. We notice that the diffusion theory calculations predict that the neutron spectrum reaches an asymptotic condition in beryllium assemblies with transverse dimensions as low as 35.56 x 35.56 cm.

From Figures 32 and 33, we notice that, in the 150 x 150 cm beryllium assembly, the diffusion theory calculation predicts a relative cold-neutron build up of 0.58 in comparison to a value of 0.6 as predicted by the S_N calculations, indicating the applicability of diffusion theory for this case. As the transverse size of the assembly is reduced, the diffusion theory heavily under-predicts the relative build up of cold neutrons. A similar behavior has been observed by Grover et al.,[56] who have analyzed the behavior of the spectrum in an infinite beryllium assembly as a function of the "poison" using the diffusion and the transport theory analyses. They have found that, as the poison concentration increases, i.e., when the spectrum distortion is more pronounced, the diffusion theory heavily under-predicts the spectral distortion and thus yields erroneous values for the spatial decay constant.

In our discrete S_N approximation analysis, recognizing the fact that there exists an additional loss term because of the transverse leakage, we have assumed that this loss term can be approximated by a diffusion theory leakage term, $D(E)\ B^2(E)$. This procedure is often used and

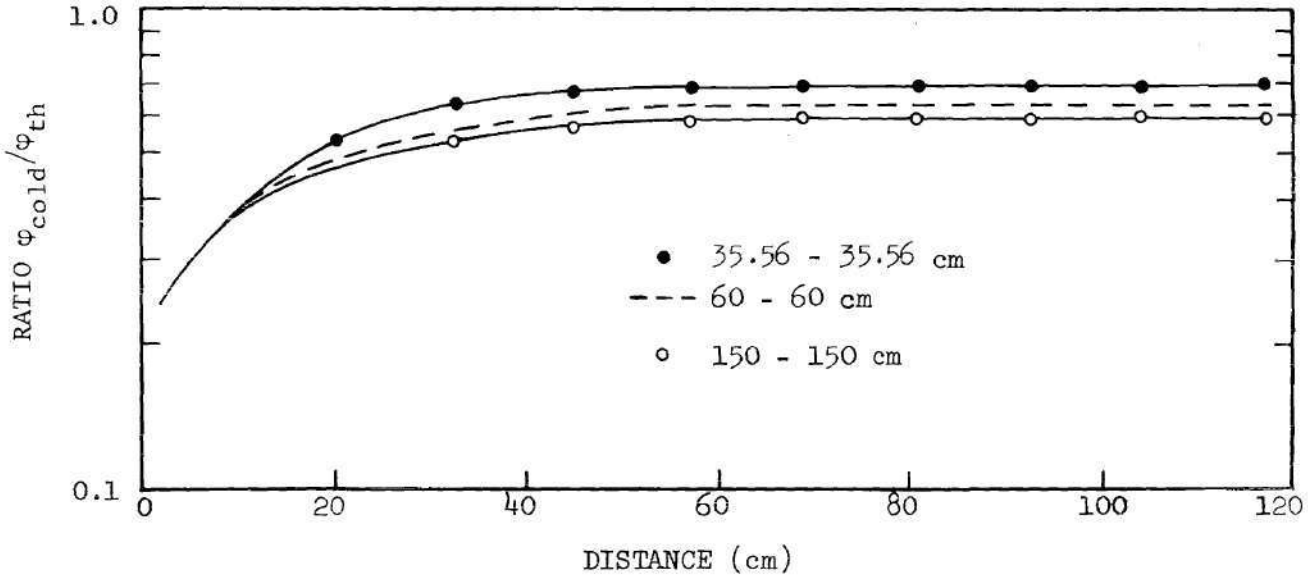

Figure 33. Spatial Behavior of the Ratio $\varphi_{cold}/\varphi_{th}$ in Beryllium Assemblies for Various Transverse Dimensions (Diffusion Theory)

has been used in the analysis of Ahmed et al.[19] The behavior of the neutron field in the z direction was treated by transport theory; i.e., no diffusion approximation was made in this direction. A closer look at this approximation is taken in Appendix C.

Let us consider the effect of introducing a $D(E)\ B^2(E)$ term, to represent the transverse leakage, on the calculated spectrum. This $D(E)\ B^2(E)$ term is independent of the direction and represents a constant loss factor for all directions, because of the way this term is treated in ANISN and several other 1-D S_N codes which we investigated. In contrast, the operators in the 3-D transport equation representing the transverse leakage, given by the second two terms of Equation 54, are directional dependent. For example, in the positive z direction, both the direction cosines η and ξ are zero and the transport of neutrons in the positive z direction has no direct influence from the leakage in the transverse directions; whereas, in our analysis the transport in the positive z direction is influenced by the loss factor $D(E)\ B^2(E)$. In beryllium this factor has a strong dependence on energy, primarily because of the large dip in the total cross section below the Bragg cut-off energy. For example, for a beryllium assembly with transverse dimensions of 35.56 x 35.56 cm, the ratio $\{D(E)\ B^2(E)/\Sigma_t(E)\}$ is of the order of 1% at above-Bragg energies and as high as 50% at below-Bragg energies.

One can raise the question about the accuracy of our conclusions with this approximation. For a qualitative discussion on the effect of the transverse leakage loss term $D(E)\ B^2(E)$, let us consider the spectrum in the positive z direction. As seen from Equation 54, in a "normal situation" there should be no direct transverse leakage loss term for the

positive z direction. But in our approximation the transport of neutrons in the positive z direction is directly influenced by the $D(E)\ B^2(E)$ term. This additional loss factor is a very large fraction of the total macroscopic cross section for sub-Bragg energies but not for above-Bragg energies. Thus, the sub-Bragg neutrons in the forward spectrum will be decaying in space at a significantly faster rate than in a "normal situation." The main effect noticeable for non-asymptotic decay is that the above-Bragg neutrons decay in space faster than the sub-Bragg neutrons. For the spectrum in the positive z direction, our analysis is in a way forcing the neutrons in the two energy ranges towards a condition more favorable for the establishment of asymptotic conditions than if the leakage term were angular dependent.

In short, if our analysis predicts a certain difference between the decay of cold and thermal neutrons in the forward flux as a function of distance, then in a "normal situation" the cold-neutron decay rate relative to the thermal neutrons will be even slower. Thus, we believe that the qualitative results and the conclusions concerning the non-asymptotic decay that were obtained using the $D(E)\ B^2(E)$ approximation would remain the same even if the correct transport equation were used for the analysis. A detailed discussion on this approximation is given in Appendix C.

Figure 34 shows the neutron energy spectrum at 57.0 cm from the source plane in a beryllium assembly with transverse dimensions of 35.56 x 35.56 cm at various angles. Comparing Figures 34 and 2, we note that our results are in good qualitative agreement with Williams' results[9] with respect to the dramatic anisotropic behavior of the flux at the Bragg cut-off energy. It should be noted that, if the transverse leakage corrections

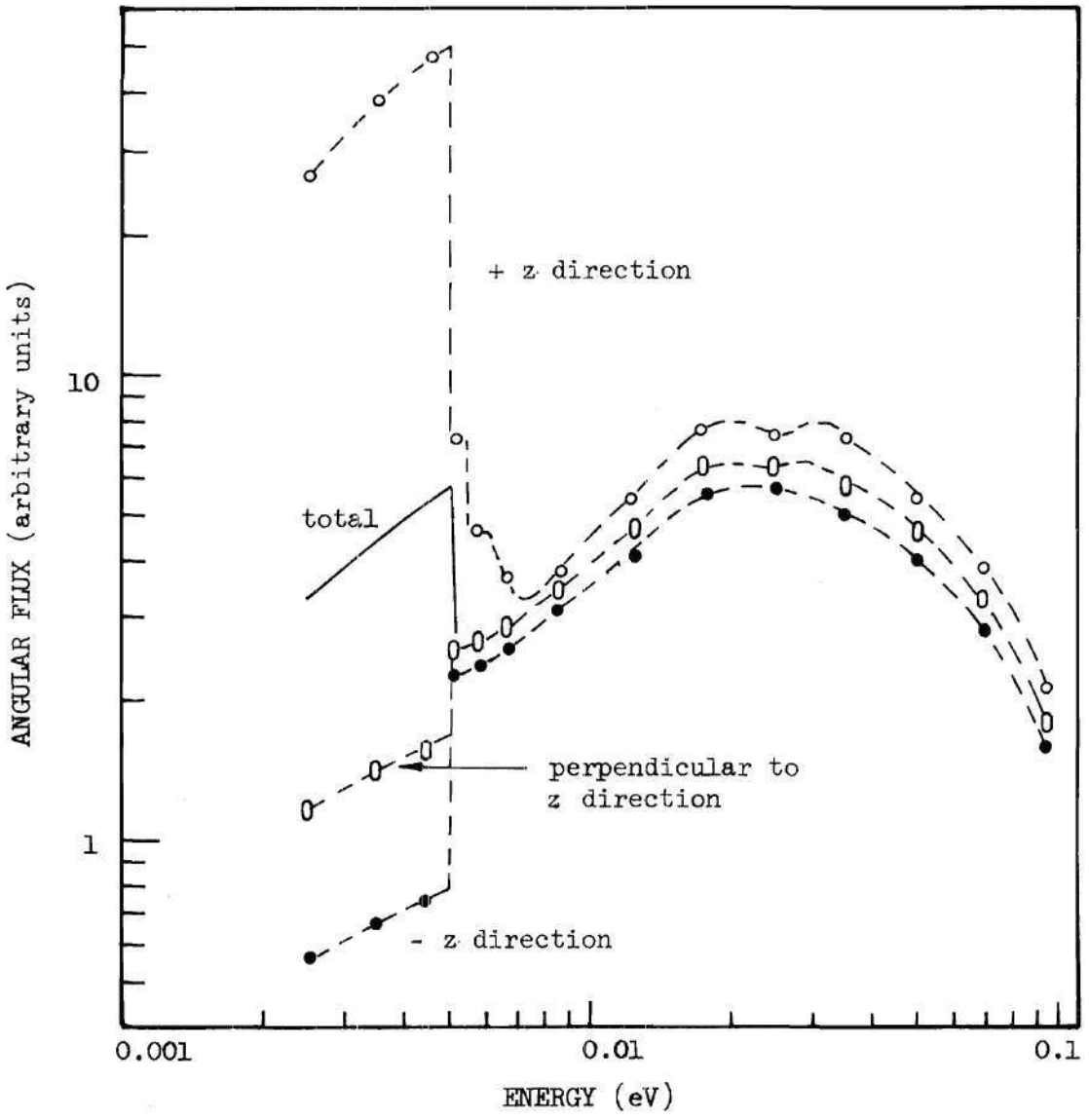

Figure 34. Neutron Energy Spectra in a 35.56 x 35.56 cm Beryllium Assembly at 57.0 cm from the Source Plane for Various z Directions (using B^2 approximation; see text)

were made angle-dependent, as they should be, the anisotropy would be even greater.

CHAPTER VI

CONCLUSIONS AND RECOMMENDATIONS

Cross Sections

Our measurements have accurately established the total cross section of beryllium, beryllium oxide, and graphite at room temperature in the sub-Bragg energy range. The sub-Bragg total cross section of these materials determines the value of $\Sigma_T(E)_{Min}$ which is a crucial parameter in establishing their critical sizes below which the neutron distribution fails to reach an equilibrium condition.

The measured sub-Bragg beryllium total cross section at room temperature is in excellent agreement with the BNL-325 data and also with the one-phonon coherent calculations of Borgonovi and Sprevak.[41] It can therefore be concluded that the sub-Bragg total cross section of beryllium has been established accurately.

Our measurement for beryllium oxide provides an accurate value of the room temperature, sub-Bragg total cross section for which there had been only one reported measurement by Zhezherun et al.[37,38] in which the sub-Bragg values are inaccurate. The experimental results show that the incoherent calculation of the thermal inelastic cross section yields an erroneous value of the sub-Bragg total cross section. It seems therefore necessary that a coherent model be developed for calculating the thermal inelastic cross section of beryllium oxide.

The measured sub-Bragg total cross section of graphite at room

temperature does not agree with any of the previously reported experimental or theoretical results. We feel that our measurement is accurate and it is not possible for us to draw any conclusion on the discrepancy between the experimental results as no details are available on the procedures or the analyses of the previously reported data. However, all the reported theoretical calculations of the thermal inelastic cross section for graphite have been made using either an incoherent approximation or an approximate model for describing the phonon frequency distribution. We, therefore, feel that a coherent calculation of the thermal inelastic cross section for graphite should be made using an accurate model for the phonon frequency distribution.

In brief, this investigation has been able to meet the objective of providing an accurate value of the sub-Bragg total cross section for beryllium, beryllium oxide, and graphite. Our measurements were limited to a small energy span below the Bragg cut-off energy of these materials. It is desirable to have a total cross section measurement covering a larger sub-Bragg energy range to determine the on-set of the λ-dependence of the total cross section, which is necessary to determine the limiting value of $v\,\Sigma_t(E)$ as the velocity variable approaches zero velocity. We could not attempt such an experiment as the neutron intensity in the GTRR thermal column was not sufficient to get any statistically meaningful results. At present the GTRR is being modified to raise the power level to 5 MW from the existing level of 1 MW. After this change the neutron intensity in the thermal column should increase in the same proportion and such an experiment might just be possible to undertake, at least for the beryllium and beryllium oxide moderators.

The measured above-Bragg total cross section of Lake-beryllium is consistently lower than the BNL-325 values showing the effect of extinction due to the presence of sufficiently large beryllium grains. We feel that with this measurement of the Lake-beryllium total cross section, the spectra measurements of Lake and Kallfelz[21,22,23] now form a complete set to be a benchmark test case.

Theoretical Spectra

The adjoint Monte Carlo analysis has produced good quantitative results in comparison with the experimental results of Lake and Kallfelz for the forward spectrum at 10.2 cm from the source plane in a 14 x 14 x 20 inch long block of beryllium. Unfortunately, due to poor particle statistics, the spectrum calculations at larger distances from the source plane could not be attempted.

Our adjoint Monte Carlo analysis is a very sophisticated one in which the full three-dimensional spatial domain has been retained and the scattering collisions have been treated accurately by using sophisticated scattering kernels. We have also proposed a simple scheme to treat exactly the anisotropy of the coherent elastic scattering collisions in the Monte Carlo method. It has been shown that the first term of the Placzek kernel has a broad shape for the energy exchange probability curve which is quite comparable to the more sophisticated Gulf kernel, and that it can do a good job of calculating the forward spectrum for this case. It has also been observed that the calculated spectrum is rather insensitive to the detailed shape of the inelastic energy exchange probability curve, as long as the inelastic kernel can predict the average energy transfer

across the Bragg cut-off energy. Our analysis has illustrated that the adjoint Monte Carlo method is advantageous over the corresponding forward Monte Carlo method for this class of problems where it is sufficient to know the fluxes at few energy points for studying the spatial behavior of the spectrum; this amounts to a reduction in the computer time for a given number of neutron histories to be followed with an increase in the statistical accuracy of the results.

Finally, the discrete ordinate S_N calculations with the energy dependent buckling approximation have shown that the equilibrium condition exists in the 150 x 150 cm beryllium assembly and that no equilibrium condition exists in the 60 x 60 cm or the 35.56 x 35.56 cm beryllium assemblies. This is in direct contradiction with the diffusion theory results of Ahmed et al.,[19] which predict that the equilibrium conditions can exist in beryllium assemblies with transverse dimensions as low as 30 x 30 cm. It should be noted that our diffusion theory analysis is also consistent with their analysis. We have shown that the diffusion theory is applicable in larger beryllium assemblies (150 x 150 cm), whereas for the smaller assemblies the theory is not applicable and yields erroneous results. These theoretical predictions are in direct agreement with the experimental results of Lake and Kallfelz,[20,22,23] who have discussed possible reasons for the failure of diffusion theory in small beryllium systems. Also, our results are in qualitative agreement with Williams' asymptotic transport theory analysis,[9] which predicts critical transverse dimensions of 127 x 127 cm.

The experimental investigations of Lake and Kallfelz were limited

to small beryllium assemblies with transverse dimensions less than 35.56 x 35.56 cm and they have studied the spatial behavior of the forward spectrum only up to distances of 40 cm from the source plane. Our S_N theoretical investigations have been made up to distances as far as 140 cm from the source plane in beryllium systems with large variations in their transverse dimensions.

Our S_N analysis is superior to the diffusion theory analysis of Ahmed et al., since the motion of neutrons in the z direction has been treated with transport theory and also, a more realistic representation of the anisotropy and the energy exchange mechanisms of the scattering collisions has been made.

The conclusion that can be drawn from this theoretical analysis is that the diffusion theory is not applicable for small beryllium systems with strong transverse leakage and one should be cautious in making quantitative conclusions regarding the critical transverse dimensions with the diffusion theory approximation.

APPENDIX A

MULTIPLE SCATTERING CORRECTION

In some of the total cross section measurements below the Bragg cut-off energy, it was necessary to keep the sample close to the detector to ensure that all the small-angle scattered neutrons entered the detector. In this sample-detector configuration, a fraction of those neutrons which undergo "normal" scattering in the sample would also enter the detector. Hence, it was necessary to correct the measured cross section data for the "multiple-scattering" contribution. Here by "multiple-scattering" contribution we mean the contributions from once scattered as well as more than once scattered neutrons.

This "multiple-scattering" contribution was calculated theoretically by the Monte Carlo method, previously described in Chapter IV. This analysis utilized a two energy-group structure, where the first and second energy groups represented the energy range below and above the Bragg cut-off energy, respectively. Isotropic scattering was assumed for both the elastic and inelastic scattering collisions. The geometry of the sample, the collimators, and the detector, as shown in Figure 6, was treated exactly.

When the sub-Bragg neutrons incident on the sample undergo a scattering event, they will always have an inelastic collision, since in this energy range the coherent elastic cross section is zero and the neutrons

have a very high probability of scattering into the higher energy range. Once the neutrons enter the high-energy group they almost always remain in this energy group. This is due to the fact that, for polycrystalline moderators like beryllium, beryllium oxide, and graphite, at room temperature, the inelastic cross section is very small in comparison to the coherent elastic cross section. Also, even if a neutron in this energy group has an inelastic collision, the probability of acquiring a sub-Bragg energy is very small.

The "multiple-scattering" contribution comes from those neutrons that collide in the sample and are scattered into the detector. This contribution depends on the sample thickness in mean free paths and the solid angle subtended by the detector at the sample. Since these two factors were small in our case, it was not possible to get any meaningful results by a direct Monte Carlo procedure. To overcome this disadvantage, the method of the expected leakage probability variance reduction scheme was utilized.

In this method a neutron is assigned a weight, w, at birth given by the non-leakage probability, $p^s = (1.0 - P^L)$, where $P^L = e^{-\Sigma_t d}$, Σ_t is the total cross section at energy E, and d is the distance to the boundary from the collision point in the flight direction $\bar{\Omega}$.

One supposes that a fraction, $w^L = P^L$, leaks out while a fraction, $w^s = P^s$, is retained. This latter fraction is now forced to make a collision somewhere on $(\bar{\Omega}x)$ by sampling from a truncated, normalized exponential distribution

$$P(x)dx = \frac{\Sigma_t(E)}{P^s} e^{-\Sigma_t(E)x} dx \qquad 0 \leq x \leq d \tag{71}$$

From this distribution the distance R to the next collision is chosen by random sampling as

$$R = - \frac{1}{\Sigma_t(E)} \log(1.0 - P^S R_N) \qquad (72)$$

where R_N is a random number which has values varying from 0 to 1, chosen from a uniform distribution. The above steps are repeated to determine a new weight for the neutron energy from this collision, after which one continues to the next collision. This method forces a neutron to always have a collision within the sample, and for this reason the neutron history is terminated by playing a Russian roulette game after the neutron's weight falls below a preset minimum.

There remains the question of the accuracy of the assumption of isotropic scattering and the use of only two energy groups in calculating the "multiple-scattering" contribution. To find an answer to this question, another Monte Carlo program was written which incorporated 21 energy groups. Also, the anisotropy of the thermal inelastic scattering collisions was described by the first term of the Placzek kernel as given by Equations 45 and 46 and the anisotropy of the coherent elastic scattering collisions was described by Equation 38.

To compare the results of two groups and 21 energy group programs, the beryllium total cross section measurements, for sub-Bragg energies, were used. As mentioned in Chapter III, this total cross section measurement was made with a 2.0 inch thick beryllium sample at 64.75 and 2.0 inches from the detector. As shown in Figure 35, the solid line represents

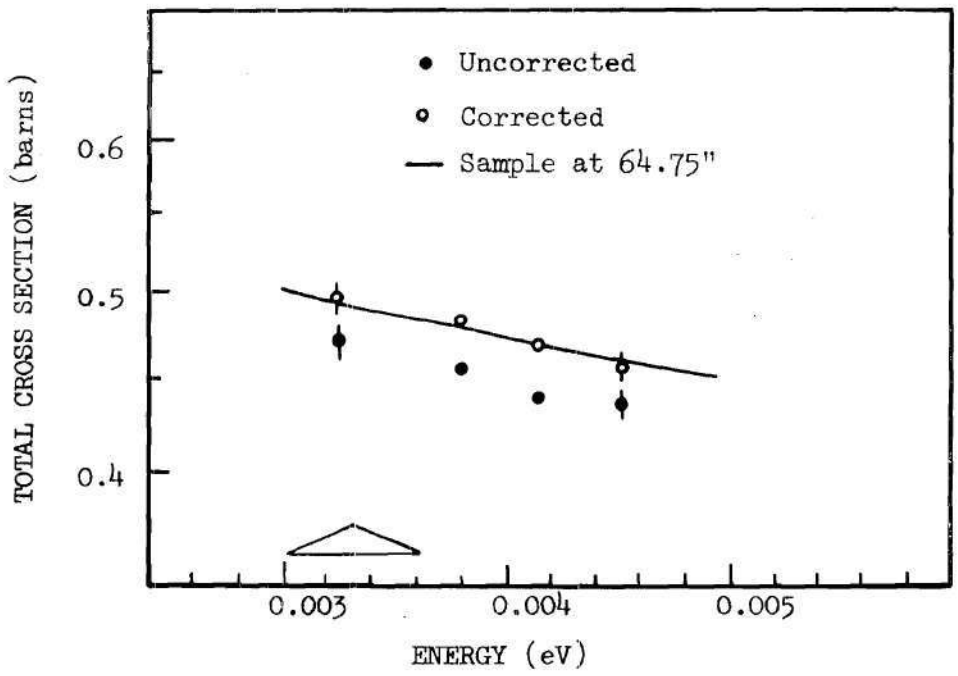

Figure 35. Effect of "Multiple-Scattering" Correction on Beryllium Cross Section Measured with Sample at 2.0 Inches

the beryllium sub-Bragg total cross section with the sample at 64.75 cm from the detector and the points represent the uncorrected cross section results in which the sample was at 2.0 inches from the detector. It has been established earlier that the small-angle scattering is negligible in beryllium and, therefore, the only significant parameter influencing this cross section measurement is the fraction of "multiple-scattered" neutrons entering the detector. As seen in Figure 35 the measured total cross section of beryllium with the sample at 2.0 inches away from the sample is lower than the solid line and this difference is indicative of the amount of "multiple-scattering" contribution.

To check the accuracy of the assumption of isotropic scattering, the 21 energy group program was used to calculate the "multiple-scattering" contribution for two cases, one with and the other without the assumption of isotropic scattering collisions. As seen in Table 8, the major difference appears in the contributions from the once collided neutrons. That is, the inclusion of an anisotropic component for the thermal inelastic interaction for the first collision yields a lower value for the "multiple-scattering" contribution. This is primarily because, in its first collision, the sub-Bragg neutrons incident on the sample will always have an inelastic scattering interaction for which the average cosine of the scattering angle is negative. Therefore, the sub-Bragg neutrons in their first collision are scattered more often away from the detector in comparison to the case where the isotropic scattering is assumed. It can also be observed from Table 8 that, from the second collision onwards, the "multiple-scattering" contribution is almost the same for both the isotropic and anisotropic cases, from which it can be postulated that, on the average for

the subsequent scatterings, the neutrons have forgotten their initial direction in the beam.

Table 8. "Multiple-Scattering" Contribution from Two- and 21-Group Programs with Isotropic and Anisotropic Scattering Assumptions

Number of Collisions	21 Energy Group		Two-Group
	Isotropic	Anisotropic	
1	0.00330	0.00181	0.00335
2	0.00196	0.00206	0.00235
3	0.00153	0.00148	0.00173
4	0.00111	0.00128	0.00124
5	0.00090	0.00090	0.00090
6	0.00079	0.00072	0.00079
Total	0.00961	0.00826	0.01040

Table 9 shows the results as calculated by the anisotropic 21 group and isotropic two group programs.

Table 9. The Effect of Two- and 21-Group "Multiple-Scattering" Correction on the Total Cross Section

Program	Multiple Scattering Contribution	Total Cross Section	
		Uncorrected	Corrected
2-group	0.01037	0.434	0.4589
21-group	0.00826	0.434	0.4517

We notice from Table 9 that the "multiple-scattering" contribution is about 25% higher than the 21 group program. However, the beryllium total

cross section, corrected for the "multiple-scattering" contribution, with these two programs differs by only 1.6%, whereas the experimental results have an accuracy of 2%. Figure 35 shows the beryllium total cross section results corrected for the "multiple-scattering" contribution as calculated by the two-group program. The figure shows that the corrected cross section is in excellent agreement with the beryllium total cross section measurement made with the sample at 64.75 inches from the detector. Thus, the 2-group program gives a reasonable estimation of the "multiple-scattering" contribution.

We have noted that the main reason for the discrepancy in the results of the 2-group program and the 21-group program is due to the assumption of isotropic scattering for the inelastic collisions. The results of the 2-group and the 21-group calculations given in Tables 8 and 9 were made for beryllium at a neutron energy of 0.0045 eV, where the final angular distribution of the inelastic collisions had an average cosine of the scattering angle, $\bar{\mu}$, equal to -0.16. The value of $\bar{\mu}$ for inelastic collisions in the sub-Bragg energy range covered in the total cross section measurement of beryllium, beryllium oxide, and graphite is within the range of $-0.11 \leq \bar{\mu} \leq -0.16$. The upper value of $\bar{\mu}$ occurs at energies just below the Bragg cut-off energy and the value of $\bar{\mu}$ moves closer to the isotropic value of $\bar{\mu} = 0$ as the energy decreases. Thus, the maximum error of $\pm$ 1.6% on the measured total cross section, due to the error in the calculated values of the "multiple-scattering" contribution using the 2-group program, is at the energy closer to Bragg cut-off energy and reduces as one moves to lower energies. To take this systematic error into account, the cross section results have been decreased systematically by 0.8% and

the error bars have been increased correspondingly.

Forward Random Walk Procedure

This section describes in detail the Monte Carlo procedure to calculate the "multiple-scattering" contribution. The sample-detector geometry used in the cross section measurement is given in Figure 6. The basic equation governing the random walk procedure is given in Equation 28. This description of the random walk procedure is for the 21-energy group structure with the anisotropy of elastic and inelastic collision incorporated in the analysis. The reduction of this analysis for the two-energy group structure with isotropic scattering is simple and straightforward.

The forward neutron random walk procedure is described in the following steps.

Step 1:

The neutron source coordinates g_o, $\bar{\Omega}_o$, and $\bar{r}_o$ are chosen from the source distribution $S_g(\bar{r},\bar{\Omega})$. The weight W_o of the neutron is set to be equal to 1.0.

The neutron source in all the cross section measurements was essentially a monoenergetic neutron beam for a given analyzer channel (the average energy is determined by the particular analyzer channel in consideration) uniformly distributed over an area of one inch in diameter with directions isotropically distributed in a cone with an apex angle of 50 minutes and centered around the positive z direction.

Step 2:

The weight of the neutrons, W, is modified as

$$W_P = (1.0 - e^{-\Sigma_t^{g_o} d}) \tag{73}$$

and

$$W = W_o \times W_P \tag{74}$$

where d is the distance to the boundary of the sample from the collision point in the direction $\bar{\Omega}_o$, and $(1-W_P)$ is the fraction of neutrons which leaks out.

Step 3:

The distance, ρ, to the next collision site is chosen as

$$\rho = -\frac{1}{\Sigma_t^{g_o}} \log(1.0 - W_P \cdot R1) \tag{75}$$

where R1 is a random number selected from a uniform distribution ranging from R1 = 0 to 1. Knowing ρ and $\bar{\Omega}_o$, it is a straightforward procedure to calculate the coordinates x_1, y_1, and z_1 of the collision site. It should be noted from the above equation that, when the random number R1 varies from 0 to 1, the value of ρ varies from 0 to d. That is, we are forcing the neutron to have a collision somewhere within the distance d, i.e., within the geometry of the sample.

Step 4:

The type of collision that the neutron can have at this collision site is determined by the inequality, $R_2 \leq \Sigma_{el}^g/\Sigma_S^g$, where Σ_{el}^g is the coherent elastic cross section. That is, if the chosen random number, R_2, is less than or equal to the ratio, Σ_{el}^g/Σ_S^g, then the neutron is assumed to undergo a coherent elastic scattering collision. Otherwise, the neutron is assumed to undergo an inelastic collision.

Step 5:

The scattered neutron energy group, g_1, is selected from the distribution

$$\frac{\Sigma_*^{g_o \to g}}{\sum_g \Sigma_*^{g_o \to g}} \tag{76}$$

and the new direction, $\bar{\Omega}_1$, is selected from the distribution

$$\frac{\Sigma_*^{g_o \to g_1}(\bar{\Omega}_o \to \bar{\Omega})}{\int d\bar{\Omega}\, \Sigma_*^{g_o - g_1}(\bar{\Omega}_o \to \bar{\Omega})} \tag{77}$$

where the subscript, *, refers to the elastic or the inelastic collision depending on the type of the scattering collision the neutron is experiencing.

Step 6:

The weight of the neutron after the collision is modified by the non-absorption probability, Σ_S^g/Σ_t^g, since we did not allow the neutron to be absorbed at any collision.

Step 7:

This step estimates the fraction of the neutron contribution at the detector from each collision site. At each collision site, if the neutron direction is such that it can reach the detector, one estimates the probability that this neutron does not collide in the remaining distance from the collision point to the boundary of the sample along the neutron direction times the probability that it does collide in the

detector. Knowing the scattered neutron direction, $\bar{\Omega}_1$, check to see if the neutron can pass through the detector. If it does not, then no scoring is made; otherwise, the scoring is done by the following steps:

A. Knowing the coordinates x_1, y_1, and z_1 of the collision site and the neutron direction $\bar{\Omega}_1$, it is a straightforward procedure to calculate the distance, L_S, from the collision site to the boundary of the sample. Then the weight of the neutron at the sample boundary is given by

$$W_S = W\, e^{-\Sigma_t^{g_1} L_S} \tag{78}$$

B. Calculate the intercept, L_o across the detector along the neutron direction $\bar{\Omega}_1$. The probability that the neutron interacts within the detector is given by

$$W_D = 1.0 - e^{-\Sigma_{t_D}^{g_1} L_o} \tag{79}$$

where $\Sigma_{t_D}^{g_1}$ is the macroscopic total cross section of the BF_3 gas contained in the detector for the energy group g_1.

C. The "multiple-scattering" contribution from this collision is then given by

$$F = W_S \cdot W_D \tag{80}$$

D. When a neutron history is terminated, the process is started from Step 1; otherwise, the process goes back to Step 2.

The neutron history was terminated when the neutron weight was

negligibly small or after the "multiple-scattering" contributions from six neutron collisions were recorded.

APPENDIX B

ERROR ANALYSIS AND ENERGY RESOLUTION

A typical cross section experiment used a TMC channel width of 64 μ sec, a chopper speed of 1800 RPM, a flight path of 2.648 meters, and a sample thickness of 4.666 cm with a number density of 0.0695 mol/cm^3. The energy range of interest was from 0.00307 to 0.00193 eV, which corresponded to analyzer channels 67 to 81. The data from these 15 channels were reduced to 5 data values by averaging 3 channels together.

The central limit theorem of probability theory states that by adding a large number of functions of arbitrary form one obtains a function which is nearly a Gaussian,[57] where the square of the standard deviation of the resultant function is equal to the square of the standard deviation of all the partial functions, assuming that none of these functions contains a systematic error. If σ_T is the standard deviation of the resultant function and $\sigma_1, \sigma_2, \ldots$ are the standard deviations of the partial functions, we have

$$\sigma_T^2 = \sigma_1^2 + \sigma_2^2 + \ldots \tag{81}$$

Also, the standard deviation of a function u, which is a function of uncorrelated variables y, z, . . ., etc., is given by

$$\sigma_u^2 = \sigma_y^2 \left(\frac{\partial u}{\partial y}\right)^2 + \sigma_z^2 \left(\frac{\partial u}{\partial z}\right)^2 + \ldots \quad (82)$$

Error Analysis

The total microscopic cross section, x, in barns is given by

$$x = \frac{1}{ND_o} \log \left\{\frac{PO}{QO-G}\right\} \quad (83)$$

where N is the sample number density, D_o is the sample thickness, G is the fraction of scattered neutrons entering the detector, PO and QO are the number of neutron counts observed in the analyzer channels for without- and with-sample measurements.

A typical set of raw experimental data is given in Table 10. Let P1, P2, and P3 be the neutron counts in a given three analyzer channels and BO be the average neutron background. The PO is given by

$$PO = (P1 + P2 + P3 - 3\ BO)/3.0 \quad (84)$$

Using Equation (82), the standard deviation is given by

$$\sigma_{PO}^2 = (\sigma_{P1}^2 + \sigma_{P2}^2 + \sigma_{P3}^2 + 3\sigma_{BO}^2)/9.0 \quad (85)$$

Noting that, $\sigma_{P1}^2 = P1$, $\sigma_{BO}^2 = BO$, etc.

$$\sigma_{PO}^2 = (P1 + P2 + P3 + 3\ BO)/9.0 \quad (86)$$

Table 10. Typical Raw Experimental Data

		Neutron Counts	
		Without Sample	With Sample
Average Background		2493	2407
Monitor Counts		3472733	3465388
Multiple Scattering Correction		0.00474 ± 0.0001	
Detector Efficiency		0.7153 ± 0.014	
Sample Thickness (cm)		4.666 ± 0.01	
Number Density (mol/cm^3)		0.0695 ± 0.002	
Channel Number	Energy (eV)		
70	0.002853	46463	40435
71	0.002753	42302	36702
72	0.002659	37953	33228

Using values from Table 10, the fractional uncertainty $\sigma_{PO}/PO = 0.31\%$. The detector dead time was found to be negligible, primarily due to the reduction of beam size by the use of a one inch diameter collimator and the intensity of the source neutrons from the thermal column is small in the sub-Bragg energy range.

Let Q1, Q2, and Q3 be the number of neutrons recorded in three consecutive channels with the sample in the neutron beam and let B1 be the average neutron background. The value of QO is

$$QO = (Q1 + Q2 + Q3 - 3\ B1)/3.0 \tag{87}$$

and the standard deviation of QO is

$$\sigma_{QO}^{2} = (Q1 + Q2 + Q3 + 3\ B1)/9.0 \tag{88}$$

Using the values from Table 10, the fractional uncertainty $\sigma_{QO}/QO = 0.33\%$. The average energy corresponding to the value of PO and QO can be obtained by averaging the corresponding energies of the three consecutive channels.

Let y be the number of uncollided and small-angle scattered neutrons as seen by the detector, then

$$y = QO - (PO/\varepsilon)M \tag{89}$$

where M is the "multiple-scattered" neutron contribution per incident neutron on the sample and ε is the detector efficiency at the corres-

ponding average neutron energy. Using Equation 82, the standard deviation of y is given by

$$\sigma_y^2 = \sigma_{QO}^2 + \sigma_{PO}^2 \left(\frac{M}{\epsilon}\right)^2 + \sigma_M^2 \left(\frac{PO}{\epsilon}\right)^2 + \sigma_\epsilon^2 \left(\frac{PO}{\epsilon^2 M}\right)^2 \tag{90}$$

Using the values from Table 10, the fractional uncertainty of y is σ_y/y = 0.34%. Define

$$K = \log\left(\frac{PO}{y}\right) \tag{91}$$

and by Equation 82

$$\sigma_K^2 = \sigma_{PO}^2 \left(\frac{1}{PO}\right)^2 + \sigma_y^2 \left(\frac{1}{y}\right)^2 \tag{92}$$

The fractional uncertainty of K is σ_K/K = 3%. Substituting Equation 91 into Equation 83, the cross section x is given by

$$x = \frac{K}{ND_o} \tag{93}$$

and

$$\sigma_x^2 = \sigma_K^2 \left(\frac{1}{ND_o}\right)^2 + \sigma_N^2 \left(\frac{K}{N^2 D_o}\right)^2 + \sigma_D^2 \left(\frac{K}{ND_o^2}\right)^2 \tag{94}$$

The fractional uncertainty in the cross section, x, is given by σ_x/x = 3.2%.

Energy Resolution

The uncertainty in the measured time of flight is composed of the chopper pulse duration and the analysis channel width. There is also an uncertainty in the flight path equal to d, the effective detector thickness, which leads to a flight time uncertainty, $\Delta t = d/v$, where v is the neutron velocity.

The chopper pulse duration is given by[58,59,60]

$$T = \frac{h}{2\omega r} ; \qquad \text{for } v > \frac{\omega r^2}{h} \tag{95}$$

$$= 2\left(\frac{h}{\omega v}\right)^{\frac{1}{2}} - 2\frac{r}{v} ; \qquad v < \frac{4\omega r^2}{h}$$

where h is the chopper slit height, ω is the chopper angular velocity, and r is the chopper slit width. The shape of the chopper pulse is approximately triangular in form with a base width T.

The standard deviation of the triangular chopper pulse can be expressed as[58]

$$\sigma_1^2 = \frac{1}{6} T^2 \tag{96}$$

The standard deviation of the rectangular analysis channel of width, t, is given by

$$\sigma_2^2 = \frac{1}{12} t^2 \tag{97}$$

The resolution function associated with the uncertainty in the flight distance due to the detector thickness has been assumed to be

rectangular in shape with a base width of $\Delta t = d/v$. Therefore,

$$\sigma_3^2 = \frac{1}{12}\frac{d^2}{v^2} \tag{98}$$

Using Equation 81, the resultant standard deviation of the time of flight is given by

$$\sigma_t^2 = \sigma 1^2 + \sigma_2^2 + \sigma_3^2 \tag{99}$$

that is,

$$\sigma_t^2 = \frac{1}{6}T^2 + \frac{1}{12}\left(t^2 + \frac{d^2}{v^2}\right) \tag{100}$$

The half width, Δt, that is, the width at half amplitude of a Gaussian function, is given by

$$\Delta t = 2.354\,\sigma_t \tag{101}$$

and

$$v = \frac{L}{t} \tag{102}$$

$$E \propto \frac{L^2}{t^2} \tag{103}$$

where E is the neutron energy and L is the flight path. Therefore,

$$\frac{\Delta E}{E} = 2v\,\frac{\Delta t}{L} \tag{104}$$

If E is measured in units of eV, and $\Delta t/L$ in units of seconds per

meter, we have

$$\frac{\Delta E}{E} = 0.028 \ (E)^{\frac{1}{2}} \ \frac{\Delta t}{L} \times 10^{-6} \tag{105}$$

From Equation 101

$$\frac{\sigma_E}{E} = \frac{\Delta E}{2.354 \ E} \tag{106}$$

The inaccuracy in measuring the flight path and the flight time should also be considered. Equation 103 gives the neutron energy in relation to the flight time and the flight path. The uncertainty in the energy due to the inaccuracy in measuring the flight time and path is

$$\frac{\sigma_E^2}{E^2} = 4 \left(\frac{\sigma_L^2}{L^2} + \frac{\sigma_t^2}{t^2} \right) \tag{107}$$

The inaccuracy in measuring the flight distance has been estimated to be 0.62 cm in a flight distance of 2.65 meters and, therefore, $\sigma_L/L = 0.48\%$.

The inaccuracy in measuring the flight time can be estimated from Equation 11. The angular preset delay has been estimated to be 3%. The uncertainty in the 82 μ sec delay between the photo transistor pulse and the trigger pulse to the TMC has been estimated to be 2%. The uncertainties in the chopper speed and the channel width are negligible and have not been considered.

From the uncertainties given by Equations 106 and 107, the resultant uncertainty can be obtained by using Equation 81. Table 11 shows

the total uncertainty in the measured neutron energy at several chopper speeds and energies.

Table 11. Total Uncertainty in the Measured Neutron Energy at Several Chopper Speeds

Chopper Speed (RPM)	Energy (eV)	$\frac{\Delta E}{E}$	$\frac{\sigma_E}{E}$
1800	0.0013	0.0666	0.0283
	0.0025	0.0873	0.0371
	0.0035	0.1008	0.0458
1800	0.0075	0.119	0.0506
	0.025	0.209	0.0887
	0.05	0.294	0.125
3954	0.0075	0.0649	0.0276
	0.025	0.1065	0.0452
	0.05	0.1457	0.0618

APPENDIX C

DISCUSSION ON APPROXIMATING THE TRANSVERSE LEAKAGE TERM IN 1-D TRANSPORT THEORY

Consider the transport equation in the rectangular geometry given by Equation 54. Expanding the flux, $\varphi(\bar{r},E,\bar{\Omega})$ in spherical harmonics and retaining only the first two terms, we have[49]

$$\varphi(\bar{r},E,\bar{\Omega}) = \frac{1}{4\pi}\left\{\varphi(\bar{r},E) + 3[\mu\ J_Z(\bar{r},E) + \sin\theta\ \sin\psi\ J_y(\bar{r},E) + \sin\theta\ \cos\psi\ J_x(\bar{r},E)]\right\} \tag{108}$$

where the direction cosines are given by

$$\mu = \cos\theta \tag{109}$$

$$\eta = \sin\theta\ \cos\psi \tag{110}$$

$$\xi = \sin\theta\ \sin\psi \tag{111}$$

These are shown in Figure 11. The total angular integrated flux is given by

$$\varphi(\bar{r},E) = \int d\bar{\Omega}\ \varphi(\bar{r},E,\bar{\Omega}) \tag{112}$$

and J_x, J_y, and J_z are the components of the neutron current density along

the x, y, and z axis.

Assuming Fick's law we have

$$J_x(\bar{r},E) = - D(E) \frac{\partial\varphi(\bar{r},E)}{\partial x} \tag{113}$$

$$J_y(\bar{r},E) = - D(E) \frac{\partial\varphi(\bar{r},E)}{\partial y} \tag{114}$$

$$J_z(\bar{r},E) = - D(E) \frac{\partial\varphi(\bar{r},E)}{\partial z} \tag{115}$$

Substituting Equations 113, 114, and 115 into Equation 108, we have

$$\varphi(\bar{r},E,\bar{\Omega}) = \frac{1}{4\pi}\left\{\varphi(\bar{r},E) - 3\,D(E)\left[\mu \frac{\partial\varphi(\bar{r},E)}{\partial z} + \sin\theta \sin\psi \frac{\partial\varphi(\bar{r},E)}{\partial y} + \sin\theta \cos\psi \frac{\partial\varphi(\bar{r},E)}{\partial x}\right]\right\} \tag{116}$$

Assuming

$$\varphi(\bar{r},E) = \varphi(z,E) \cos(B_x(E)x) \cos(B_y(E)y) \tag{117}$$

where the transverse buckling for a square block is given by

$$B_x^2(E) = B_y^2(E) = \left\{\frac{\pi}{D_T + 1.42\,\lambda_{tr}(E)}\right\}^2 \tag{118}$$

and the terms are defined in Equation 67. The energy dependence of B_x, B_y, and D will be suppressed for the sake of convenience.

Substituting Equation 117 into Equation 116, we have

$$\varphi(\bar{r},E,\bar{\Omega}) = \frac{1}{4\pi}\Big[\varphi(z,E)\cos(B_x x)\cos(B_y y) \tag{119}$$

$$- 3D\Big\{\mu\cos(B_x x)\cos(B_y y)\frac{\partial\varphi(\bar{r},E)}{\partial z}$$

$$+ \sin\theta\sin\psi\,\varphi(z,E)\cos(B_x x)(-B_y)\sin(B_y y)$$

$$+ \sin\theta\cos\psi\,\varphi(z,E)(-B_x)\sin(B_x x)\cos(B_y y)\Big\}\Big]$$

Therefore, at x=0 and y=0, that is, along the z axis, we have

$$\frac{\partial\varphi(\bar{r},E,\bar{\Omega})}{\partial y}_{x=y=0} = \frac{3D}{4\pi}\sin\theta\sin\psi\,B_y^2\,\varphi(z,E) \tag{120}$$

and

$$\frac{\partial\varphi(\bar{r},E,\bar{\Omega})}{\partial x}_{x=y=0} = \frac{3D}{4\pi}\sin\theta\cos\psi\,B_x^2\,\varphi(z,E) \tag{121}$$

Substituting Equations 120 and 121 into Equation 54, the transport of neutrons along the z axis is given by

$$\mu\frac{\partial\varphi(z,E,\bar{\Omega})}{\partial z} + \frac{3D(E)}{4\pi}\sin^2\theta\,\{\sin^2\psi\,B_y^2 + \cos^2\psi\,B_x^2\} \tag{122}$$

$$\times\,\varphi(z,E) + \Sigma_t(E)\,\varphi(z,E,\bar{\Omega}) = Q(z,E,\bar{\Omega})$$

Integrating over ψ and using Equations 60, 61, and 62, we have

$$\mu\frac{\partial\varphi(z,E,\mu)}{\partial z} + \frac{3}{4}D(E)\,B^2(E)\sin^2\theta\,\varphi(z,E) + \Sigma_t(E)\,\varphi(z,E,\mu) \tag{123}$$

$$= Q(z,E,\mu)$$

where the transverse buckling $B^2(E)$ is defined in Equation 67 and $Q(z,E,\mu)$ is given by Equation 62.

As mentioned in Chapter IV, we have used the computer code ANISN[49] to analyze the behavior of $\varphi(z,E,\mu)$ in beryllium moderators for different transverse dimensions. In ANISN, the assumption is made that the effect of the transverse leakage could be approximated by adding the term, $D(E)\ B^2(E)\ \varphi(z,E,\mu)$, to the one-dimensional transport equation. This means that we are solving an equation of the form

$$\mu\ \frac{\partial F(z,E,\mu)}{\partial z} + D(E)\ B^2(E)\ F(z,E,\mu) + \Sigma_t(E)\ F(z,E,\mu) = Q^*(z,E,\mu) \qquad (124)$$

where the function Q^* is the same as the function Q except that $\varphi(z,E,\mu)$ is replaced by $F(z,E,\mu)$. The function F has the same definition as that of the function φ. It is desirable to solve Equation 123, instead of Equation 124, since the derivation of it can be mathematically justified within the framework of the assumptions that were made while deriving Equation 123.

The main difference between the two equations (123 and 124) is in the second term which describes the transverse leakage. In Equation 123, the coefficient in the second term is angle-dependent, whereas it is not so in Equation 124. However, the interesting part is that, when these two equations are integrated over $d\mu$ from -1 to +1, they are transformed into a set of integral equations which are identical in their formulation.

From Equation 123 we have

$$\int d\mu\ \mu\ \frac{\partial \varphi(z,E,\mu)}{\partial z} + \{\Sigma_t(E) + D(E)\ B^2(E)\}\ \varphi(z,E) \qquad (125)$$

$$= S(z,E) + \int dE'\ \Sigma_{SO}(E' \rightarrow E)\ \varphi(z,E)$$

and from Equation 124 we have

$$\int d\mu\ \mu\ \frac{\partial F(z,E,\mu)}{\partial z} + \{\Sigma_t(E) + D(E)\ B^2(E)\}\ F(z,E) \qquad (126)$$

$$= S(z,E) + \int dE'\ \Sigma_{SO}(E' \rightarrow E)\ F(z,E)$$

Here it should be noted that, when the source term $Q(z,E,\mu)$, defined by Equation 62, is integrated over $d\mu$, all the terms vanish except the $\ell=0$ term.

Comparing Equations 125 and 126, we notice that the two integral equations are identical in form with the same operators and the same boundary conditions. This suggests that the total angle-integrated flux values calculated from Equations 123 and 124 will not be very different from each other. At least, we believe that the broad conclusions, that were made in Chapters V and VI about the applicability of the diffusion theory in determining the critical transverse buckling for beryllium moderator, will remain essentially unaltered.

The main effect noticeable for a non-asymptotic decay is that the above-Bragg neutrons decay in space faster than those in the sub-Bragg region. As discussed in Chapter V, for the positive z direction, the use of an angle-independent transverse leakage term causes the relative below-

Bragg decay rate to be faster than if the leakage term was angle-dependent. This also indicates that the conclusions that were made in Chapter VI would remain unaltered.

Let us compare some of the assumptions made in Ahmed's analysis[19] with our analysis. In the analysis used by Ahmed et al., the following assumptions have been made:

1. Diffusion approximation
2. Flux is separable in x, y, and z
3. Energy-dependent buckling concept
4. Anisotropy of the scattering collisions is described by retaining only the first two terms of the Legendre expansion of the differential scattering cross section.

In our analysis the main feature is that the diffusion approximation is used only to estimate the transverse leakage term, whereas the motion of neutrons in the z direction is treated with transport theory. Also, the anisotropy of the scattering collisions is treated more accurately by retaining the first four terms in the Legendre expansion of the differential scattering cross section. Our analysis uses assumptions 2 and 3 given above. Therefore, we believe that our analysis is superior to the complete diffusion theory approximation.

APPENDIX D

ESTIMATION OF THE SOURCE SPATIAL DISTRIBUTION

The theoretical procedure to estimate the source spatial distribution of neutrons coming into the 35.56 x 35.56 cm beryllium block from the GTRR graphite thermal column is described here. The purpose of this analysis was to check on the accuracy of the source spatial distribution (Figure 9) used in our adjoint Monte Carlo analysis and to investigate the validity of our assumption that the source distribution is separable in space and energy. The geometry of the graphite thermal column, the Plexiglass plate, and the beryllium block have been described in Chapter IV.

A two-dimensional discrete ordinate transport computer code,[61] DOT-III, was used in this theoretical analysis. The required cross sections and the scattering kernels, which have been described in Chapter IV, are the same as those used in the ANISN-calculations. The R-Z geometry used in the DOT-analysis is shown in Figure 36. The 152 x 152 cm rectangular graphite block and the 35.56 x 35.56 cm rectangular beryllium block were converted into equivalent cylindrical blocks of radius 80 cm and 26 cm, respectively. This conversion was made by equating the corresponding bucklings of the rectangular and the cylindrical blocks. The buckling defined by Equation 67 is strongly energy-dependent around the Bragg cut-off energy, since the transport mean-free-path fluctuates drastically at this energy. An average value of the above- and below-Bragg

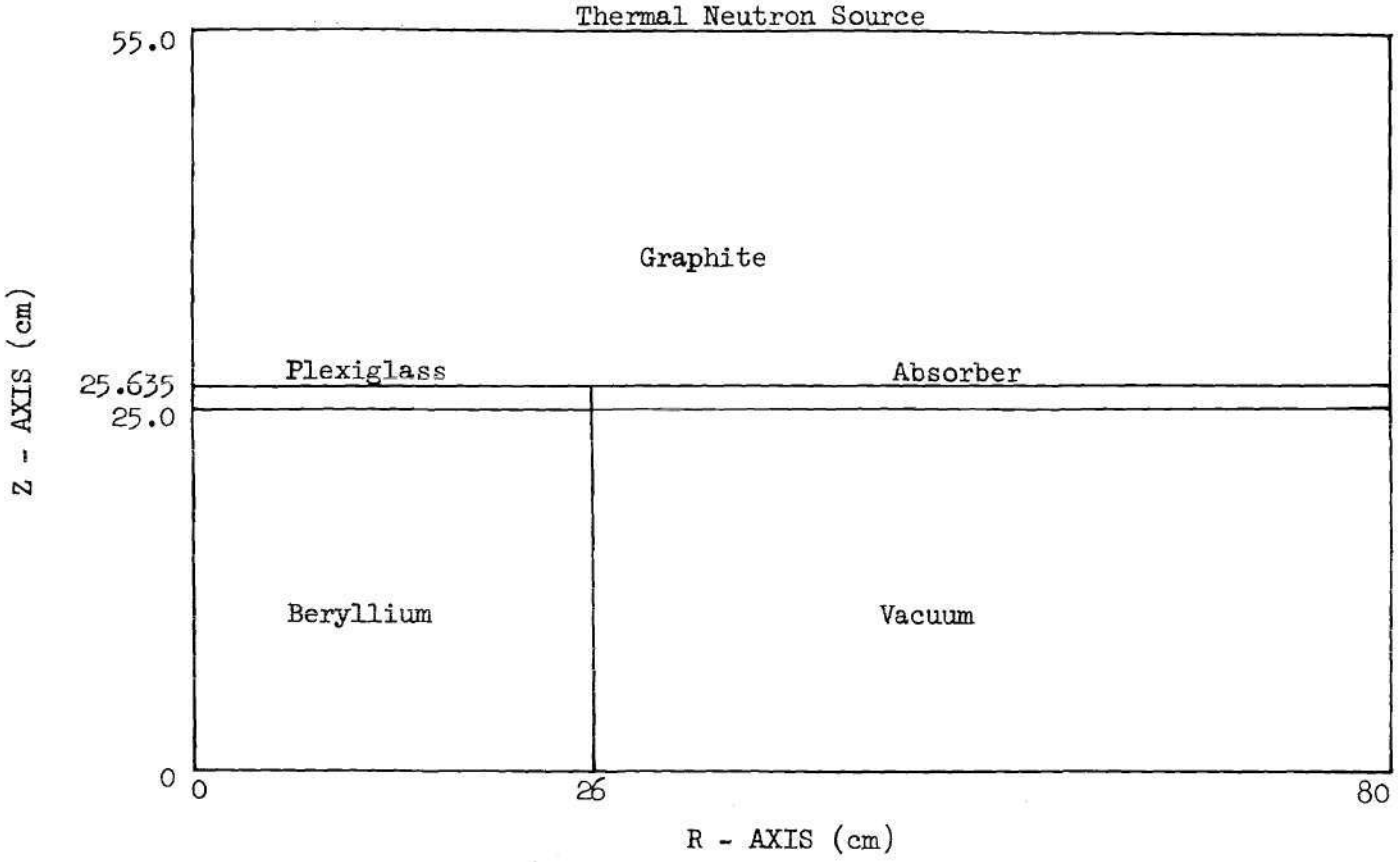

Figure 36. R-Z Geometry Used in the DOT-III Calculations

transport mean-free-paths was used in estimating the buckling of the beryllium block. This procedure was not used for the graphite and the Plexiglass blocks, since they have large transverse neutronic dimensions. A region of strong neutron absorber was used as shown in Figure 36, to simulate a non-reentrant boundary condition for the beryllium and Plexiglass blocks. The isotropic thermal neutron source at the end of the graphite block was assumed to be Maxwellian in energy distribution with a cosine spatial distribution over the 80 cm transverse dimension. The objective of the DOT-calculation was to determine the radial distribution of neutrons coming into the beryllium block across a z-plane very close to the meeting-plane of the beryllium and the Plexiglass blocks.

Figure 37 shows the behavior of the transverse total flux distribution as one moves away from the graphite region into the beryllium region. The radius of 26 cm of the cylindrical beryllium block has been normalized to 17.78 cm, which is one-half of the corresponding rectangular block width, for making comparisons of the spatial distributions in the two blocks as a function of the relative distance from the block center to its edge. In Figure 37, we notice that, in the graphite region, the transverse distribution has a broad shape and as one moves towards the beryllium block the distribution starts depressing in the region around a transverse distance of 18 cm. At 24.5 cm along the z-axis, i.e., 0.5 cm inside the beryllium block, the transverse distribution has a relatively broader shape than the corresponding cosine distribution. Also, at this z-position, the total flux distribution has almost the same shape as that of the distribution for the incoming neutrons into the beryllium block. In Figure 37, the distribution shown is for 0.0045 eV (below-

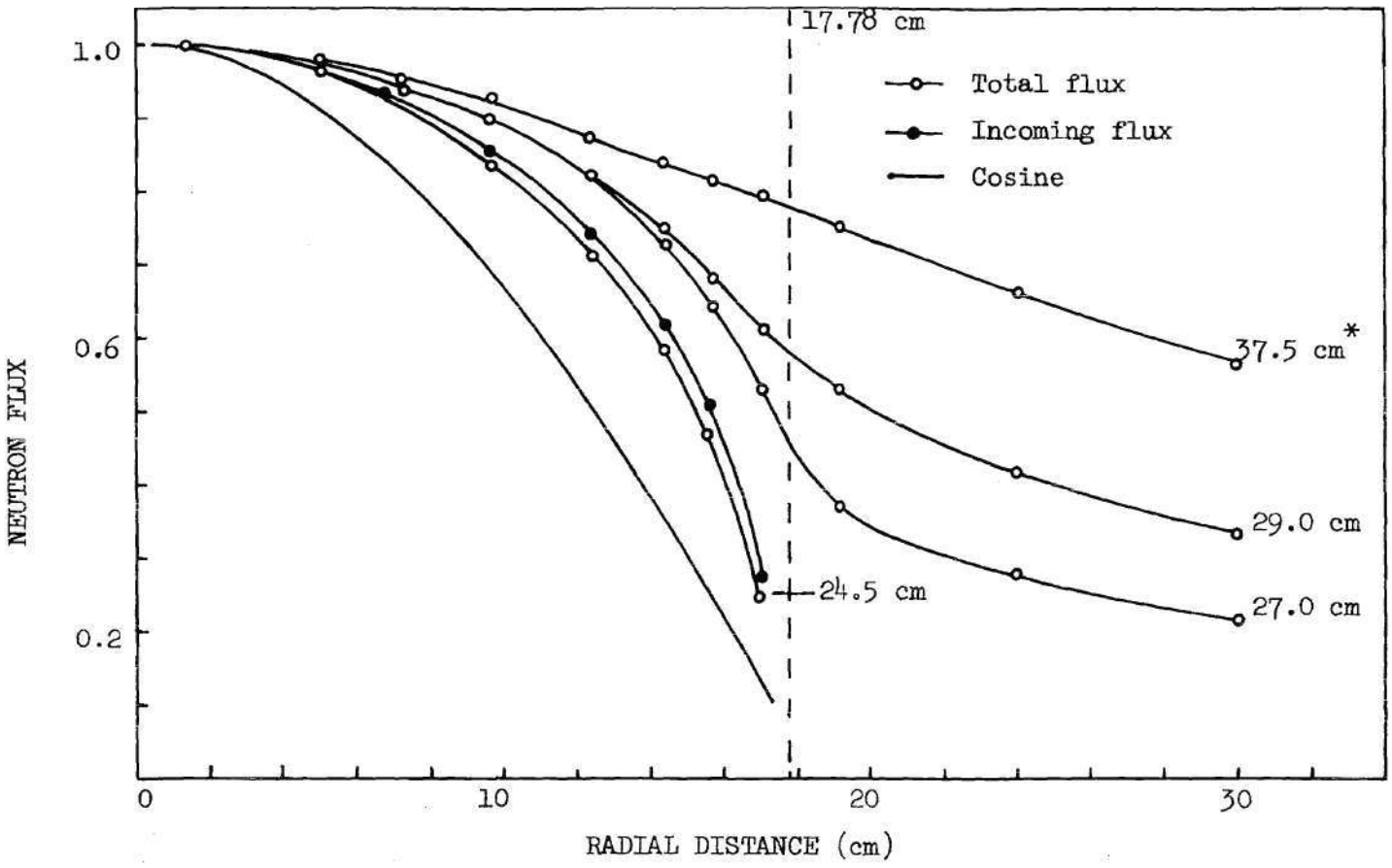

Figure 37. Spatial Behavior of the Transverse Flux Distribution Along the z Axis for 0.0045 eV Neutrons (* - distances along z axis)

Bragg) neutrons; the behavior is the same for the above-Bragg neutrons.

Figure 38 shows the transverse distribution of neutrons coming into the beryllium block at 0.5 cm from the Plexiglass plate for above- (0.035 eV) and below-Bragg (0.0045 eV) energies. This is the spatial distribution of the source neutrons for the beryllium block. We notice that the transverse distributions for the above- and below-Bragg energies are the same and are in agreement with the experimental result used in our adjoint Monte Carlo analysis, which was taken from Figure 9.

Figure 39 shows the ratio of the incoming source neutron flux at 0.0045 eV (below-Bragg) to that at 0.035 eV (above-Bragg) across the source plane for the beryllium block. The ratio stays constant over a large central region showing that our assumption of space-energy separability is valid except at regions very close to the edges.

This analysis has shown that the distribution shown in Figure 9 is quite adequate in representing the source transverse distribution. It should be noted that the buckling of the beryllium block could only be estimated and one cannot be certain whether the transverse leakage from the sides of the block is treated exactly in our DOT-calculation. At this point, we can say that the relative peaking of the sub-Bragg neutrons in the forward spectrum at 10.2 cm from the source plane could be in error by less than 10% due to the assumptions made about the source angular distribution. This has been discussed in Chapter IV.

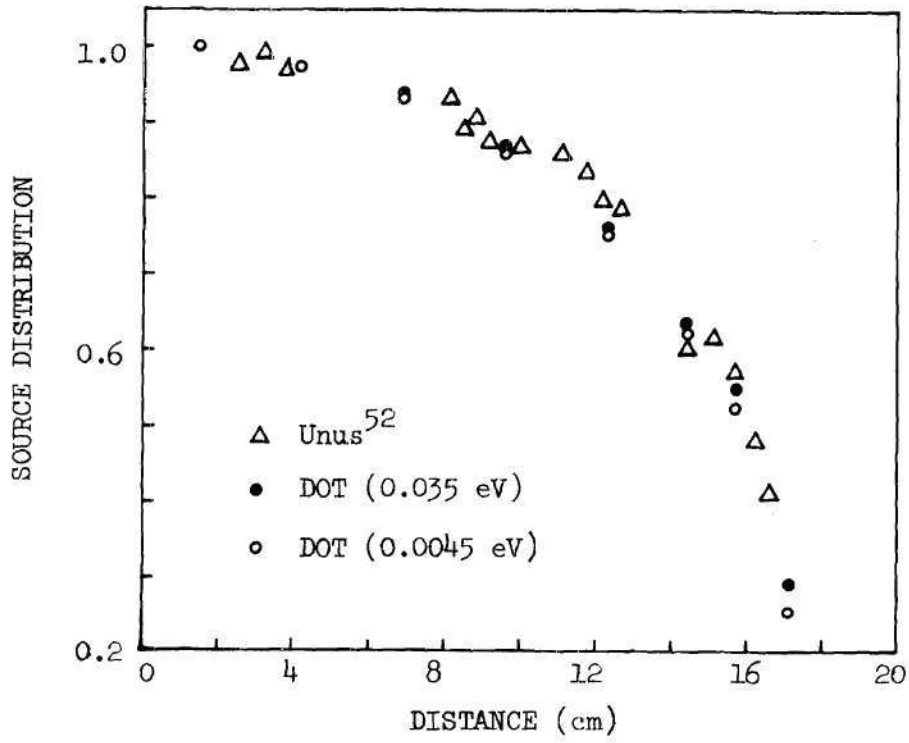

Figure 38. Source Transverse Spatial Distribution Across the Source Plane of the Beryllium Block

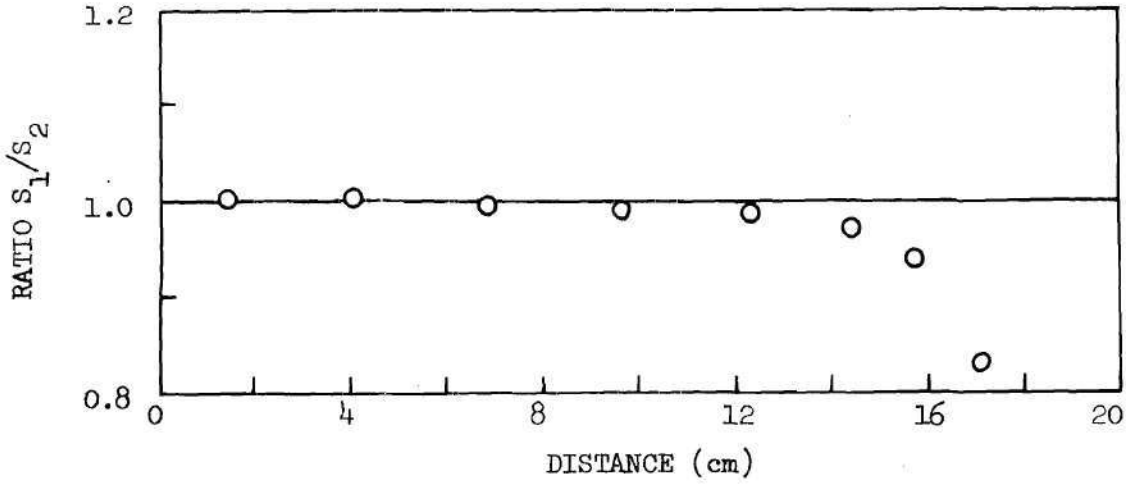

Figure 39. Ratio of Incoming Source Neutron Flux at 0.0045 eV to That at 0.035 eV Across the Source Plane of the Beryllium Block

BIBLIOGRAPHY

1. K. H. Beckurts and K. Wirtz, Neutron Physics, translated by L. Dresner, Springer-Verlag, New York, 1964.

2. F. Ahmed and A. K. Ghatak, "On the Space-Energy Separability of the Fundamental Mode of the Neutron Transport Operator with Isotropic Scattering," Nuclear Science and Engineering, 33, 106 (1968).

3. M. M. R. Williams, "Space, Time and Energy Separability in the Pulsed Neutron Experiment," Nukleonik, 10:5, 252 (1967).

4. J. Wood and M. M. R. Williams, "The Validity of the Buckling Concept and the Importance of Spatial Transients in the Pulsed Neutron Experiment," Journal of Nuclear Energy, 21, 113 (1967).

5. N. Corngold and P. Michael, "Some Transient Phenomena in Thermalization. II. Implications for Experiment," Nuclear Science and Engineering, 19, 91 (1964).

6. M. M. R. Williams, "Existence of a Diffusion Length in a Finite Prism of Pure Moderator," Proc. Symp. on Neutron Thermalization and Reactor Spectra, IAEA, Ann Arbor, 1967, pp. 27-43.

7. M. M. R. Williams, "Approximate Solutions of the Neutron Transport Equation in Two and Three Dimensional Systems," Nukleonik, 9:7, 305 (1967).

8. M. M. R. Williams, The Slowing Down and Thermalization of Neutrons, John Wiley and Sons, Inc., New York, 1966.

9. M. M. R. Williams, "The Energy Dependent Diffusion Length Problem with Transverse Leakage," Nukleonik, 11:5, 219 (1968).

10. D. J. Hughes and R. B. Schwartz, "Neutron Cross Sections," BNL-325, 2nd Ed., Brookhaven National Laboratory (1959).

11. M. Nelkin, "Asymptotic Solutions of the Transport Equations for Thermal Neutrons," Physica, 29, 261 (1963).

12. N. Corngold, "Some Transient Phenomena in Thermalization. I. Theory," Nuclear Science and Engineering, 19, 80 (1964).

13. R. Conn and N. Corngold, "Pulsed Neutron Decay Constants in Crystalline Moderators," Transactions of the American Nuclear Society, 10:2, 628 (1967).

BIBLIOGRAPHY (Continued)

14. R. Conn and N. Corngold, "Analysis of Pulsed Neutron Experiments in Polycrystalline Media Using a Model Kernel," Nuclear Science and Engineering, 37, 94 (1969).

15. R. Conn and N. Corngold, "A Theory of Pulsed Neutron Experiments in Polycrystalline Media," Nuclear Science and Engineering, 37, 85 (1969).

16. M. T. Rainbow and A. I. M. Ritchie, "Measurements in Pulsed BeO Assemblies with Decay Constants in the Region of Corngold's Limit," Journal of Nuclear Energy, 22, 735 (1968).

17. M. T. Rainbow and A. I. M. Ritchie, "Some Measurements of Decay Constants Close to $(\nu \Sigma_{inel})_{min}$ in Pulsed BeO Assemblies," Nuclear Science and Engineering, 28, 306 (1967).

18. J. A. DeJuren and V. A. Swanson, "Cold Neutron Effects in Graphite Diffusion Measurements," Journal of Nuclear Energy A/B, 20, 905 (1966).

19. F. Ahmed, L. S. Kothari, and A. Kumar, "Effect of Transverse Dimensions on the Diffusion Length of Neutrons in Crystalline Moderator Assemblies," Nuclear Science and Engineering, 46, 203 (1971).

20. M. M. R. Williams, "Comments on the Effect of Transverse Dimensions on the Diffusion Length in Crystalline Moderator Assemblies," Nuclear Science and Engineering, 47, 498 (1972).

21. J. A. Lake and J. M. Kallfelz, "Space Dependent, Steady State Thermal Neutron Spectra in Beryllium Above the Critical Buckling," Transactions of the American Nuclear Society, 13, 690 (1971).

22. J. A. Lake and J. M. Kallfelz, "Measurements of Steady-State, Space Dependent Thermal Neutron Spectra in Beryllium Assemblies with Strong Transverse Leakage," Nuclear Science and Engineering (to be published).

23. J. A. Lake, "Measurement of Steady State Space Dependent Thermal Neutron Spectra in Beryllium," Unpublished Doctoral Thesis, Georgia Institute of Technology (1972).

24. J. Wood, "Pseudo-Exponential Decay of a Neutron Pulse in Small Beryllium Systems," Journal of Nuclear Energy A/B, 20, 649 (1967).

25. G. E. Bacon, Neutron Diffraction, Clarendon Press, Oxford, 1962.

26. W. Gläser, "Scattering Law Studies for Moderators," Proc. Symp. on Neutron Thermalization and Reactor Spectra, IAEA, 1968, p. 235.

BIBLIOGRAPHY (Continued)

27. J. U. Koppel and J. A. Young, "Scattering Kernel for Beryllium," Nuclear Science and Engineering, 19, 367 (1964).

28. P. A. Egelstaff, "The Slow-Neutron Cross Section of Graphite," Journal of Nuclear Energy, 5, 203 (1957).

29. L. S. Kothari and K. S. Singwi, "Thermal Inelastic Scattering of Cold Neutrons in Polycrystalline Graphite," Physical Review, 106, 230 (1959).

30. R. J. Weiss, "Small Angle Scattering of Neutrons," Physical Review, 83, 379 (1951).

31. H. H. A. Krueger, D. Meneghetti, G. R. Ringo, and L. Winsberg, "Small Angle Scattering of Thermal Neutrons," Physical Review, 80, 507 (1950).

32. A. K. Ghatak and H. C. Honeck, "On the Feasibility of Measuring High Time Decay Constants," Nuclear Science and Engineering, 21, 227 (1965).

33. W. W. Clendenin, "Neutron Diffusion Lengths of Graphite-Absorber Mixtures between 200 and 2000°K," Nuclear Science and Engineering, 36, 1 (1969).

34. P. G. Khubchandani, L. S. Kothari, and K. S. Singwi, "Thermal Inelastic Scattering of Cold Neutrons in Polycrystalline Graphite II," Physical Review, 110, 70 (1959).

35. J. Krumhansl and H. Brooks, "The Lattice Vibration Specific Heat of Graphite," The Journal of Chemical Physics, 21, 1663 (1953).

36. R. Conn, "Approximate Dispersion Relations and the Total Coherent Inelastic Neutron Scattering Cross Section for Graphite," Nuclear Science and Engineering, 40, 17 (1970).

37. I. F. Zhezherun and A. A. Chernyshov, "The Influence of Temperature on the Scattering of Thermal Neutrons on Baked Beryllium Oxide," AEC-tr-4688 (1960).

38. I. F. Zhezherun et al., "Study of Beryllium and Beryllia as Neutron Moderators," Proc. of the Third International Conference on the Peaceful Uses of Atomic Energy, Geneva, United Nations, New York, 3, 1964, p. 362a.

39. GASKET, "A Unified Code for Thermal Neutron Scattering," by J. U. Koppel, J. R. Triplett, and Y. D. Naliboff, GA-7417 (1967).

BIBLIOGRAPHY (Continued)

40. FLANGE, "A Code for Thermal Neutron Scattering," GA-6824 (1966).

41. G. M. Borgonovi and D. Sprevak, "A Calculation of the Coherent Neutron Scattering from Polycrystalline Beryllium," Nuclear Science and Engineering, 42, 137 (1970).

42. E. Fermi, W. J. Sturm, and R. G. Sachs, "The Transmission of Slow Neutrons Through Micro-crystalline Materials," Physical Review, 71, 589 (1947).

43. L. S. Kothari and K. S. Sinwi, "Interaction of Thermal Neutrons with Solids," Solid State Physics, 8, 109 (1959).

44. Specifications Sheet, Beryllium Block-High Purity Grade N-50-C, Brush Wellman, Inc., Cleveland, Ohio (1972).

45. P. Landry, Ventron Corporation, Private Communication.

46. A. E. Goldman, Union Carbide Corporation, Private Communication.

47. A. I. M. Ritchie, K. J. Maher, and G. D. Trimble, "Calculation of Decay Constants in Beryllium Oxide in the Region of $(v \Sigma_{inel})_{min}$," Journal of Nuclear Energy, 24, 151 (1969).

48. A. I. M. Ritchie, Private Communication to Dr. J. M. Kallfelz (1973).

49. ANISN, "A One Dimensional Discrete Ordinates Transport Code," Oak Ridge National Laboratory, CCC-82 (1973).

50. E. A. Starker, P. N. Stevens, D. C. Irving, and V. R. Cain, "The MORSE Code--A Multigroup Neutron and Gamma-Ray Monte Carlo Transport Code," Oak Ridge National Laboratory, ORNL-4585 (1970).

51. D. C. Irving, "The Adjoint Equation and Its Simulations by Monte Carlo," ORNL-TM-2879 (1970).

52. I. J. Unus, Unpublished Report, Georgia Institute of Technology, Atlanta, 1972.

53. HEXSCAT, "Coherent Elastic Scattering of Neutrons by Hexagonal Lattices," Y. D. Naliboff and J. U. Koppel, GA-6026 (1964).

54. J. U. Koppel and D. H. Houston, "Reference Manual for ENDF Thermal Neutron Scattering Data," GA-8774 (1968).

BIBLIOGRAPHY (Concluded)

55. C. E. Lee, "The Discrete S_n Approximations to Transport Theory," LA-2595 (1962).

56. P. S. Grover, L. S. Kothari, and A. K. Ghatak, "Comparison of Neutron-Transport and Diffusion Theories of Isotropic Scattering," Nuclear Science and Engineering, 31, 314 (1968).

57. P. R. Bevington, Data Reduction and Error Analysis for the Physical Sciences, McGraw-Hill Book Co., Inc., New York, 1969.

58. V. F. Turchin, Slow Neutrons, Moscow, 1963; translated by the Israel Program for Scientific Translations, Ltd., 1965.

59. R. S. Stone and K. E. Slovacek, "Reactor Spectrum Measurements Using a Neutron Time-of-Flight Spectrometer," KAPL-1499, Knowles Atomic Power Laboratory (1956).

60. J. Spalek, "Neutron Time-of-Flight Spectrometry," ANL-6990, Argonne National Laboratory (1965).

61. DOT-III, "A Two-Dimensional Discrete Ordinate Transport Code with General Anisotropic Scattering," ORNL-TM-4280 (1972).

VITA

Bangalore Inamati Shamasundar was born on July 22, 1942 in Mysore, Karnataka State, India. He attended public schools in Davanagere, Karnataka State and graduated from Government High School in 1958. He attended the College of Engineering, Davanagere and received the degree of Bachelor of Mechanical Engineering "with University Rank" in January 1964. He entered the Indian Institute of Science in August 1964 and obtained the degree of Master of Engineering in Mechanical Engineering in June 1966.

From 1966 to 1969 Mr. Shamasundar was employed as a Design Engineer at Hindustan Motors Limited, Calcutta, India, where he was engaged in design, development, and testing of automotive components.

In January 1970, Mr. Shamasundar came to Georgia Institute of Technology, Atlanta, in the United States of America, to continue his education in Nuclear Engineering. He completed his Master of Science degree in Nuclear Engineering in 1971 after which he began work toward the Doctor of Philosophy in the School of Nuclear Engineering.

Mr. Shamasundar is married to the former Padmareka Katti of Davanagere and they have a son, Gopal. Mr. Shamasundar is a member of the American Nuclear Society and the honor Society of Sigma Xi.